(Eg) J. Johnson
J. DeSHON

NUREG/CR-0300
TREE-1268
for U.S. Nuclear Regulatory Commission

GAP CONDUCTANCE TEST SERIES-2 TEST RESULTS REPORT FOR TESTS GC 2-1, GC 2-2, AND GC 2-3

RICHARD W. GARNER
RICHARD H. SMITH
DAVID H. SCHWIEDER
DANIEL T. SPARKS
PAUL H. KLINK
PHILIP E. MACDONALD

November 1978

EG&G Idaho, Inc.

IDAHO NATIONAL ENGINEERING LABORATORY

DEPARTMENT OF ENERGY

IDAHO OPERATIONS OFFICE UNDER CONTRACT EY-76-C-07-1570

Available from
National Technical Information Service
Springfield, Virginia 22161
Price: Printed Copy A19; Microfiche $3.00

The price of this document for requesters outside the North American continent can be obtained from the National Technical Information Service.

NUREG-CR-0300
TREE-1268
R3

GAP CONDUCTANCE TEST SERIES-2

TEST RESULTS REPORT FOR

TESTS GC 2-1, GC 2-2, AND GC 2-3

Richard W. Garner
Daniel T. Sparks
Richard H. Smith
Paul H. Klink
David H. Schwieder
Philip E. MacDonald

EG&G Idaho, Inc.
Idaho Falls, Idaho 83401

Published November 1978

PREPARED FOR THE
U.S. NUCLEAR REGULATORY COMMISSION
AND THE U.S. DEPARTMENT OF ENERGY
IDAHO OPERATIONS OFFICE
UNDER CONTRACT NO. EY-76-C-07-1570
NRC FIN NO. A6041

ACKNOWLEDGMENT

The authors would like to gratefully acknowledge the consultation, support, and interest of Dr. Robert VanHouten (NRC).

ABSTRACT

Light water reactor (LWR) fuel behavior studies are being conducted by the Thermal Fuels Behavior Program of EG&G Idaho, Inc. These studies are being performed in the Power Burst Facility (PBF) at the Idaho National Engineering Laboratory (INEL). As a part of the fuel behavior studies, a series of tests to evaluate gap conductance in LWR design fuel rods has been initiated. The results obtained from three of these tests, Gap Conductance Tests GC 2-1, GC 2-2, and GC 2-3, are presented in this report. The experiment data were used as a basis for evaluating the effects of variations in LWR fuel rod design parameters of initial pellet-to-cladding gap width, fill gas composition, and fuel density on the thermal response of fuel rods and the heat transfer coefficient (gap conductance) across the pellet-to-cladding gap. On the basis of the experiment data, the thermal conductivity of the UO_2 fuel and the gap conductance are affected by pellet cracking. An empirical model has been developed for estimating an effective cracked pellet fuel thermal conductivity as a function of temperature. Also, the Ross and Stoute gap conductance correlation has been compared with steady state gap conductance values obtained from experiment data and the model has been modified to account for the effects of pellet cracking and pellet fragment relocation on the gap conductance. Gap conductance values have also been obtained by the power oscillation method, and an evaluation of the power oscillation experimental method for use in obtaining gap conductance in irradiated fuel rods is presented. Details of the design and operation of the tests, the observed thermal response of the fuel, and the analysis methods used for obtaining effective fuel thermal conductivity and steady state and power oscillation gap conductance values are provided as appendices.

SUMMARY

Gap Conductance Test Series-2 is being conducted by the Thermal Fuels Behavior Program of EG&G Idaho, Inc., under contract to the United States Department of Energy as part of the Nuclear Regulatory Commission's Water Reactor Safety Research Program. This report describes the test results and analysis of three gap conductance tests performed in the Power Burst Facility (PBF) at the Idaho National Engineering Laboratory (INEL). These tests are identified as Tests GC 2-1, GC 2-2, and GC 2-3, and are the first three tests of a series of five tests designed on the basis of a 3 x 3 fractional factorial design for evaluating the effects of variations in the fuel rod design parameters on the thermal response of light water reactor fuel rods. The rod design parameter variations used in Tests GC 2-1, GC 2-2, and GC 2-3 encompass variations in initial gap widths, fuel densities, and expected fill gas composition.

Although additional data will be forthcoming from Tests GC 2-4 and GC 2-5, the data from the three tests performed to date have provided a basis for evaluating the effects of fuel design parameter variations on (a) fuel rod thermal response (that is, temperature response), (b) effective fuel thermal conductivity, and (c) pellet-to-cladding gap conductance as a function of rod power density. Data for evaluating gap conductance were obtained by steady state ($\int$kdT) and power oscillation experimental methods and the steady state results also provide a basis for evaluation of the power oscillation method for obtaining pellet-to-cladding gap conductance in light water reactor (LWR) design rods.

Generally, the test rod steady state thermal responses were as expected, except that the xenon and argon filled rods were hotter at low powers than was expected. Initial gap width has a strong effect on the fuel centerline and pellet surface temperatures in helium filled rods when the gap width is increased from 2.2 to 3.4% of the pellet diameter, but only a small effect was observed when the gap width was increased from 0.94 to 2.2%. However, for argon and xenon filled rods, the effect of gap width between 0.94 and 2.2% gap rods was much greater. The stronger effect of gap width in the argon and xenon filled rods than in the helium filled rods is interpreted to be due to the strong effect of pellet cracking and fill gas inclusion on the effective thermal conductivity of the fuel. Inclusion of the low conductivity fill gases of argon and xenon in the fuel cracks strongly inhibits heat conduction across the cracks. At high powers, however, fuel restructuring and contact pressure somewhat offset the effect of cracking and gas inclusion in the xenon filled test rods.

In all test rods, the fuel centerline temperatures increased much more than did the off-center (pellet surface) temperatures when the initial gap width was increased. This indicates that when the pellets crack, part of the thermal resistance normally associated with the pellet-to-cladding gap is redistributed within the fuel pellet, especially in moderate and large gap rods. This result further illustrates that pellet cracks and the movement of pellet fragments degrade the fuel thermal conductivity while improving the gap conductance.

The xenon filled rods showed the highest fuel temperatures at a specified power level. However, the differences in the fuel centerline temperatures between xenon and argon rods were much smaller than the differences in the off-center (pellet surface) temperatures for the same rods. This result indicates that the gap thermal resistance and the fuel thermal conductivity are reduced in both xenon and argon filled rods, but that the reduction in fuel thermal conductivity in the high temperature xenon filled rod is somewhat offset by some other effect, possibly fuel restructuring.

The effect of fuel density on the observed thermal response was small for fuel centerline temperatures, and indistinguishable from normal scatter in the data for off-center temperatures.

Under actual operating conditions, pellet cracking, relocation, and fill gas inclusion significantly alter the thermal conductivity of UO_2 fuel pellets. An analytical procedure was developed for evaluating the "effective fuel thermal conductivity" that takes these effects into account. To be of use in predicting fuel rod effective thermal conductivities, an empirical correlation was developed on the basis of evaluated effective thermal conductivities from Tests GC 2-1, GC 2-2, and GC 2-3. The correlation was obtained for all the helium filled test rods in terms of (a) a nominal "hot gap width," (b) the initial cold gap width, and (c) the fuel density. Although the fuel density has small effect as an individual parameter, it did serve as a multiplier to fine-tune the relationship for the various helium test rods.

Pellet-to-cladding gap conductance was evaluated as a function of test rod power density by the steady state ($\int$kdT) and power oscillation experimental methods. The steady state values were very consistent between similar rods in the three tests, and showed relatively small azimuthal variations in a given rod. The effect of initial gap width was significant for the helium filled rods between the wide gap and narrow gap rods. Only medium and narrow gap xenon and argon rods were tested and the effect of gap width was small between the different gap rods for both xenon and argon.

The low thermal conductivities of the xenon and argon fill gases significantly decrease the gap conductance in these rods with respect to the relatively high conductivity helium fill gas rods. However, the effect of fill gas is offset somewhat, but not entirely, by high fuel temperatures which result in greater fuel expansion, pellet cracking, and pellet fragment relocation, all of which increase the gap conductance by decreasing the gap width.

A correlation was developed which provides a simple method for estimating the gap conductance of a particular LWR design fuel rod under a specific set of rod conditions. In the development of the correlation for predicting gap conductance it was observed that all but three of the test rods in the three tests could be predicted quite well by the Ross and Stoute gap conductance correlation, modified to account for pellet cracking and pellet fragment relocation by assuming nonuniform thermal expansion of the cracked pellets. The nonuniform thermal expansion model takes into consideration that the pellets have been heated and cracked. Upon cooldown the pellet fragments do not usually fit together well enough to completely close the relocated cracks. Upon reheating, the relocated cracks must

be filled before thermal expansion contributes to closing the existing pellet-to-cladding gap. A nonuniform thermal expansion model that allowed only 30% of the integrated fuel pellet radial thermal expansion to be communicated to the relocated pellet-to-cladding gap was determined to fit the data best.

For the other three rods (the narrowest initial gap width rods; Rods GC 502, GC 522-2, and GC 523-3), a uniform thermal expansion model provided the best fit with experimental data. For Rod GC 502, the narrow gap helium filled rod, data were also obtained that would better be fit by a nonuniform expansion model. These data were obtained during the power oscillation portion of the test and may be indicative of a definite change in the thermal response of the rod after the power was cycled several times. The xenon (Rod GC 523-2) and argon (Rod GC 522-2) filled narrow gap rods exhibited high fuel temperatures at low power levels, because of the low thermal conductivity fill gases, resulting in early gap closure. With gap closure at low power levels, subsequent thermal expansion would be expected to be essentially the same as for a solid pellet; that is, uniform thermal expansion.

Gap conductance values determined by the power oscillation method were generally in agreement with the steady state values at low powers, but deviated significantly (much higher values) at high powers. A direct correlation exists between the power levels at which the two methods deviate and the occurrence of waveshape changes in the fuel and cladding temperature oscillations. The waveshape changes are believed to be due to pellet-to-cladding contact during the oscillations, possibly indicating gap closure during the power increase and gap reopening during the power decrease.

Azimuthal variations within a rod were much greater for the power oscillation method than for the steady state method. Many of the indicated power oscillation values at high powers were unrealistically high (greater than 40 $kW/m^2 \cdot K$). Pellet-to-cladding contact is postulated to have occurred during the high power oscillations, with possible gap closure during the increase in power and gap reopening during the decrease in power. Gap closure and reopening during the power oscillation cycle would alter the measured phase lag of the cladding surface temperature oscillation by introducing higher harmonics. The analytical methods used to evaluate gap conductances do not account for higher harmonics and may result in unrealistic values.

Analyses are described that were performed to identify cladding surface temperature waveform distortions and to quantitatively determine the effect of observed nonlinearities on the results obtained by the power oscillation method. Nonlinearities in the waveforms were identified for both pressurized water reactor (PWR) and boiling water reactor (BWR) design rods, but the nature of the nonlinearities were different for the two designs; that is, the amount of signal distortion increased in the BWR rods as the nominal rod power increased, but the signal distortion was greatest at low power levels in the PWR rods. The amount of signal distortion observed at a specific power level suggests that the PWR design fuel rods maintained a more stable fuel stack geometry during the power oscillations. The fuel pellet central expansion is possibly compensated for by the dished ends of the PWR fuel

pellets, but it contributes to an unstable geometry in the initially flat ended BWR pellets during a power oscillation.

A major objective of the PBF gap conductance tests has been to provide experimental data for evaluating the power oscillation method for obtaining gap conductances. On the basis of the results obtained from Tests GC 2-1, GC 2-2, and GC 2-3, the power oscillation method does not provide reliable and consistent gap conductance values for BWR design rods over the range of power levels of interest. These results are in contrast to the evaluation of the power oscillation method based on the "piggyback" tests with PWR design rods. The analyses should continue in an attempt to determine why the power oscillation method appears to provide acceptable results for PWR design rods but not for BWR design rods. Tests GC 2-4 and GC 2-5 will provide additional low power data to better identify the range of applicability of the oscillation method. These results may also provide further insight as to why the method works for one rod design and not the other.

CONTENTS

FIGURES

Data Plots - Test GC 2-1 Power Calibration Period

Data Plots - Test GC 2-1 Preconditioning Period

Data Plots - Test GC 2-1 Power Oscillation Period

Data Plots - Test GC 2-2 Power Calibration Period

Data Plots - Test GC 2-2 Preconditioning Period

Data Plots - Test GC 2-2 Power Oscillation Period

Data Plots - Test GC 2-3 Power Calibration Period

Data Plots - Test GC 2-3 Preconditioning Period

Data Plots - Test GC 2-3 Power Oscillation Period

TABLES

GAP CONDUCTANCE TEST SERIES-2

TEST RESULTS REPORT FOR

TESTS GC 2-1, GC 2-2, AND GC 2-3

I. INTRODUCTION

Light water reactor fuel behavior studies are being conducted by the Thermal Fuels Behavior Program of EG&G Idaho, Inc., under contract to the United States Department of Energy. This work is part of the Nuclear Regulatory Commission's Water Reactor Safety Research Program[1] under which experimental data for verification of analytical models developed to predict the behavior of light water nuclear fuel rods under normal and postulated accident conditions are being obtained from a variety of in-reactor and out-of-reactor experiments.

On the basis of analytical predictions, the heat transfer rate across the fuel-to-cladding gap (gap conductance) is considered to be an important factor in determining the response of light water reactor (LWR) fuel rods to postulated accidents.

A series of five tests to evaluate gap conductance in LWR design fuel rods has been designed to be performed in the Power Burst Facility (PBF) at the Idaho National Engineering Laboratory (INEL). This series of tests is being performed to evaluate the effects of variations in the design parameters of initial gap width, fill gas composition, and fuel density on the thermal response of LWR fuel rods, and to provide a basis for evaluating the power oscillation experimental method for obtaining data from which gap conductance values can be determined. Specific objectives of each test are to (a) provide experimental data for evaluating gap conductance by both the steady state $\int kdT$ and power oscillation experimental methods, (b) provide information from which effective fuel thermal conductivities can be determined, and (c) provide data for evaluating the effects of variations in the three design parameters (initial pellet-cladding gap width, fill gas composition, and fuel density) on the gap conductance values and the effective fuel thermal conductivity.

This series of tests has been designated Series-2, and the individual tests are identified as Tests GC 2-1 through GC 2-5. Tests GC 2-1, GC 2-2, and GC 2-3 have been performed and consisted of basic boiling water reactor (BWR) design test rods with variations in the initial diametral gap widths of 0.94, 2.2, or 3.4% of the pellet diameter; fill gas compositions of pure helium, xenon, or argon; and fuel densities of 92, 95, or 97% theoretical density (TD). The data obtained from Tests GC 2-1, GC 2-2, and GC 2-3 have been analyzed and correlations have been developed from which gap conductance values and effective fuel thermal conductivities can be estimated for any LWR design fuel rod.

The purpose of this report is to present the experimental and analytical results from Tests GC 2-1, GC 2-2, and GC 2-3, and to provide a preliminary evaluation, based on analysis of data from these first three tests, of the capability for the power oscillation experimental method to provide data from which gap conductance values can be determined.

Section II discusses the basis for performing in-reactor gap conductance tests and briefly describes the steady state $\int kdT$ and power oscillation experimental methods. Section III summarizes the important test rod and test assembly design characteristics and test conduct procedures for each test. The effects of rod design parameter variations on experiment results, in terms of measured thermal responses, are discussed and correlated with postirradiation examination results in Section IV. Section V describes analyses for evaluating effective fuel thermal conductivities and gap conductance values and the effects of rod design parameter variations on these quantities. In addition, correlations for evaluating effective fuel thermal conductivities and gap conductance values for any LWR design fuel rod are presented. Analysis of the power oscillation experimental results and an evaluation of the power oscillation experimental method for obtaining gap conductance values are provided in Section VI.

Appendix A provides detailed information on the experiment instrumentation, evaluation of data uncertainties, and conduct of each test. Detailed test results are provided in Appendix B in the form of thermal response data plots and time-dependent data plots for each measurement transducer used in the tests. Appendix C provides descriptions of the analysis methods used to (a) correct the off-center fuel temperature measurements for perturbation effects and effects of fuel pellet eccentricity, (b) to estimate effective fuel thermal conductivities and gap conductance values, (c) to evaluate gap conductance by the power oscillation experimental method, and (d) to evaluate test rod power densities and uncertainties. Part of the evaluation of the power oscillation experimental method involves analysis of data obtained during the power-cooling-mismatch tests, Tests PCM-2 and PCM-3, in the PBF. Descriptions of the test design and conduct for the gap conductance portions of Tests PCM-2 and PCM-3 (identified as Tests GC PCM-2 and GC PCM-3) are provided in Appendix D. All appendices are provided on microfiche and are attached to the back cover.

II. BASIS FOR IN-REACTOR GAP CONDUCTANCE EXPERIMENTS

In the event that an accident, such as a postulated loss-of-coolant accident, should occur in a light water power reactor, the fuel rod thermal response depends on the thermal energy stored in the fuel at the time the postulated accident occurs, the mechanisms involved in heat transfer from the fuel rods following the accident, and the steps taken to mitigate the consequences of the accident. On the basis of analytical predictions, the fuel-to-cladding gap conductance is considered to be an important factor in the determination of the response of LWR fuel to postulated accidents.

The thermal conductance across the fuel-to-cladding gap is by means of contact conductance at points of fuel-to-cladding contact, and convection through a gap gas environment. For nominally open gaps, gap size and the thermal conductivity of the gap gas dominate the functional relationship. For closed gaps, contact pressure becomes dominant. Affecting gap conductance to a lesser extent are surface roughness of the fuel and cladding, and gap gas pressure (as it influences the accommodation coefficients, and, therefore, the thermal conductivity of the light gases). All of the parameters affecting gap conductance are highly temperature-dependent and are complex functions of the changes occurring within the fuel rod during irradiation.

Gap size and contact pressure are, in turn, influenced by a number of factors including initial gap size; fuel pellet cracking; thermal expansion of fuel and cladding (a function of power); fuel swelling and densification; and creep, and elastic and plastic deformations of the cladding material. The first three factors (initial gap size, pellet cracking, and thermal expansion) are most significant during the early operating life of the fuel rod. The fuel pellet cracking phenomenon is not well understood and is not modeled accurately in current gap conductance codes. Present experimental knowledge suggests, however, that pellet cracking is dependent on the initial fuel density and the pellet center-to-surface temperature gradients (functions of power). Pellet cracking is considered to be particularly significant during initial power ramps.

The effect of gap-gas thermal conductivity on gap conductance is dependent on the initial backfill pressure and composition of the fill gas, the generation and release of gaseous fission products, and the release of fuel impurities (primarily nitrogen, carbon dioxide, and hydrogen). Initial backfill pressure and composition of the fill gas are also most influential during early life.

In summary, those parameters that are thought to have a significant and direct effect on gap conductance during early life are:

(1) Power level

(2) Initial pellet-to-cladding gap size

(3) Fuel density (fuel cracking effects)

(4) Gap gas composition

(5) Backfill pressure

(6) Surface roughness of fuel and cladding.

The first four of the listed parameters are the most important. In-reactor experiments are required to obtain information on the effects of these parameters on fuel rod thermal response.

Gap conductance as such is not a directly measureable quantity and must be inferred from other measured variables. Two experimental methods are being employed in the Thermal Fuels Behavior Program at the INEL for obtaining gap conductance information from in-reactor tests – the steady state ($\int$kdT) method[2] and the thermal oscillator or power oscillation method, described in Appendix C. The $\int$kdT method requires cladding surface temperature measurements and a detailed knowledge of the temperature distribution in the test rod fuel. To experimentally obtain the latter information requires internal fuel temperature measurements, which cannot be made in preirradiated fuel rods.

The thermal oscillator method relates fuel-to-cladding gap conductance to the phase relationship between a sinusoidal test fuel rod power density oscillation and the corresponding test rod cladding surface temperature oscillation. During a power oscillation, the two signals will oscillate at the same frequency, but with a phase lag between the power signal and the cladding surface temperature signal. Theoretically, the gap conductance can be determined from analytical relationships between the measured phase lag and the gap conductance. The major advantage of the thermal oscillator technique is that only external fuel rod measurements of cladding surface temperature and test fuel rod power are required to obtain gap conductance information. A detailed description of the power oscillation method is provided in Appendix C.

III. EXPERIMENT DESIGN AND CONDUCT

The PBF Gap Conductance Test Program Test Series-2, was designed on the basis of a 3 x 3 fractional factorial design to obtain the maximum amount of information with a minimum number of tests. The test series consists of five tests, each test being performed with four, instrumented, basically BWR-design test rods. The test rod designations and variations in rod design parameters of fuel density, initial gap width, and gap gas composition are shown in Table I. Test rod length is limited to 0.91 m in the PBF in-pile tube. The common nominal design characteristics for all rods in Tests GC 2-1, GC 2-2, and GC 2-3 are provided in Table II. Specific measurements of the pretest fuel pellet and cladding characteristics are provided in References 3, 4, and 5.

For each test, the instrumented fuel rods were installed in the four-rod hardware (designated 4X-A or 4X-B) and positioned in the PBF in-pile tube. The 4X hardware positions the fuel rods symmetrically within the in-pile tube. A zircaloy shroud around each test rod maintains the independence of each rod and provides coolant flow upward past each rod. The test train is designed to facilitate easy removal and replacement of the fuel rods and shrouds after each test.

Measurements were made directly in or on the test rods to obtain data for evaluating rod thermal response, effective fuel thermal conductivity, and pellet-to-cladding gap conductance values, and in the coolant system to determine thermal hydraulic conditions and test rod power densities. During Tests GC 2-1, GC 2-2, and GC 2-3, three of the rods in each test contained a fuel centerline thermocouple; three equally spaced, azimuthally, off-center thermocouples at the same axial location as the centerline thermocouple; three equally spaced, azimuthally, cladding surface thermocouples at the same axial location as the centerline and off-center thermocouples; and two cladding surface thermocouples at a lower axial position on the fuel rods. The fourth rod in each test contained a centerline thermocouple, only one off-center fuel thermocouple, and cladding surface thermocouples in the same arrangement as on the other three rods. Specific details of the test instrumentation for all three tests are provided in Appendix A.

The purpose of the off-center thermocouples was to measure fuel temperatures close to the pellet surface in an attempt to better determine the pellet surface temperature; to reduce the uncertainty in the resulting steady state gap conductance values, in conjunction with the centerline thermocouples; and to provide a means for determining an effective (in-pile, cracked pellet) fuel thermal conductivity. The cladding surface thermocouples were used to estimate the temperature drop across the gap and to obtain phase angles used in evaluating power oscillation gap conductance values.

Each of the tests consisted basically of three parts performed in the following sequence: (a) steady state operation (power calibration) over a range of PBF core power levels during which each of the four test fuel rod power densities was determined and calibration constants between test rod power and core power were obtained, (b) a preconditioning period during which test rod peak power densities were cycled between low

TABLE I

PBF GAP CONDUCTANCE TEST SERIES-2
TEST ROD PARAMETER VARIATIONS

Test	Test Rod Designation and Designs			
	GC 501	GC 502	GC 503	GC 504
GC 2-1	2.2% gap[a] 97% TD fuel 2.6 MPa Xe	0.94% gap 97% TD fuel 2.6 MPa He	2.2% gap 95% TD fuel 2.6 MPa He	2.2% gap 95% TD fuel 2.6 MPa Ar
	GC 522-1	GC 522-2	GC 522-3	GC 522-4
GC 2-2	2.2% gap 92% TD fuel 2.6 MPa Xe	0.94% gap 95% TD fuel 2.6 MPa Ar	0.94% gap 95% TD fuel 2.6 MPa He	3.4% gap 95% TD fuel 2.6 MPa He
	GC 523-1	GC 523-2	GC 523-3	GC 523-4
GC 2-3	0.94% gap 92% TD fuel 2.6 MPa He	0.94% gap 95% TD fuel 2.6 MPa Xe	3.4% gap 97% TD fuel 2.6 MPa He	2.2% gap 92% TD fuel 2.6 MPa Ar
	GC 524-1	GC 524-2	GC 524-3	GC 524-4
GC 2-4	2.2% gap 95% TD fuel 2.6 MPa He	2.2% gap 92% TD fuel 2.6 MPa He	2.2% gap 97% TD fuel 2.6 MPa He	2.2% gap 97% TD fuel 2.6 MPa Ar
	GC 525-1	GC 525-2	GC 525-3	GC 525-4
GC 2-5	2.2% gap 92% TD fuel 2.6 MPa He	0.94% gap 95% TD fuel 2.6 MPa Ar	0.94% gap 95% TD fuel 2.6 MPa He	3.4% gap 92% TD fuel 2.6 MPa He

[a] All gap sizes are expressed in percent of nominal design pellet diameter.

and high power levels for three cycles (the purpose of the preconditioning period was to obtain data from which fuel pellet cracking and rearrangement effects on gap conductance values could be evaluated), and (c) a power oscillation period during which the power was oscillated about several nominal power levels at a variety of oscillation magnitudes and periods. Steady state data were obtained during all phases of each test. Power oscillation gap conductance data were obtained only during the oscillation periods. System conditions were nominally 538 K inlet temperature, 7.17 MPa coolant pressure, and 250 to 1000 cm^3/s

TABLE II

COMMON NOMINAL DESIGN CHARACTERISTICS OF BWR DESIGN TEST FUEL RODS FOR GAP CONDUCTANCE TESTS GC 2-1, GC 2-2, and GC 2-3

Rod Parameter	Nominal Design Value
Cladding outside diameter (mm)	12.50
Cladding inside diameter (mm)	10.79
Wall thickness (mm)	0.86
Fuel material	UO_2
Cladding material	Zircaloy-2
Pellet shape	Flat ends
Pellet length (mm)	10.57
Rod overall length (mm)	990.6
Fuel stack length (mm)	914.4
Plenum length (mm)	55.12
Plenum volume	
Fuel volume	0.08
Plenum spring	Coiled carbon steel
Internal pressure (MPa)	2.58
Shroud inside diameter (mm)	19.30
Pellet enrichment (wt% U-235)	10

coolant flow during the power calibration and preconditioning periods, and 478 K inlet temperature, 7.17 MPa coolant pressure, and 500 cm^3/s coolant flow during the oscillation period. Variations in the specific operation conditions and performance sequence between the three tests are discussed in Appendix A.

IV. EXPERIMENT RESULTS – EFFECTS OF FUEL ROD DESIGN PARAMETER VARIATIONS ON THERMAL RESPONSE AND CORRELATION WITH POSTIRRADIATION EXAMINATIONS

Experimental data obtained during a PBF gap conductance test include: (a) coolant inlet and outlet temperatures, separate coolant differential temperature (ΔT) data, coolant mass flow rates, and coolant pressure, from which test rod average power densities are determined for each rod; (b) fuel pellet centerline, off-center, and cladding surface temperatures from which test rod thermal response, steady state gap conductance values, test rod stored energies, and effective fuel thermal conductivities are determined; (c) test rod power and cladding surface temperature oscillation data from which pellet-to-cladding gap conductance values are estimated; and (d) neutron flux wire and self-powered neutron detector (SPND) data from which axial weighting factors are determined for evaluating local test rod power densities.

Test rod average power densities, fuel centerline and cladding surface temperatures, cladding surface temperature phase angles, and axial weighting factors are determined directly from measured variables. The measured fuel off-center temperatures must be corrected for perturbation effects, and evaluations of effective thermal conductivity and steady state and power oscillation gap conductance values require additional analyses and computer calculations to obtain the desired results.

For each test, steady state thermal response data were obtained over a range of test rod peak power densities from approximately 2 to 52 kW/m. These data were obtained during the power calibration and preconditioning periods and immediately prior to and following power oscillations during the oscillation portions of the tests.

This section describes the steady state thermal response data obtained from Tests GC 2-1, GC 2-2, and GC 2-3; the effects of variations in test rod design parameters on the thermal response; and correlation of observed thermal response with postirradiation examination results. Detailed descriptions of the response of each individual temperature measurement in each test rod and the effects of power cycling on the response are provided in Appendix B. The general conclusion from the evaluations described in Appendix B is that there are no identifiable effects of power cycling on the thermal response of the rods.

1. EFFECT OF INITIAL GAP WIDTH

Helium filled fuel rods with initial pellet-to-cladding gap widths of 0.94, 2.2, and 3.4% of the initial fuel pellet diameters were tested during Tests GC 2-1, GC 2-2, and GC 2-3. Representative effects of variations in the initial gap width on the fuel centerline

temperatures in the helium filled rods are shown in Figure 1[a]. These results show that the initial gap width has a strong effect on the fuel centerline temperature in helium filled rods at higher power levels; for example, approximately 600 K higher temperatures were measured in the wide gap (3.4%) rod (Test GC 2-2, Rod 522-4) than in the narrow gap (0.94%) rod (Test GC 2-2, Rod GC 522-3) at a power density of 35 kW/m. However, temperatures in the medium gap (2.2%) rod (Test GC 2-1, Rod GC 503) were only approximately 100 K higher than in the narrow gap rod, at the same power density. The effect of initial gap width on centerline temperatures in the helium filled rods increases nonlinearly with gap width.

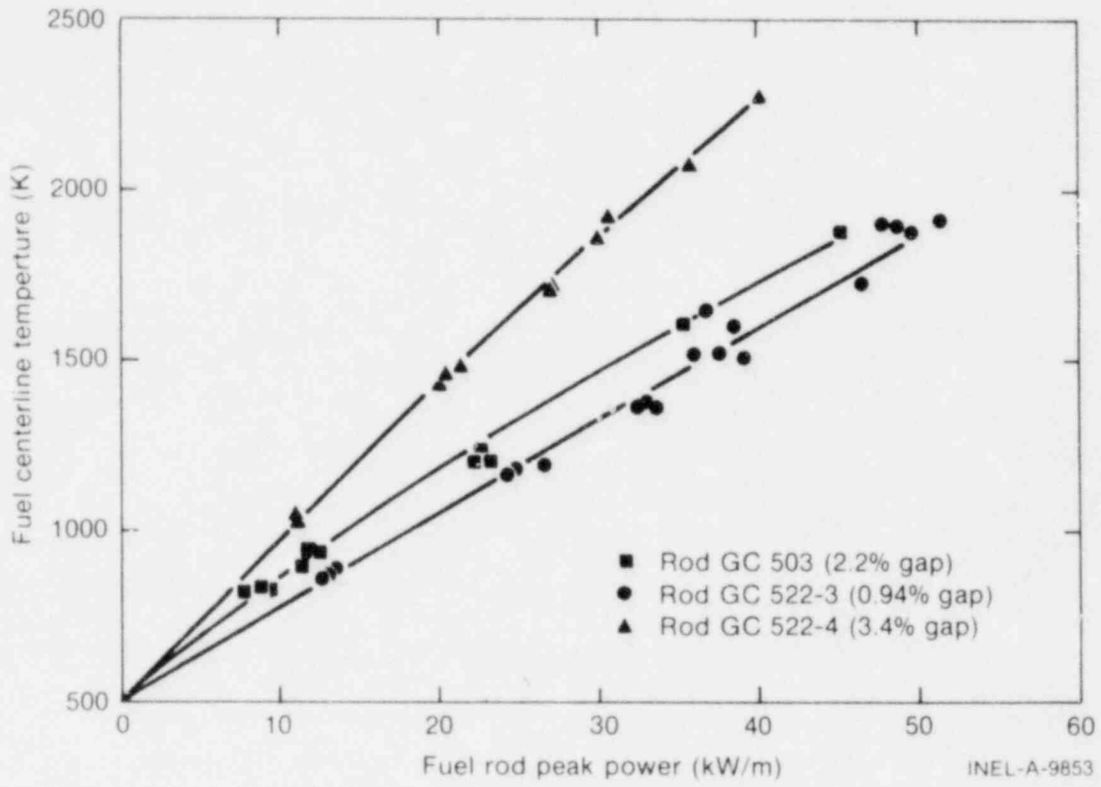

Fig. 1 Composite plot of fuel centerline temperature measurements showing effect of initial gap width in helium filled rods.

The same trend was observed in the off-center temperature measurements in the helium filled rods, as shown in Figure 2. Although the absolute magnitude of the difference at 35 kW/m (approximately 250 K) is less than for the centerline temperature measurements, the nonlinear effect is quite evident. Figure 2 also shows the relative dispersion in the azimuthally oriented off-center temperature measurements for each test rod.

---

[a] The solid line curve shown in the figure is an approximation to the data points drawn by the authors to illustrate the trend of the data. Such curves are used frequently in this report, particularly where several sets of data are shown in the same figure. Unless otherwise noted, these curves represent neither mathematical fits to the data nor analytical calculations of behavior.

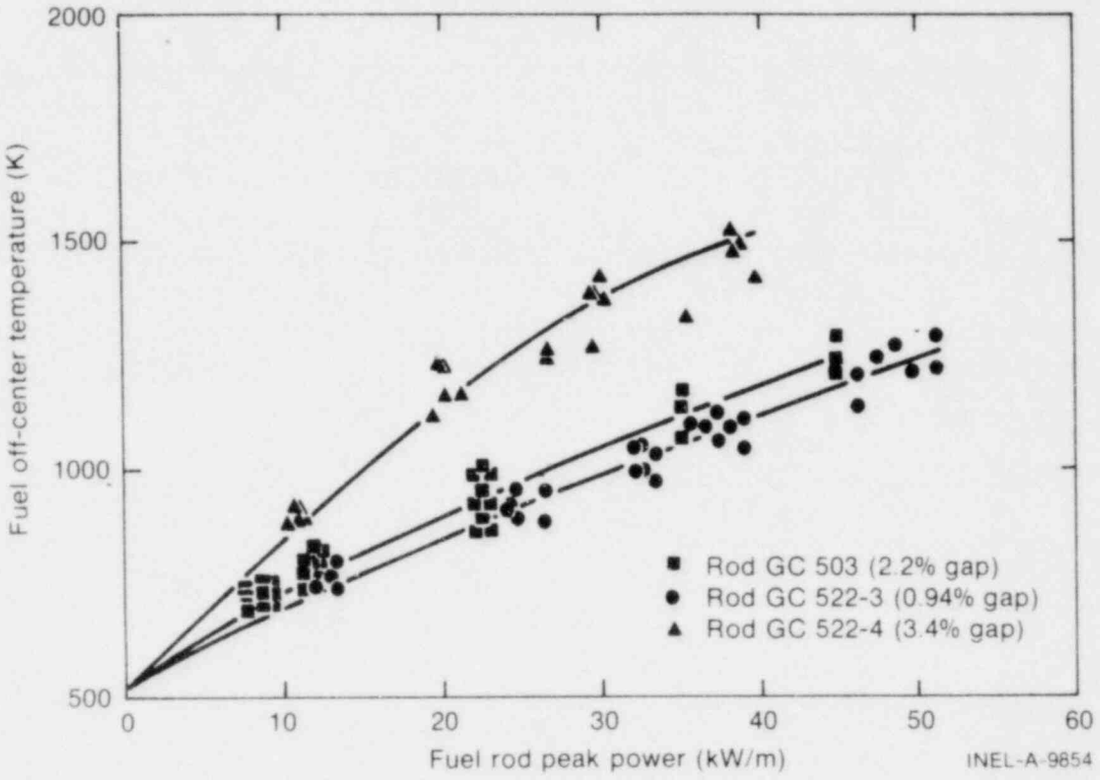

Fig. 2 Composite plot of fuel off-center temperature measurements showing effect of initial gap width in helium filled rods. This plot also shows the range of variation in the azimuthally distributed temperature measurements for each test rod.

The larger effect of gap width on the centerline temperatures than on the off-center temperatures in helium filled rods means that the radial temperature distribution will also be different, with a steeper temperature gradient in the wide gap (3.4%) rod than in the narrow gap (0.94%) rod. This effect is apparently due to a decrease in the effective fuel thermal conductivity of the wide gap rod relative to the narrow gap rod, probably resulting from cracking and relocation of the fuel pellets, effectively redistributing the initial radial gap inward toward the center of the pellet in the wide gap rod. This conclusion is supported by the postirradiation examination (PIE) photomicrographs shown in Figures 3, 4, and 5 for the helium filled rods of Figures 1 and 2. Figures 3 and 4 show that there are only slight differences in the cracking patterns between the small and medium gap rods, supporting the observed similar thermal responses for these rods. Figure 5, however, shows that the wide gap rod provides space for larger cracks and eccentric positioning of the fuel pellets, also supporting the higher fuel temperatures in the wide gap rod.

Representative effects of initial gap width on the thermal response of argon filled test rods are shown in Figures 6 and 7 for the fuel centerline and off-center temperature measurements, respectively. Initial gap widths in the argon filled rods that have been tested (Test GC 2-1, Rod GC 504; Test GC 2-2, Rod GC 522-2; and Test GC 2-3, Rod GC 523-4) were 0.94 and 2.2%. The representative data in Figure 6 show large differences in centerline temperature measurements between the 0.94 and 2.2% initial gap widths. At a power density of 20 kW/m, the measured temperature in the medium gap (2.2%) rod was

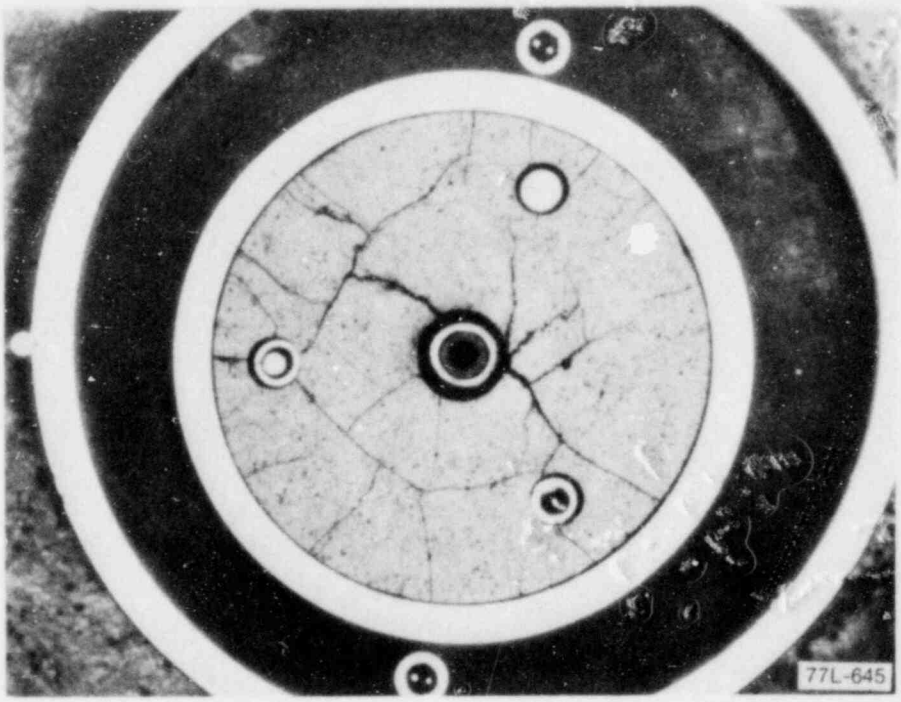

Fig. 3 Photomicrograph showing crack patterns in fuel of Rod GC 522-3 (He, 0.94% gap) at 451.5 mm.

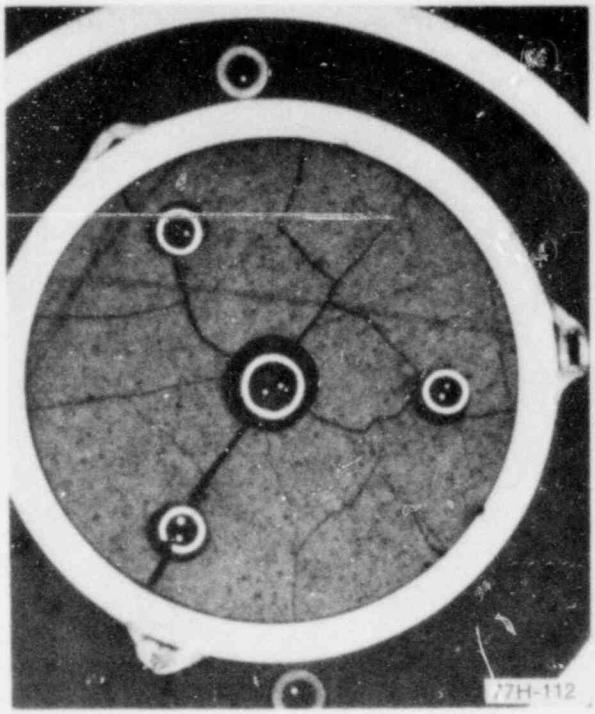

Fig. 4 Photomicrograph showing crack patterns in fuel of Rod GC 503 (He, 2.2% gap) at 487 mm.

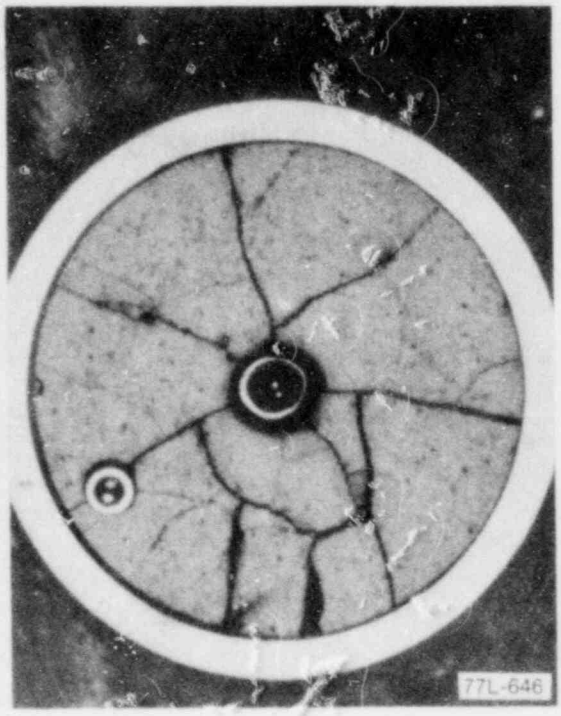

Fig. 5 Photomicrograph showing crack patterns in fuel of Rod GC 522-4 (He, 3.4% gap) at 488 mm.

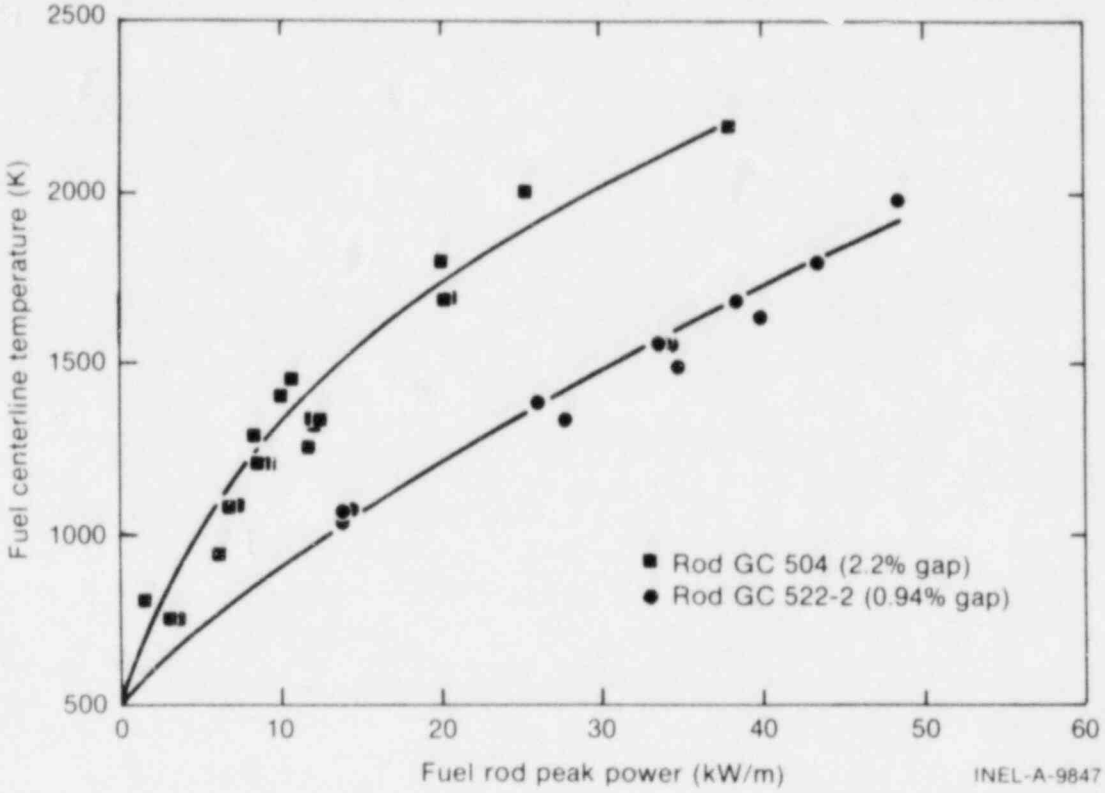

Fig. 6 Composite plot of fuel centerline temperature measurements showing effect of initial gap width in argon filled rods.

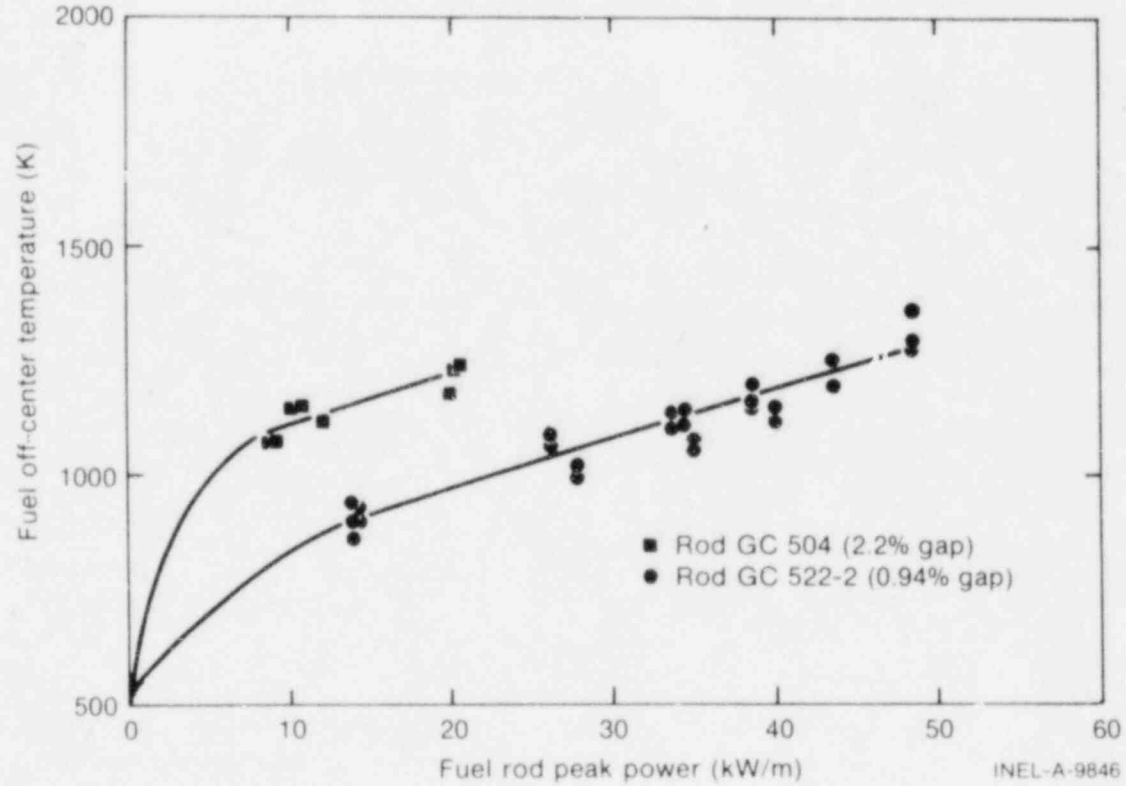

Fig. 7 Composite plot of fuel off-center temperature measurements showing effect of initial gap width in argon filled rods. Plot also shows range of variation in the azimuthally distributed temperature measurements in Rod GC 522-2.

approximately 500 K higher than in the narrow gap (0.94%) rod. This difference in centerline temperatures between the medium and narrow gap argon rods is significantly larger than the approximately 100 K difference observed between the medium and narrow gap rods with helium fill gas. In addition, the absolute magnitude of the centerline temperature (~1750 K) in the 2.2% argon filled rod was approximately 550 K higher than the measured (~1200 K) temperature in the 2.2%, helium filled rod at 20 kW/m. The higher fuel temperatures in the argon rods resulted in different fuel cracking patterns than in the helium rods, and, consequently, different effective fuel thermal conductivities, as discussed in Section V.

The effects of initial gap width on the off-center fuel temperatures are shown in Figure 7 for the argon filled rods with the 0.94 and 2.2% initial gaps. The solid circle symbols shown in Figure 7 indicate the azimuthal variation in the three measured off-center temperatures in Rod GC 522-2 (0.94% gap) from Test GC 2-2. Rod GC 504 (2.2% gap) from Test GC 2-1 contained only one off-center thermocouple. The difference in off-center temperatures between the narrow (0.94%) and medium (2.2%) gap argon filled rods was approximately 300 K at 20 kW/m, indicating that the shape of the radial temperature profile is different in the two argon filled rods to approximately the same extent as observed between the wide gap and narrow gap helium rods.

The PIE photomicrographs shown in Figures 8 and 9 for the narrow and medium gap argon filled rods, respectively, also show that more extensive cracking and significantly wider cracks occur in the medium gap rod than in the narrow gap rod. The increased crack area in Rod GC 504 would be expected to cause a decrease in effective fuel thermal conductivity, with resulting higher fuel temperatures than in the narrow gap rod, Rod GC 522-2.

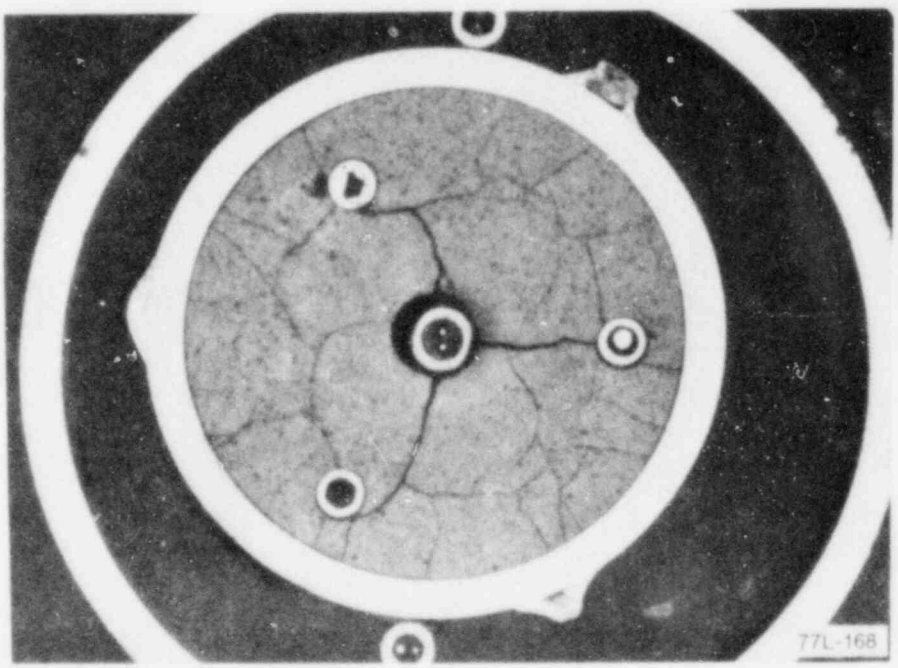

Fig. 8 Photomicrograph showing crack patterns in fuel of Rod GC 522-2 (Ar, 0.94% gap) at 451 mm.

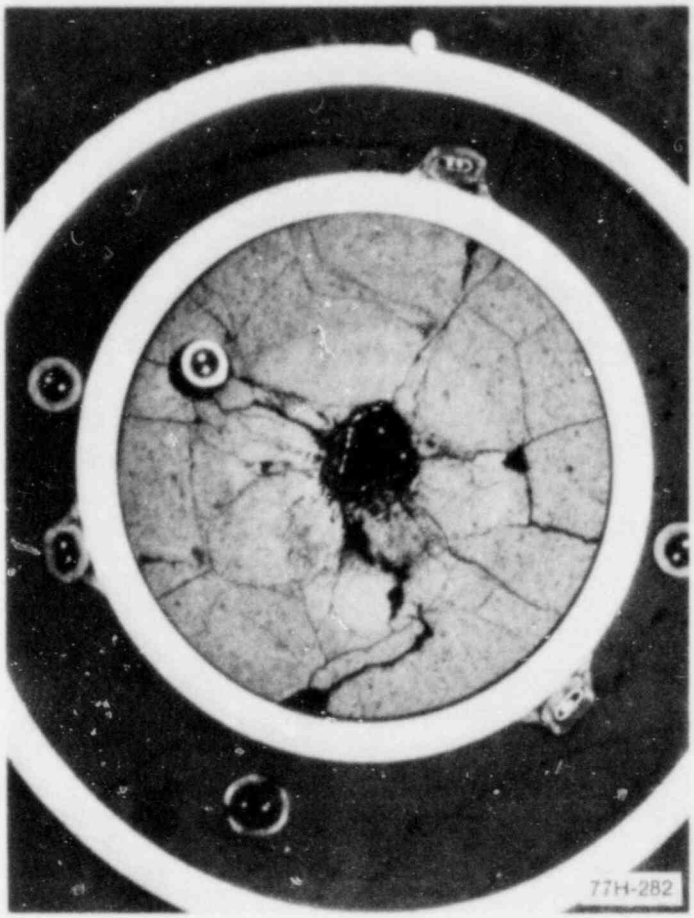

Fig. 9 Photomicrograph showing crack patterns in fuel of Rod GC 504 (Ar, 2.2% gap) at 489.5 mi

Tests GC 2-1, GC 2-2, and GC 2-3 have also provided data on the effect of initial gap width (0.94 and 2.2%) on the thermal response of rods backfilled with xenon fill gas. Comparisons of fuel centerline and off-center temperature measurements as functions of test rod power density for initial gap widths of 0.94 and 2.2% are shown in Figures 10 and 11, respectively. As would be expected because of the low thermal conductivity of the xenon gas as compared with that of helium and argon, the measured fuel temperatures are significantly higher in the xenon rods. Although the fuel densities of the three rods were also different (92, 95, and 97% TD), the effect of density is small compared with the effect of gap width, as discussed in Section IV-3, and is not considered to influence interpretation of the effect of gap width. The effect of initial gap width is also quite pronounced in the xenon filled rods. The fuel centerline temperatures were approximately 500 K higher in the medium (2.2%) gap rod than in the narrow (0.94%) gap rod, at a power density of 35 kW/m. The off-center temperature differences were approximately 250 K at the same power level. The absolute fuel centerline and off-center temperatures in the xenon rods were approximately 2300 and 1900 K, respectively, for the medium gap rods. These temperatures are approaching the reliable limits for both the centerline and off-center thermocouples and the thermocouples showed signs of possible failure at power densities above approximately 35 kW/m.

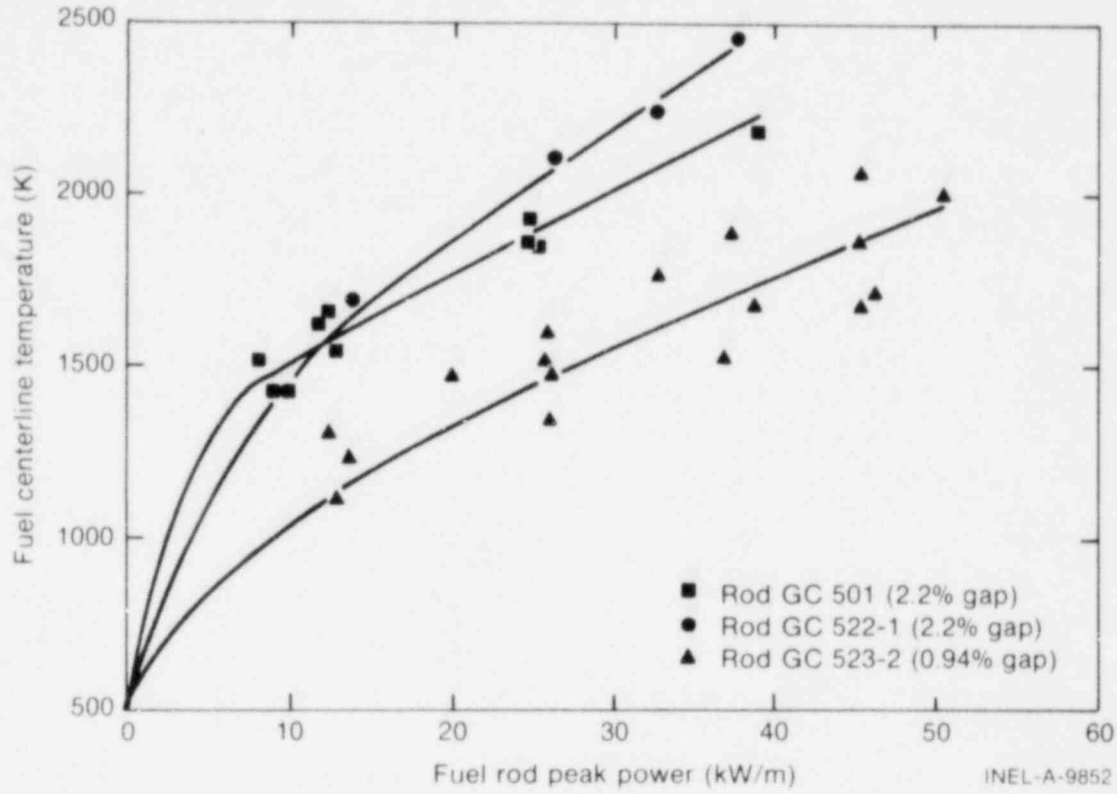

Fig. 10 Composite plot of fuel centerline temperature measurements showing effect of initial gap width in xenon filled rods. The effect of fuel density is also shown between Rods GC 501 (97% TD) and GC 522-1 (92% TD).

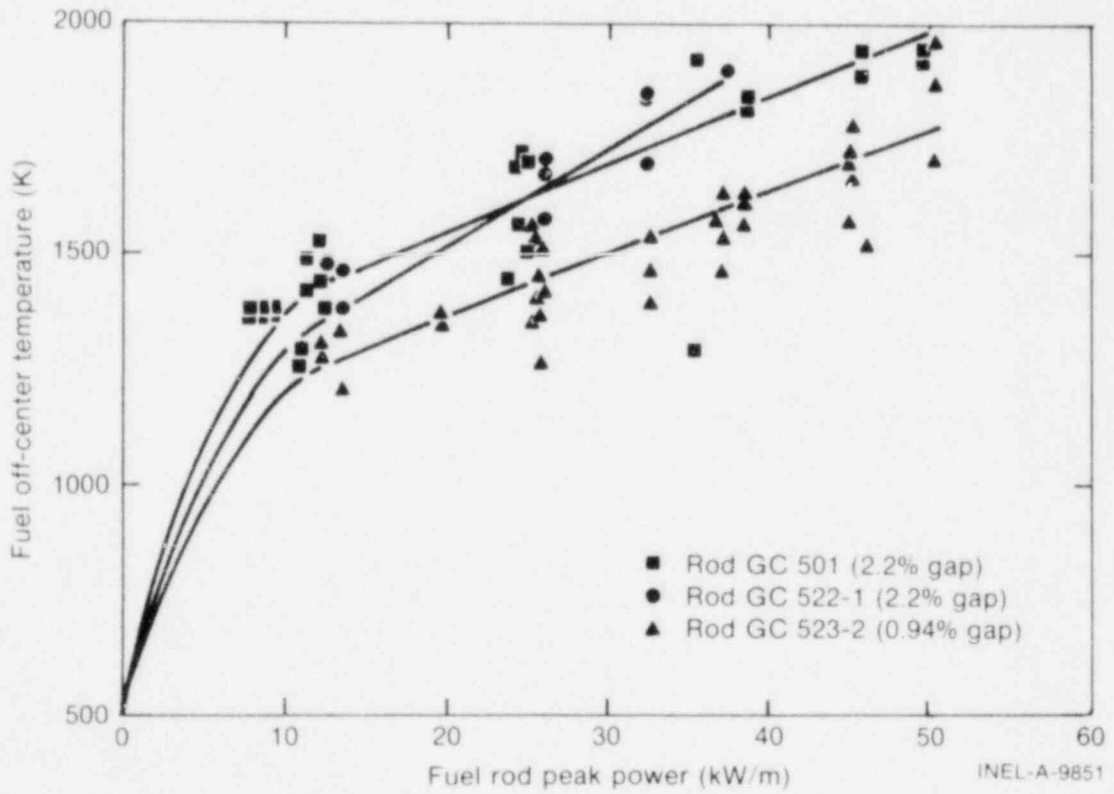

Fig. 11 Composite plot of fuel off-center temperature measurements showing effect of initial gap width in xenon filled rods.

PIE photomicrographs are shown in Figures 12 and 13 for narrow gap (Rod GC 523-2) and medium gap (Rod GC 501) xenon filled rods, respectively. Again, the cracking is more extensive in the medium gap rod than in narrow gap rod, leading to higher fuel temperatures, and both pictures show melting of the centerline and off-center thermocouple sheaths. It is postulated that during the increase in power density the fuel restructured into columnar grains, significantly increasing the fuel thermal conductivity and causing the rate of temperature increase to be significantly reduced. However, as the fuel temperature increased, pellet cracking and pellet fragment relocation degraded the fuel thermal conductivity, although they improved the gap conductance. The high fuel temperatures resulted in an interaction between the fuel thermocouple sheaths (for both centerline and off-center thermocouples) and the UO_2 fuel, causing a low-melting-point eutectic or oxide which destroyed the fuel thermocouples in the medium gap xenon rods. Figure 14 shows crack patterns and crack widths for Rod GC 522-1 (another medium gap, xenon filled rod) similar to those for Rod GC 501 in Figure 13.

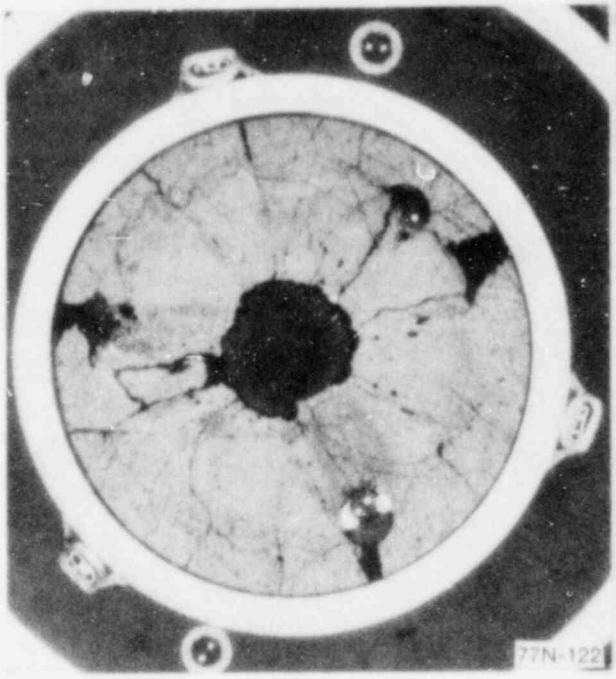

Fig. 12 Photomicrograph showing crack patterns in fuel of Rod GC 523-2 (Xe, 0.94% gap) at 469 mm.

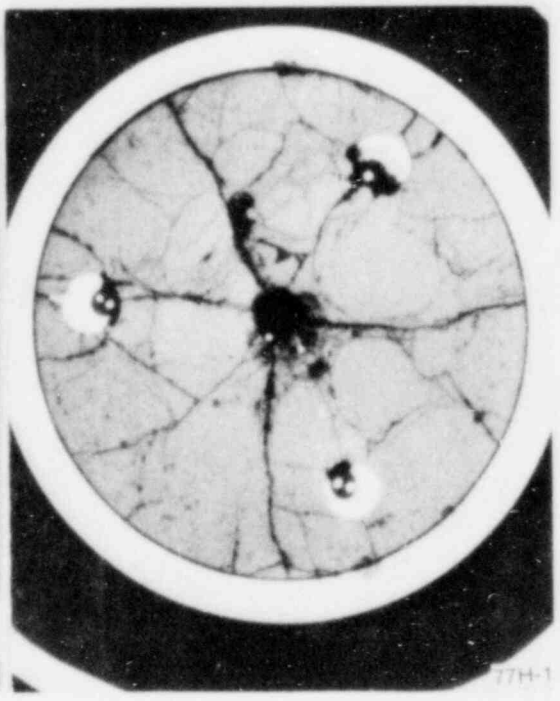

Fig. 13 Photomicrograph showing crack patterns in fuel of Rod GC 523-2 (Xe, 2.2% gap) at 477.8 mm.

The dispersion among the off-center fuel temperature measurements in the xenon rods was significantly greater than was observed in the argon or helium filled rods, as shown in Figure 11. Also, the differences among the three off-center temperature readings (at a given power) are significantly greater in the medium gap rod, Rod GC 501 (~300 K), than in the narrow gap rod, Rod GC 523-2 (~150 K). Since xenon gas has a very low thermal conductivity, stochastic variations in pellet cracking and pellet fragment movement should induce more dispersion among the off-center fuel temperature measurements in the xenon rods. Also, more pellet fragment movement would be expected in a moderate gap rod than

in a small gap rod and, consequently, more dispersion would be expected among the off-center temperature measurements in a moderate gap rod than in a small gap rod.

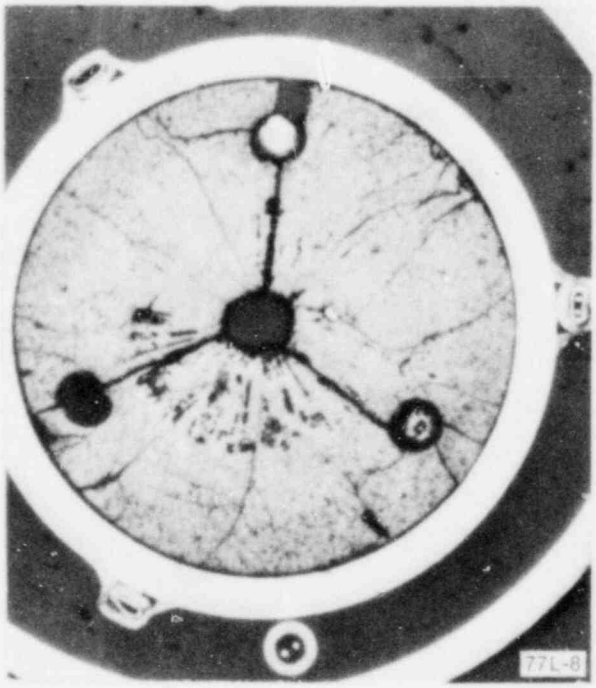

Fig. 14 Photomicrograph showing crack patterns in fuel of Rod GC 522-1 (Xe, 2.2% gap) at 454 mm.

In summary, the effect of variations in initial gap width in all the test rods was to increase the fuel temperatures as the gap width increases. In the helium filled rods, the increase in temperature at a power density of 35 kW/m was relatively low (∿100 K for centerline temperatures and ∿50 K for off-center temperatures) when the gap was increased from 0.94 to 2.2%, but a large increase in temperatures (∿500 K centerline, ∿250 K off-center) was observed when the gap was increased from 2.2 to 3.4%. In the argon and xenon rods the increase in temperatures was much higher (∿500 K for centerline and ∿250 K for the off-center measurements) when the gap was increased from 0.94 to 2.2%. Wide gap (3.4%) rods have not been tested with argon or xenon fill gases.

The fuel centerline temperatures increased much more than did the off-center temperatures when the initial gap was increased in either the helium, argon, or xenon filled rods. This greater increase indicates that part of the thermal resistance normally associated with the pellet-to-cladding gap actually resides in the fuel after pellet cracking occurs in moderate and large gap rods. Apparently, pellet cracks and the movement of pellet fragments degrade the nominal fuel thermal conductivity while improving the gap conductance in these rods. This conclusion is also supported by the fact that the magnitude of the off-center fuel temperature measurement dispersions can be related to the initial gap size and fill gas composition.

2. EFFECT OF FILL GAS COMPOSITION

Representative effects of fill gas composition on the measured fuel temperatures are shown in Figures 15 and 16 for centerline and off-center temperatures, respectively, in the 2.2% initial gap rods. As would be expected, the xenon filled rods showed the highest temperatures. However, an approximately 200 K difference existed between the centerline temperatures of the xenon and argon rods at the power level of 20 kW/m, but about 400 K difference existed between the off-center temperatures in these same rods at the same power levels. This result indicates that the gap thermal resistance and the fuel thermal conductivity are reduced in both rods, due primarily to relocation of fuel fragments, but the reduction in fuel thermal conductivity in the high temperature xenon filled rod is offset somewhat by some other effect, probably fuel restructuring (columnar grain growth or crack healing). Photomicrographs for the three rods represented in Figures 15 and 16 are shown in Figures 17, 18, and 19 for the helium, argon, and xenon filled rods, respectively. Figures 18 and 19 (argon and xenon, respectively) show that both the argon and xenon filled rods had a central region with restructured fuel consisting of radially elongated (columnar) grains. The figures also show that the centerline thermocouples in both rods had melted, dispersing sheath material in the fuel. In the xenon filled rod, the off-center thermocouple sheaths had also melted and metallic inclusions were found in the fuel between the centerline and off-center thermocouple holes. The comparable fuel centerline temperatures for the argon and xenon filled rods shown in Figure 15 could also be due to thermocouple shunting and the resulting junctions being at different axial positions in the two rods.

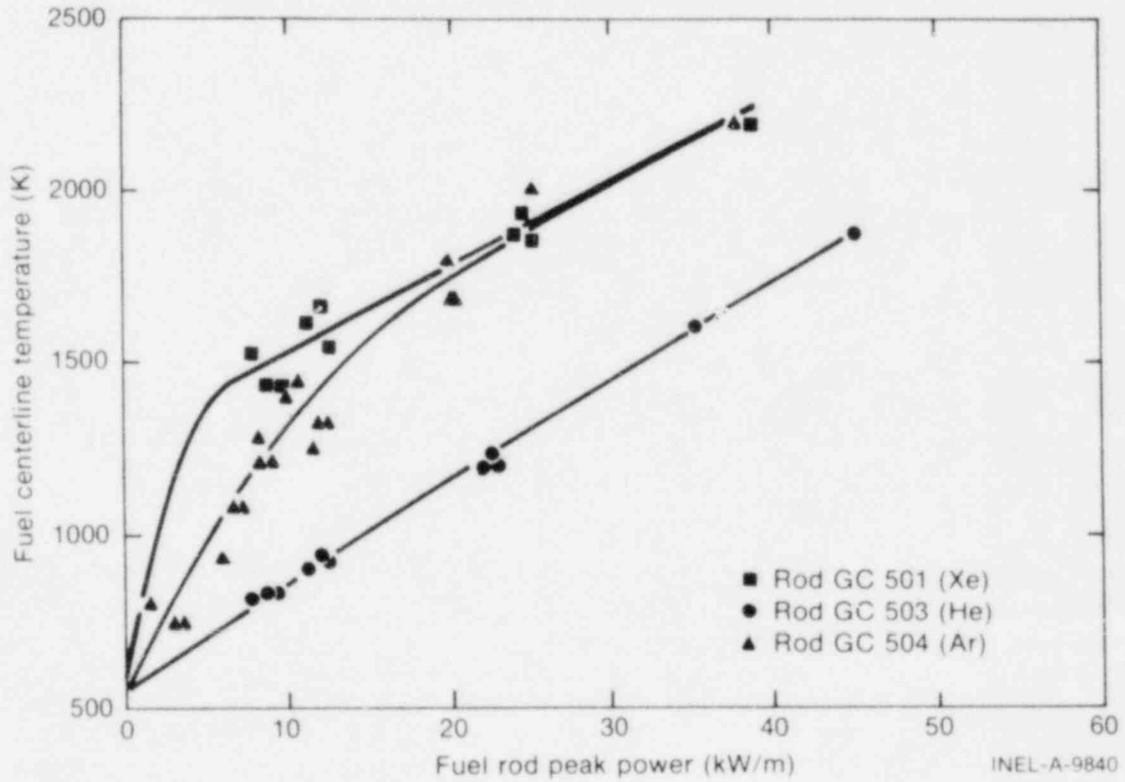

Fig. 15 Composite plot of fuel centerline temperature measurements showing effect of fill gas composition in 2.2% initial gap rods.

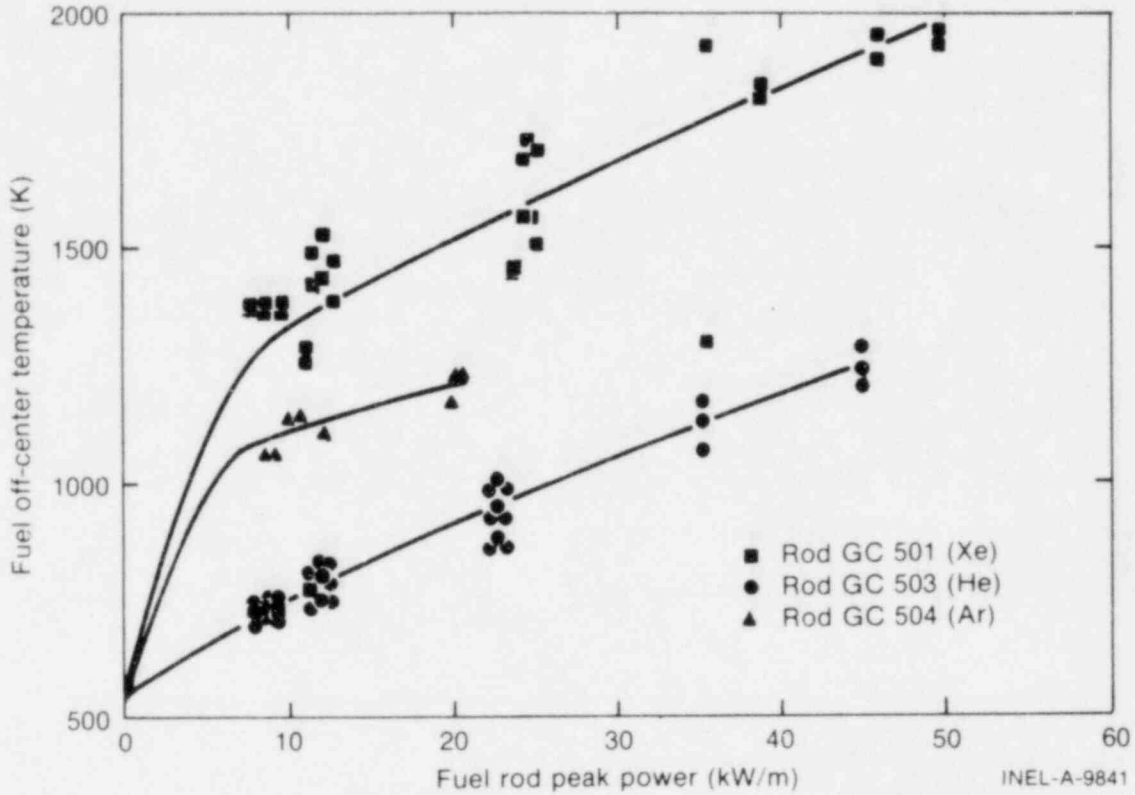

Fig. 16 Composite plot of fuel off-center temperature measurements showing effect of fill gas composition in 2.2% initial gap rods.

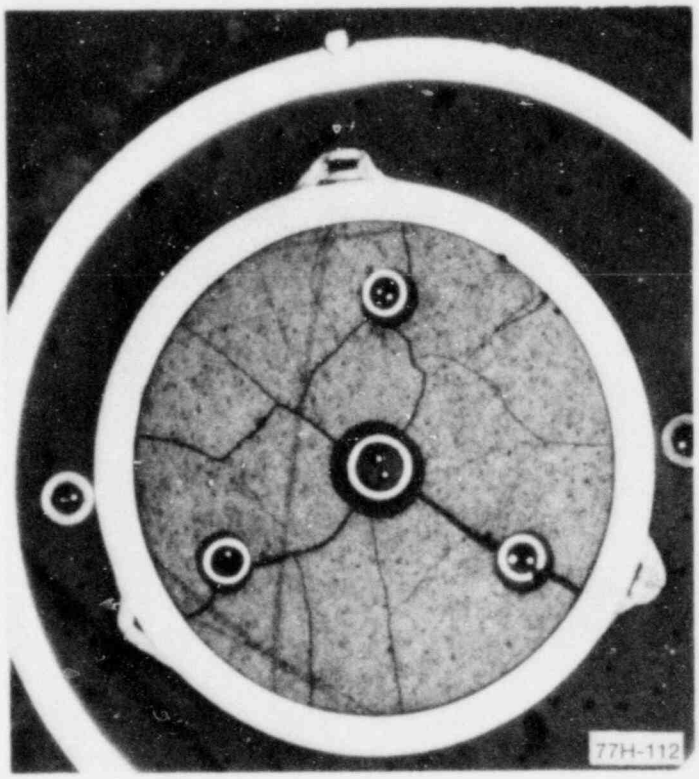

Fig. 17 Photomicrograph showing crack patterns in fuel of Rod GC 503 (He, 2.2% gap) at 486.7 mm.

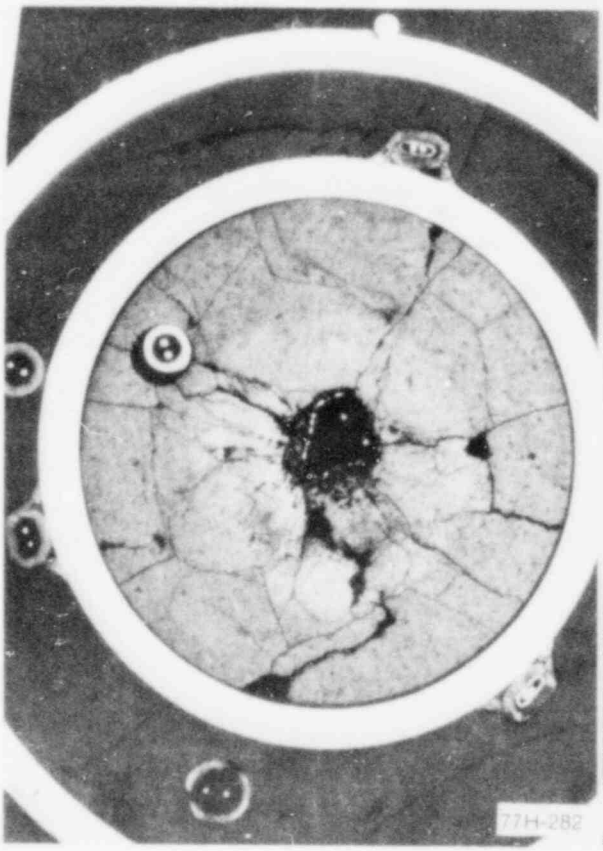

Fig. 18 Photomicrograph showing crack patterns in fuel of Rod GC 504 (Ar, 2.2% gap) at 489.5 mm.

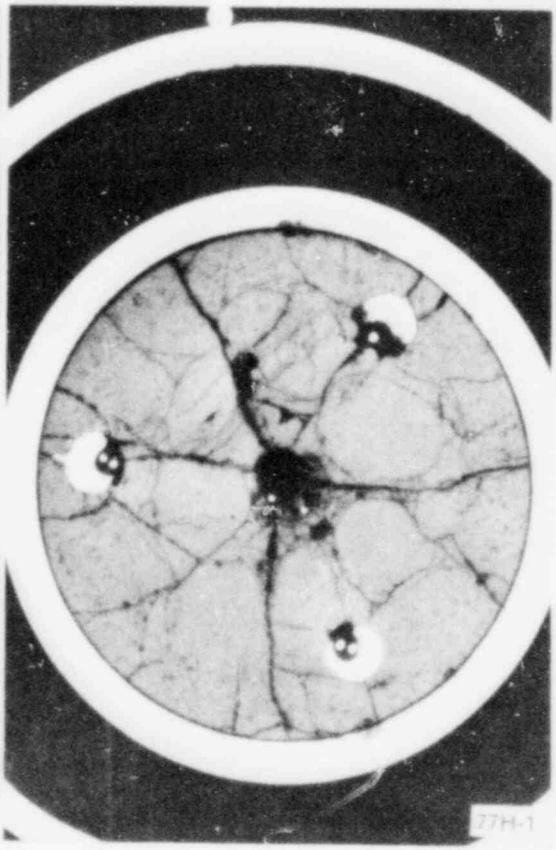

Fig. 19 Photomicrograph showing crack patterns in fuel of Rod GC 501 (Xe, 2.2% gap) at 477.8 mm.

Figure 16 also illustrates the effects of fill gas conductivity on the dispersion of the off-center temperature measurements. As discussed above, the measurements from the xenon filled rod are much more scattered than the measurements from the argon or helium rods.

The effect of fill gas composition on the measured fuel temperatures in the rods with a 0.94% initial pellet-to-cladding gap is shown in Figures 20 and 21. These data again show the expected highest temperatures in the xenon rods, lowest temperatures in the helium rods, and intermediate temperatures in the argon rods for both centerline and off-center temperatures. However, at high powers the centerline temperature measurements in the xenon filled rod are only slightly above the values measured in the argon and helium filled rods, whereas the off-center temperatures in the xenon rod are approximately 500 K higher than in the argon and helium rods. Again, this apparent improvement in the xenon filled rod fuel thermal conductivity, as compared with that for the argon filled rod, may be due to extensive restructuring (or possibly instrument disintegration and error).

Figures 20 and 21 also indicate that the argon and helium filled rods' centerline and off-center temperatures tend to converge at high powers. This tendency is probably due to gap closure and pellet-to-cladding contact pressure buildup in these initially small gap rods.

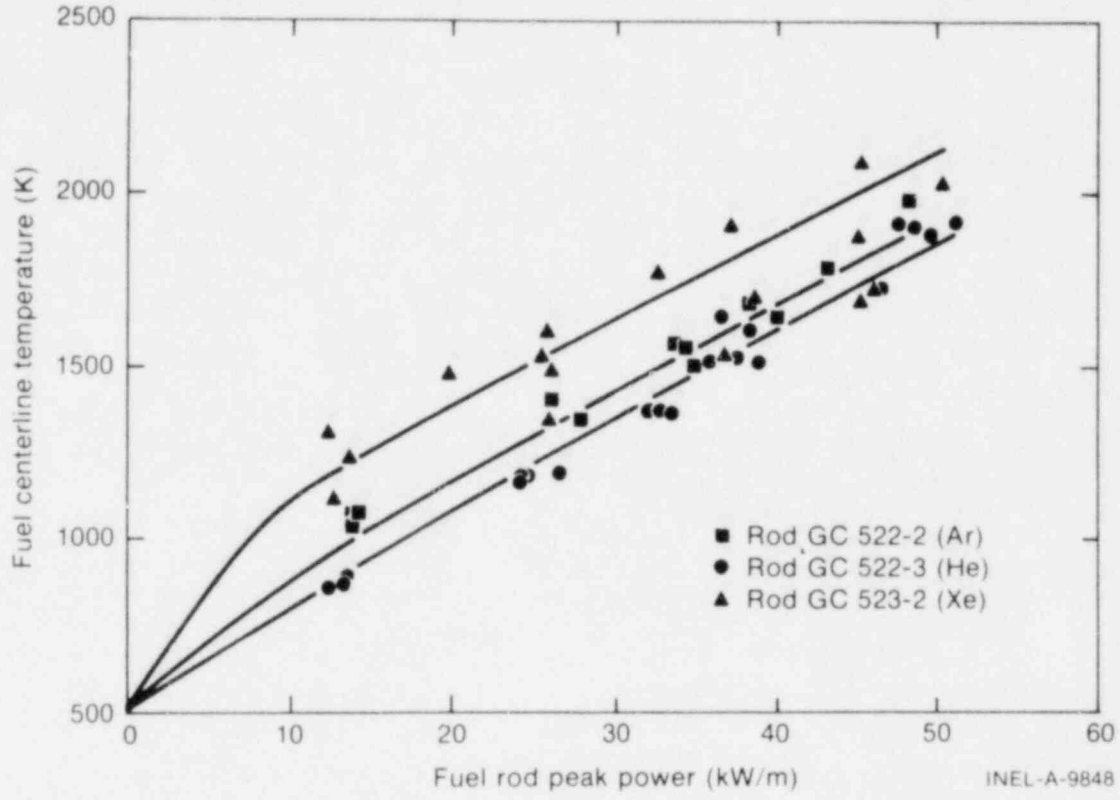

Fig. 20 Composite plot showing effect of fill gas composition on measured fuel centerline temperatures in rods with 0.94% initial gap width.

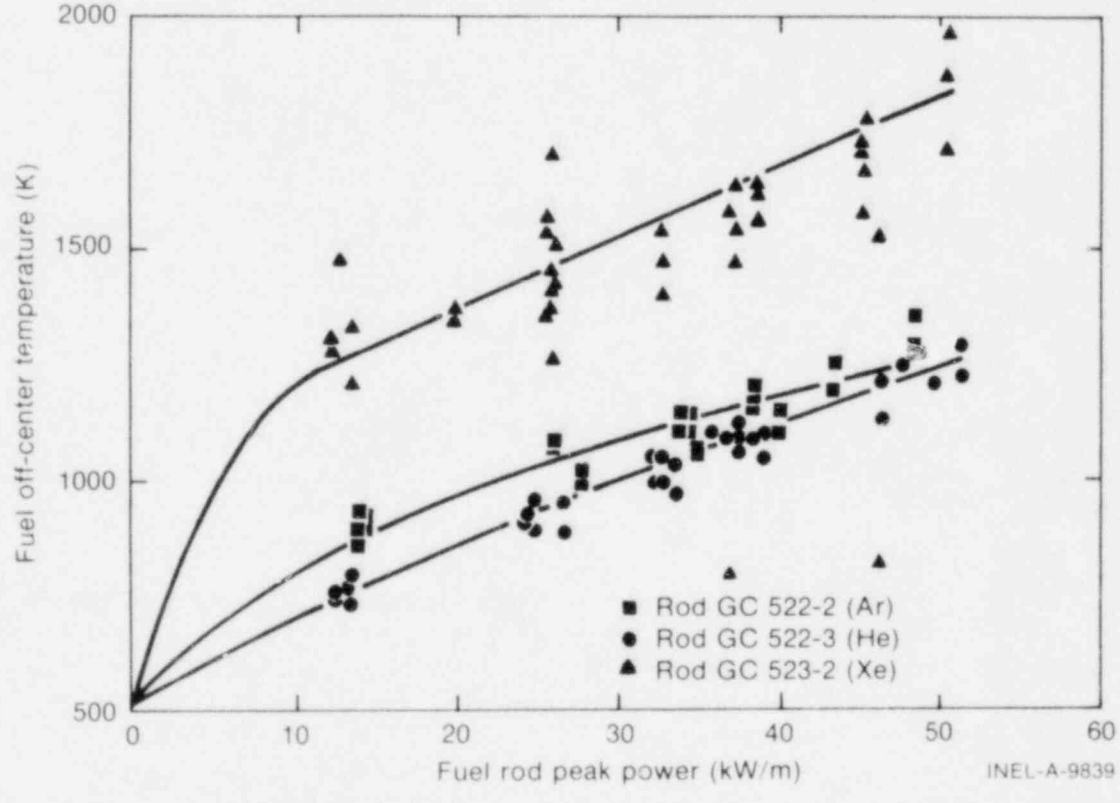

Fig. 21 Composite plot showing effect of fill gas composition on measured fuel off-center temperatures in rods with 0.94% initial gap width.

This same tendency for the argon and helium filled rods' temperatures to converge at high powers is evident in Figures 15 and 16 for the moderate (2.2%) gap rods; however, the point of convergence appears to be at much higher powers in the moderate gap rods than in small gap rods.

The PIE photomicrographs of the 0.94% initial gap rods are shown in Figures 22, 23, and 24. Figure 24 shows restructured fuel with metallic inclusions in the fuel for the narrow gap, xenon filled rod, but Figures 22 and 23 show normal fuel structures in the helium and argon filled rods.

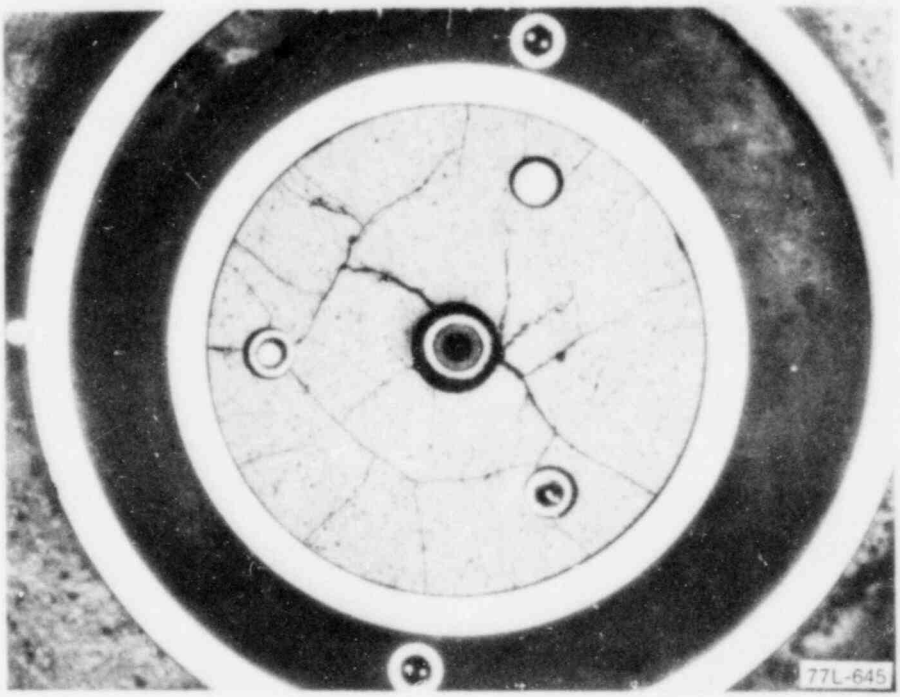

Fig. 22 Photomicrograph showing crack patterns in fuel of Rod GC 522-3 (He, 0.94% gap) at 451.4 mm.

The formation of a melted material region in the xenon rods is suspected to have significantly altered the thermal characteristics of these rods. However, the oxide or eutectic reactions, or both, probably occurred after failure of the respective instruments. Other fuel structural changes such as columnar grain growth or pellet crack healing probably occurred well before instrument failure and resulted in the lower fuel centerline temperatures in the xenon filled rods (as compared with the argon filled rods). The high off-center temperature measurements in the xenon filled rods are probably simply due to the very low thermal conductivity of the xenon fill gas.

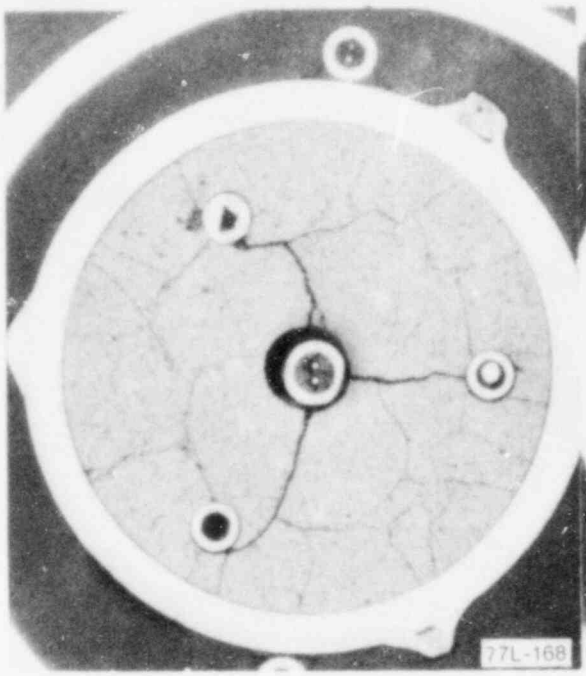

Fig. 23 Photomicrograph showing crack patterns in fuel of Rod GC 522-2 (Ar, 0.94% gap) at 451 mm.

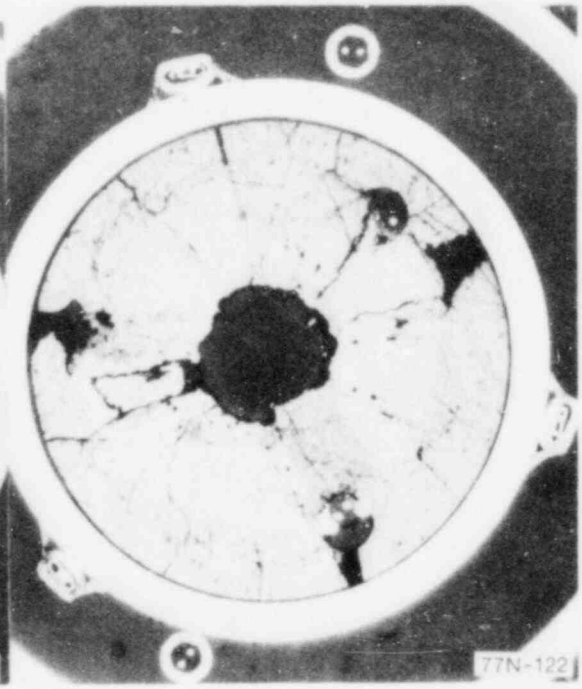

Fig. 24 Photomicrograph showing crack patterns in fuel of Rod GC 523-2 (Xe, 0.94% gap) at 469 mm.

3. EFFECT OF FUEL DENSITY

The effect of fuel density on measured fuel temperatures is relatively small compared with the effects of initial gap width and gas composition. Figures 25 and 26 show the effect on centerline and off-center temperatures, respectively, for helium filled rods with an initial gap of 0.94%. Generally, the measured fuel centerline temperatures decrease as the density increases. These results are consistent with generally expected behavior and Maxwell-Euiken theory. The off-center temperature measurements from the high density helium filled rod, Rod GC 502 (97% TD fuel), also show a slight tendency to be lower than the fuel off-center measurements from the lower fuel density helium filled rods (Figure 26). This slight effect may simply be due to data scatter.

From PIE photomicrographs of these same three rods (Rods GC 502, GC 522-3, and GC 523-1) (Figures 27, 28, and 29) it is not obvious that the density effects are discernible.

Figures 30 and 31 present the measured fuel centerline and off-center temperatures as a function of power at the thermocouple locations for the argon filled test rods with an initial gap of 2.2%. The off-center temperatures are similar; however, the fuel centerline temperatures of the higher density rod (Rod GC 504, 95% TD fuel) appear to be somewhat higher than the fuel centerline temperatures of the low density rod (Rod GC 523-4, 92% TD fuel). Postirradiation examinations of both of these rods showed that the centerline and off-center thermocouples had failed at some time during the tests. In particular, the PIE

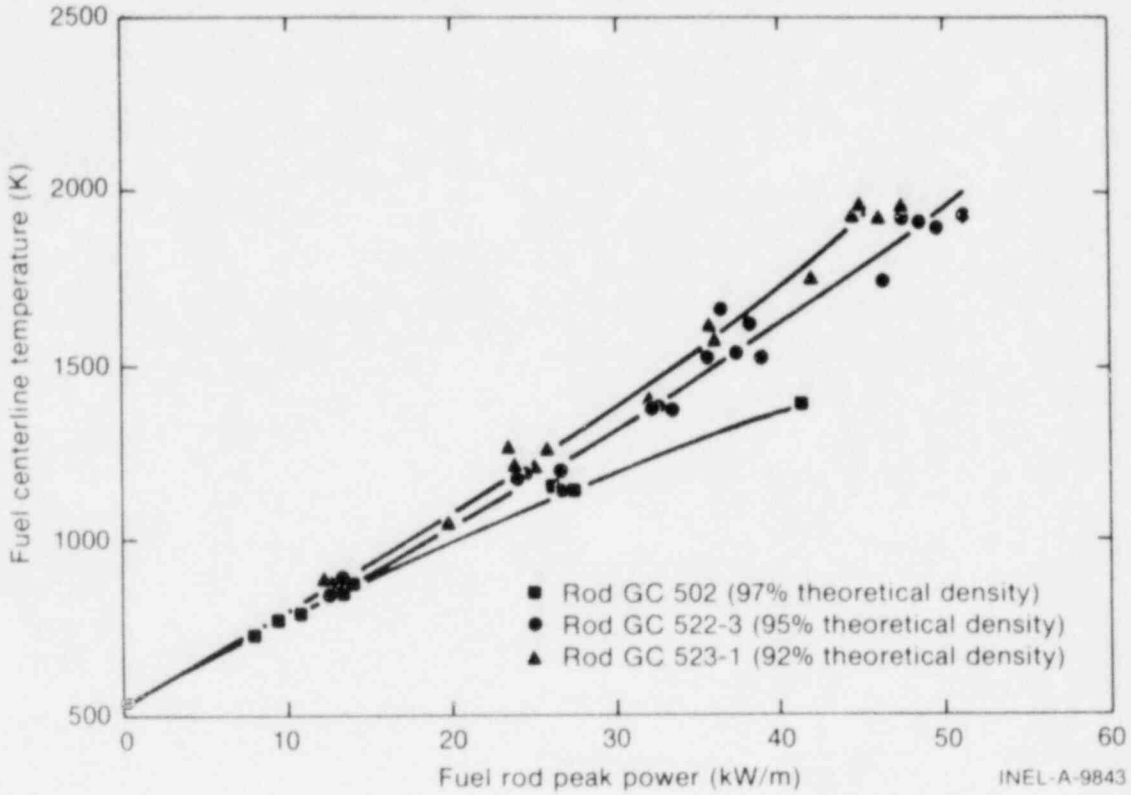

Fig. 25 Composite plot showing effect of fuel density on measured fuel centerline temperatures in helium filled rods with 0.94% initial gap widths.

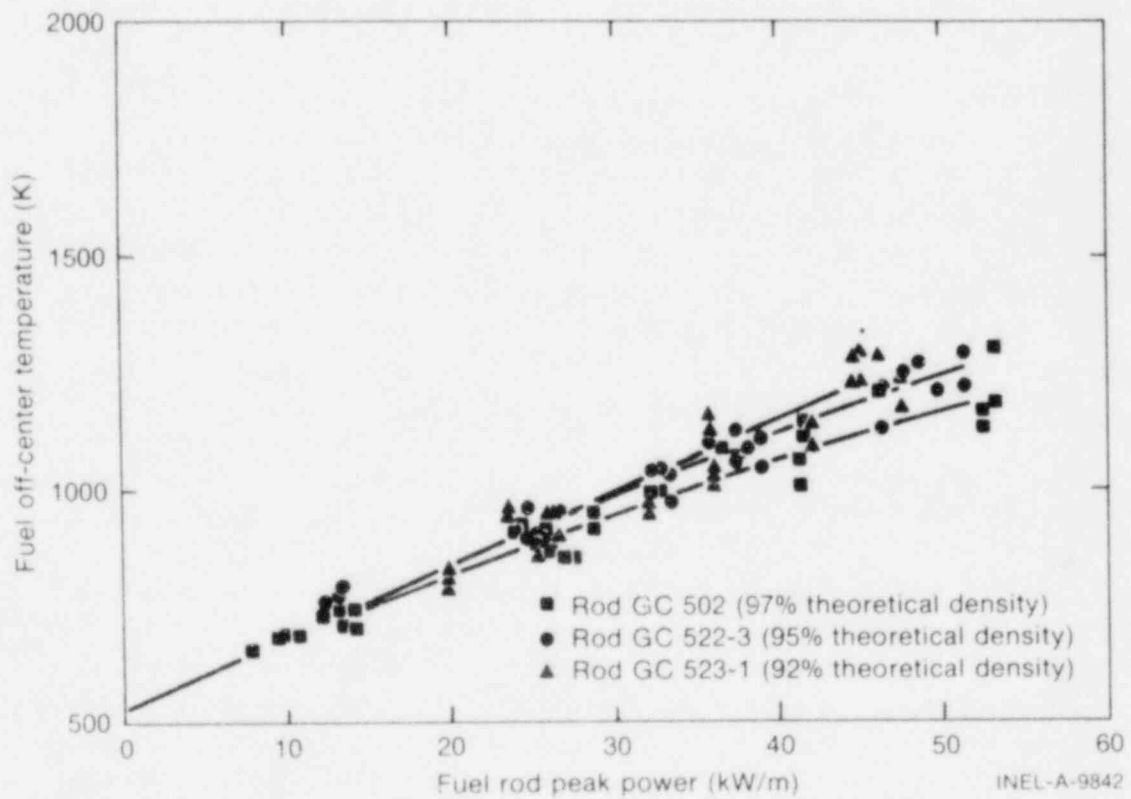

Fig. 26 Composite plot showing effect of fuel density on measured fuel off-center temperatures in helium filled rods with 0.94% initial gap widths.

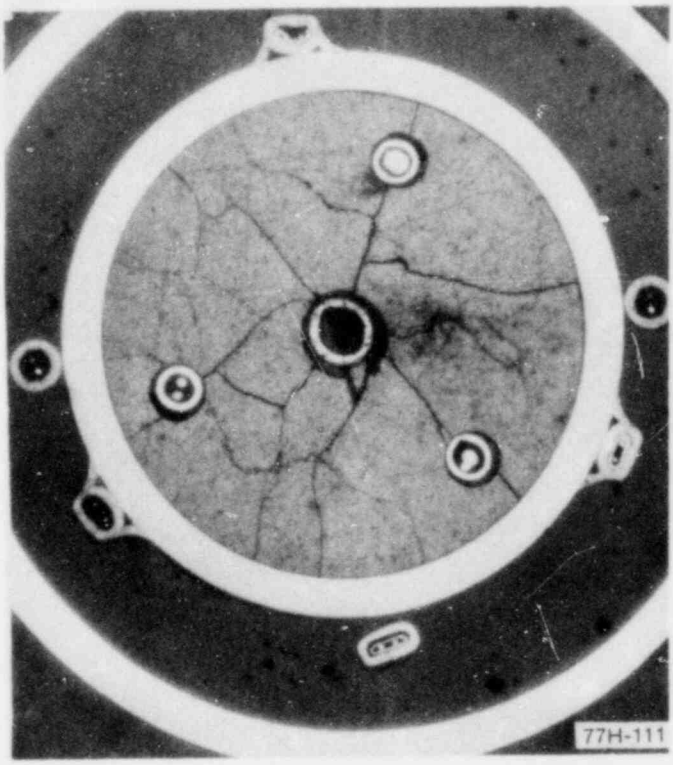

Fig. 27 Photomicrograph showing crack patterns in fuel of Rod GC 502 (He, 0.94% gap, 97% TD) at 486.9 mm.

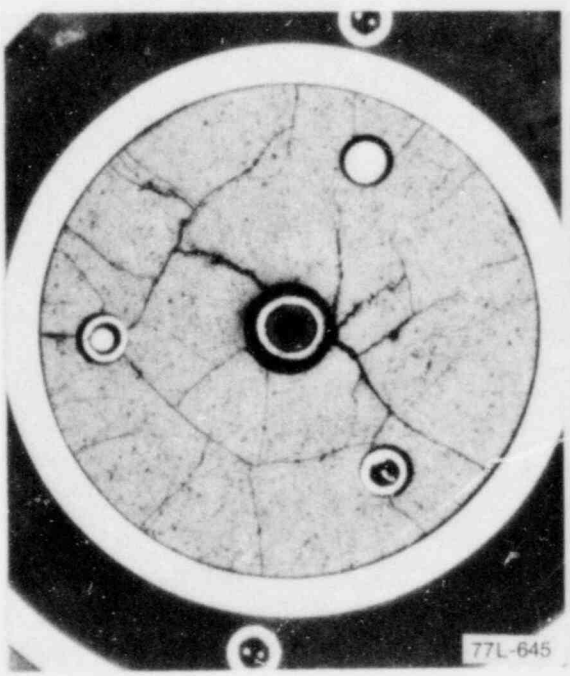

Fig. 28 Photomicrograph showing crack patterns in fuel of Rod GC 502 (He, 0.94% gap, 95% TD) at 451.4 mm.

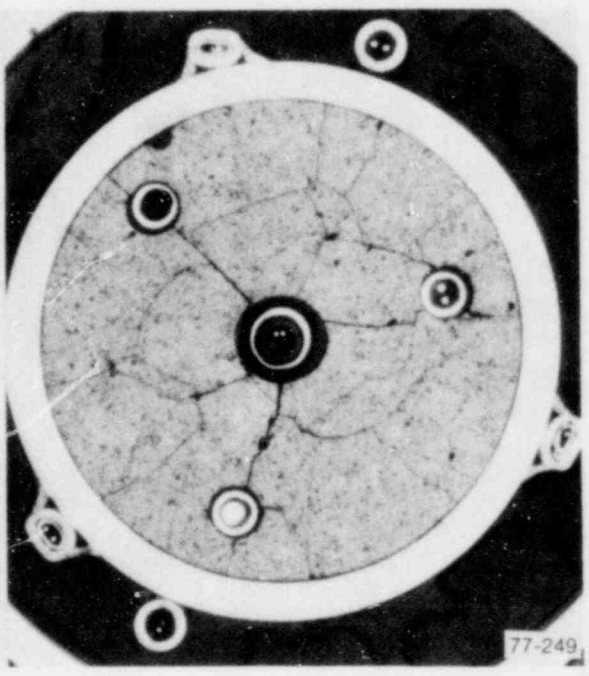

Fig. 29 Photomicrograph showing crack patterns in fuel of Rod GC 523-1 (He, 0.94% gap, 92% TD) at 476 mm.

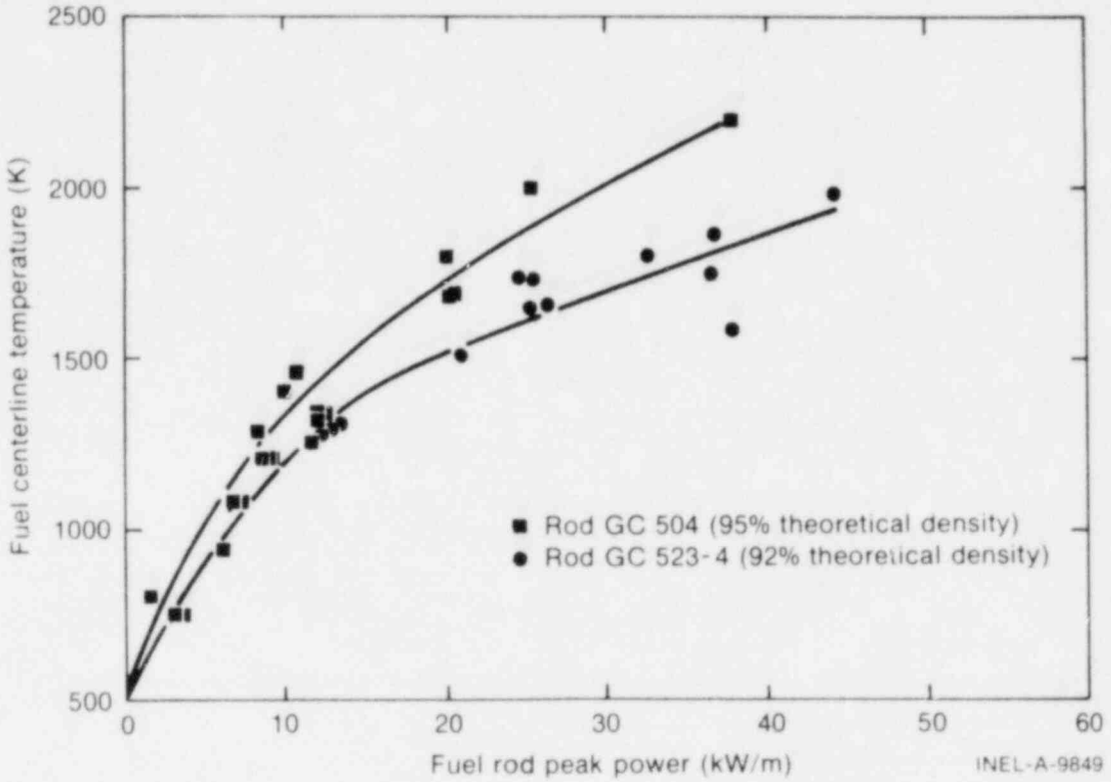

Fig. 30 Composite plot showing effect of fuel density on measured fuel centerline temperatures in argon filled rods with 2.2% initial gap widths.

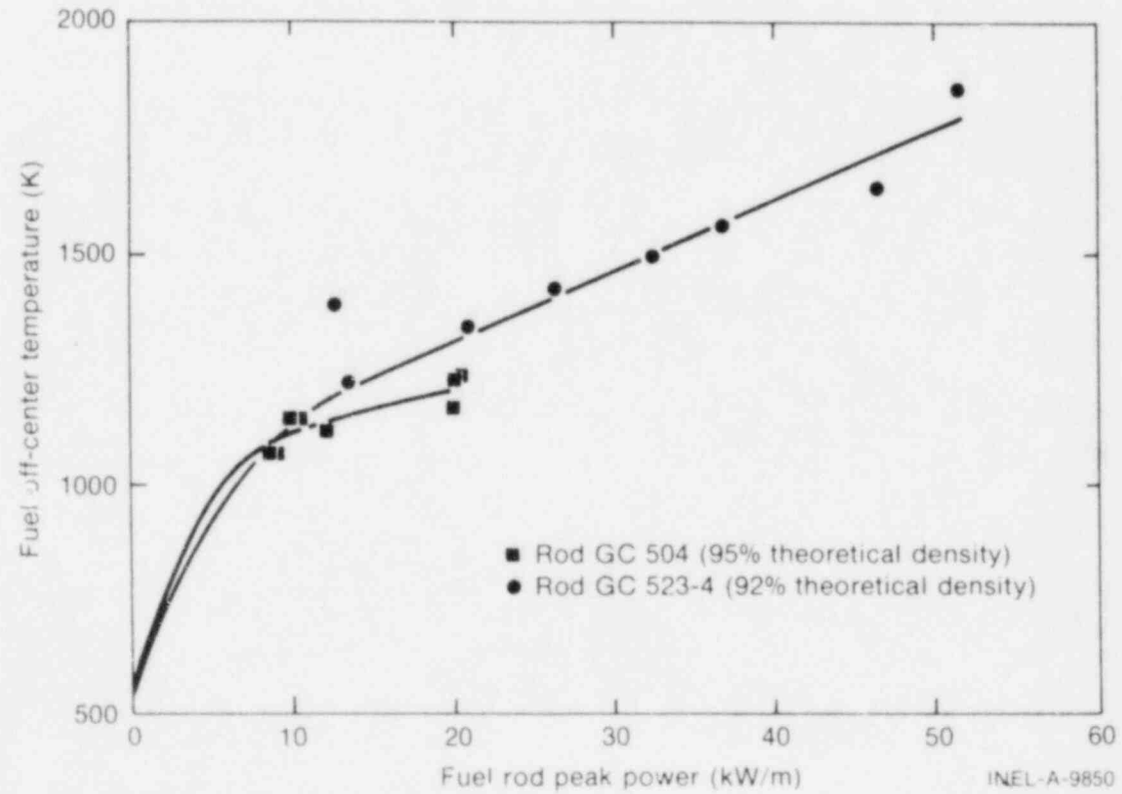

Fig. 31 Composite plot showing effect of fuel density on measured fuel off-center temperatures in argon filled rods with 2.2% initial gap widths.

photomicrographs (Figures 32 and 33) show that the off-center thermocouple in Rod GC 523-4 had broken off at some position above the junction, and that the centerline thermocouple had disintegrated above the junction. The PIE photomicrographs show that the off-center thermocouple in Rod GC 504 was apparently in good condition at the location of the junction, but the centerline thermocouple was disintegrated at the same axial location. The relative physical conditions of the centerline thermocouples during the tests probably biased the results.

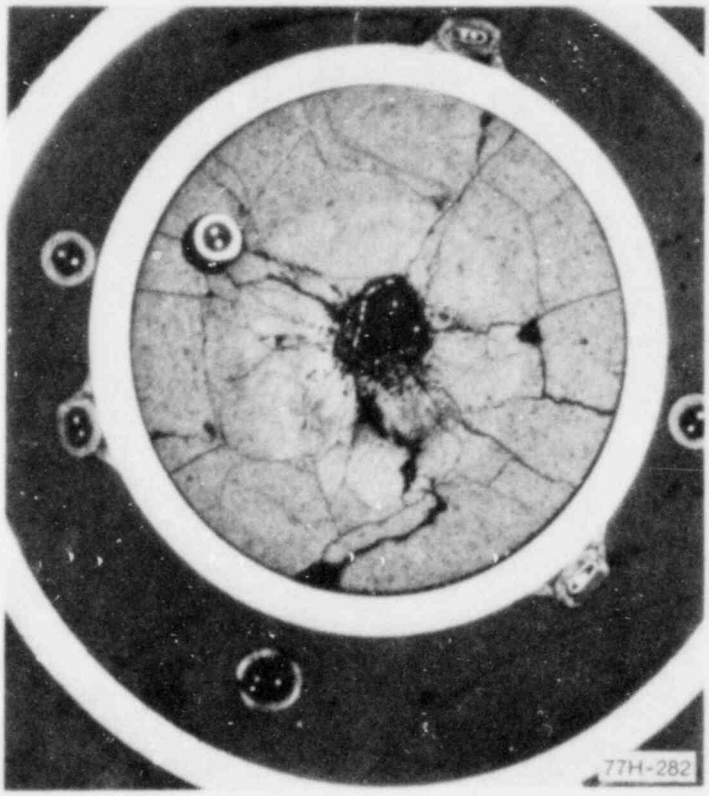

Fig. 32 Photomicrograph showing crack patterns in fuel of Rod GC 504 (Ar, 2.2% gap, 95% TD) at 489.5 mm.

Figures 34 and 35 show the effect of fuel density on the measured fuel centerline and off-center temperatures, respectively, of xenon filled rods with a 2.2% initial gap width. The same trend as for the helium filled rods is shown, with the lower density rods indicating the highest fuel centerline temperatures and relatively similar off-center temperatures. However, the PIE photomicrographs from both of these rods (Rod GC 501, Figure 36, and Rod GC 522-1, Figure 37) also show disintegrated fuel centerline thermocouples, and possible damaged or disintegrated off-center thermocouples at the intended junction elevations. Although the data shown in Figures 34 and 35 may have been obtained before the thermocouples disintegrated, it is obvious the results must be used with caution.

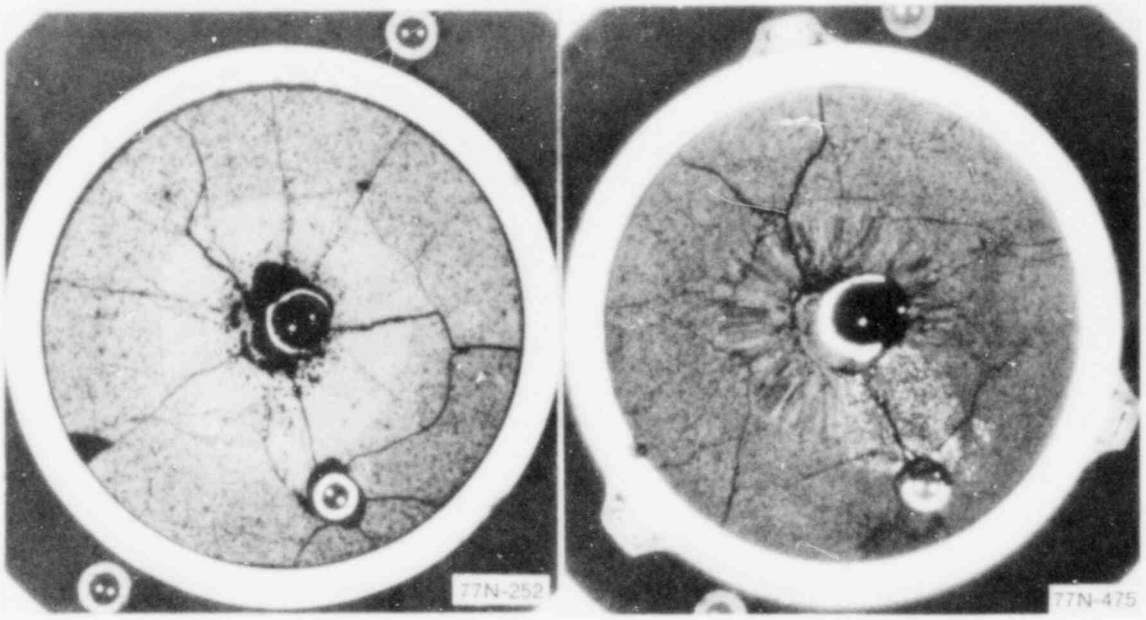

Fig. 33 Photomicrograph showing crack patterns in fuel of Rod GC 523-4 (Ar, 2.2% gap, 92% TD) at 458 and 468 mm.

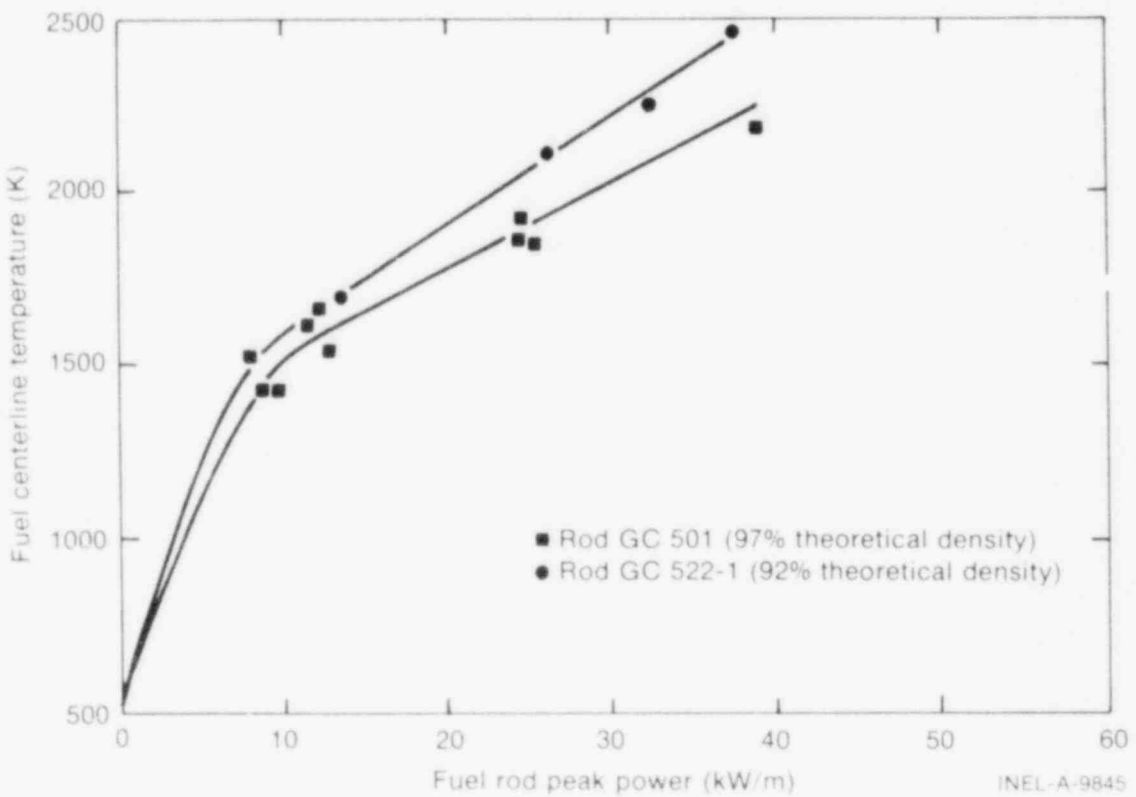

Fig. 34 Composite plot showing effect of fuel density on measured fuel centerline temperatures in xenon filled rods with 2.2% initial gap widths.

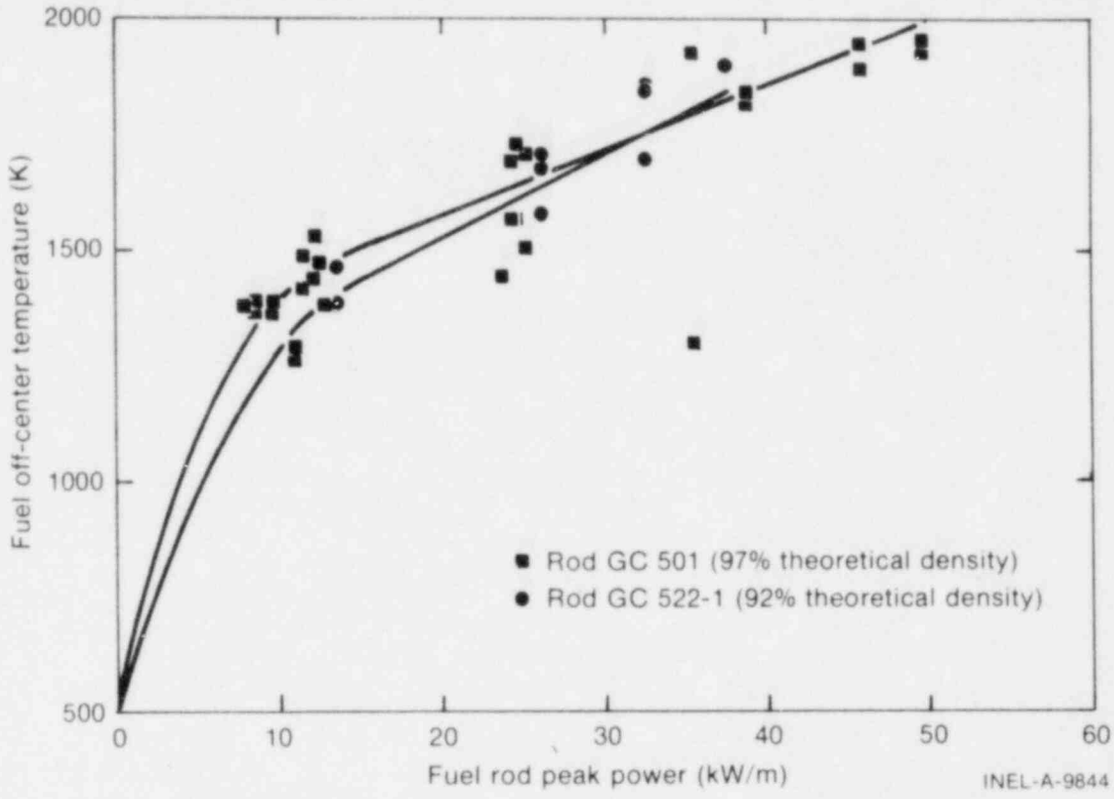

Fig. 35 Composite plot showing effect of fuel density on measured fuel off-center temperatures in xenon filled rods with 2.2% initial gap widths.

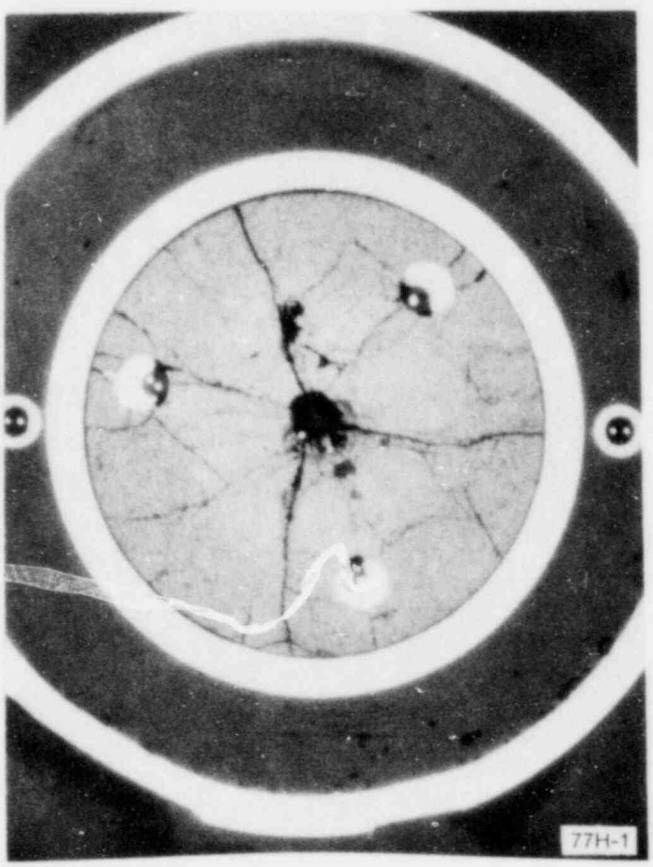

Fig. 36 Photomicrograph showing crack patterns in fuel of Rod GC 501 (Xe, 2.2% gap, 97% TD) at 477.8 mm.

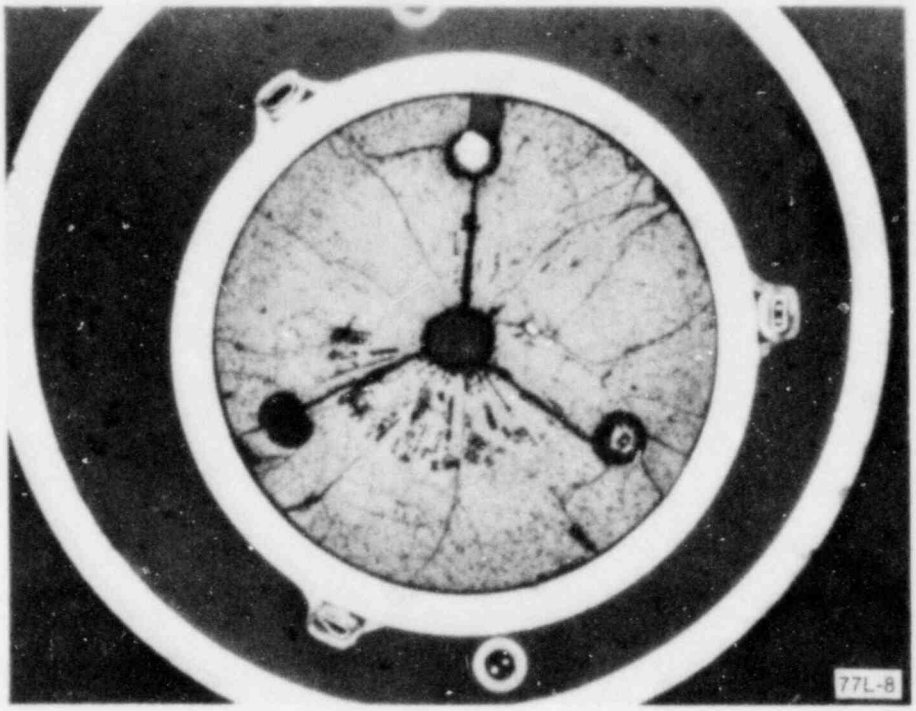

Fig. 37 Photomicrograph showing crack patterns in fuel of Rod GC 522-1 (Xe, 2.2% gap, 92% TD) at 454 mm.

4. CONCLUSIONS

The observed thermal response of the test fuel rods in Tests GC 2-1, GC 2-2, and GC 2-3 was as expected. Generally, higher fuel temperatures are associated with wide gap rods than narrow gap rods. However, temperatures of the medium gap rods are significantly closer to the temperatures of the narrow gap rods than to the temperatures of the wide gap rods, indicating a strong nonlinear effect of gap width on temperature. The fuel centerline temperatures increased much more than did the off-center temperatures when the initial gap was increased in either the helium, argon, or xenon filled rods. This greater increase indicates that pellet cracking and pellet fragment relocation degrade the nominal fuel thermal conductivity, and the greater increase is also supported by the fact that the magnitude of the off-center fuel temperature measurement dispersions can be related to the initial gap size and fill gas composition.

Significantly higher fuel temperatures were observed in the xenon and argon filled test rods than in the helium filled rods. This would be expected because of the large differences in the thermal conductivities of the gases. The initial rate of the fuel centerline temperature increases in the xenon and argon filled rods indicated that extremely high temperatures would occur; however, the rate of increase slowed down above power levels of approximately 5 to 10 kW/m, indicating that fuel restructuring into columnar grains

significantly increased the fuel thermal conductivity. Further temperature increases resulted in pellet cracking and pellet fragment relocation which decreased the fuel thermal conductivity but increased the gap conductance. A somewhat unexpected result, however, was that the high temperatures in the medium gap xenon and argon rods resulted in an interaction between the fuel and the thermocouple sheath materials that altered the structure of the fuel.

The effect of fuel density on the off-center thermocouple response was indistinguishable from normal scatter in the data. There was a slight tendency for lower fuel centerline temperatures in the high density, helium filled rods.

Postirradiation examination (of photomicrographs) showed significantly different fuel cracking patterns in the narrow gap rods as compared with the medium and wide gap rods (small, relatively few cracks in the narrow gap rods and large, numerous cracks in the medium and wide gap rods). Some of the wider gap rods showed eccentric pellet positioning, which may have resulted from thermal expansion and pellet cracking effects, or may have occurred during the initial pellet loading or handling of the rods prior to or following testing.

The generally higher temperatures in the wide gap rods and the unexpectedly high temperatures in the xenon and argon filled rods can, in part, be explained in terms of a decrease in the effective thermal conductivity of the fuel due to redistribution of the initial gap inward toward the center of the pellets when the pellets crack and fragments relocate. In some cases, azimuthal variations in the off-center temperature measurements can also be explained in terms of pellet fragment relocation effects.

The analyses for effective fuel thermal conductivities and steady state gap conductances described in the next section provide considerable insight into the effects of pellet cracking and fragment relocation on the thermal response of the fuel rods.

V. ANALYSIS OF EXPERIMENT STEADY STATE RESULTS

As a fuel rod is operated at power, thermal stresses cause the fuel pellets to crack and pieces of the fuel to relocate in such a manner that some of the initial gap area is redistributed toward the center of the pellet. Consequently, pellet cracking and relocation alter both the fuel thermal conductivity and the pellet-to-cladding gap. A change in either the fuel thermal conductivity or gap conductance will alter the radial temperature distribution and, consequently, will affect the amount of stored energy in the fuel rod at any given time. Therefore, evaluation of fuel rod stored energy and subsequent thermal response requires an evaluation of both the "effective" fuel thermal conductivity and the pellet-to-cladding gap conductance. An objective of the PBF gap conductance tests is to obtain experimental data for developing a model that accurately predicts both effective fuel thermal conductivities and gap conductances and relates these to measurable or calculable fuel rod variables. This section briefly describes the analyses performed and the results obtained for effective fuel thermal conductivities, which reflect fuel cracking and relocation effects, and for the effects of fuel rod design on pellet-to-cladding gap conductance values by the steady state ($\int$kdT) experimental method. Correlations are also developed that permit estimates of effective fuel thermal conductivity and gap conductance values for any LWR design fuel rod.

1. EVALUATION OF EFFECTIVE FUEL THERMAL CONDUCTIVITY[a]

In evaluating effective fuel thermal conductivities, radial temperature profiles were calculated for the test fuel rods at specific power levels, then the UO_2 thermal conductivity relationship used in the calculations was adjusted and the profiles were recalculated until the calculated radial profiles coincided with the measured fuel centerline and off-center (corrected for perturbation effects as described in Appendix C) temperature measurements. These calculations were performed using a simple $\int$kdT computer code called FUELCON[b] that was developed for this purpose. The FUELCON code is described in detail in Appendix C.

The basic fuel thermal conductivity relationship that was used in the FUELCON calculations was that described in MATPRO[6]. This relationship had been developed using experimental data obtained from solid pellets under controlled conditions during which the pellets generally did not crack and relocate. The resulting FUELCON-calculated effective

---

[a] A correlation is developed in this section for the effective fuel thermal conductivity of helium filled LWR fuel rods. The data from the xenon and argon filled rods were ignored because of the fuel restructuring and fuel centerline thermocouple problems discussed in Section III.

[b] EG&G Idaho, Inc., Configuration Control Number H003151B.

fuel thermal conductivity is simply the MATPRO conductivity modified to account for fuel cracking effects, based on experimental data. Figure 38 shows a representative comparison between a radial temperature profile calculated with the unadjusted MATPRO thermal conductivity relationship and an adjusted thermal conductivity as determined by FUELCON.

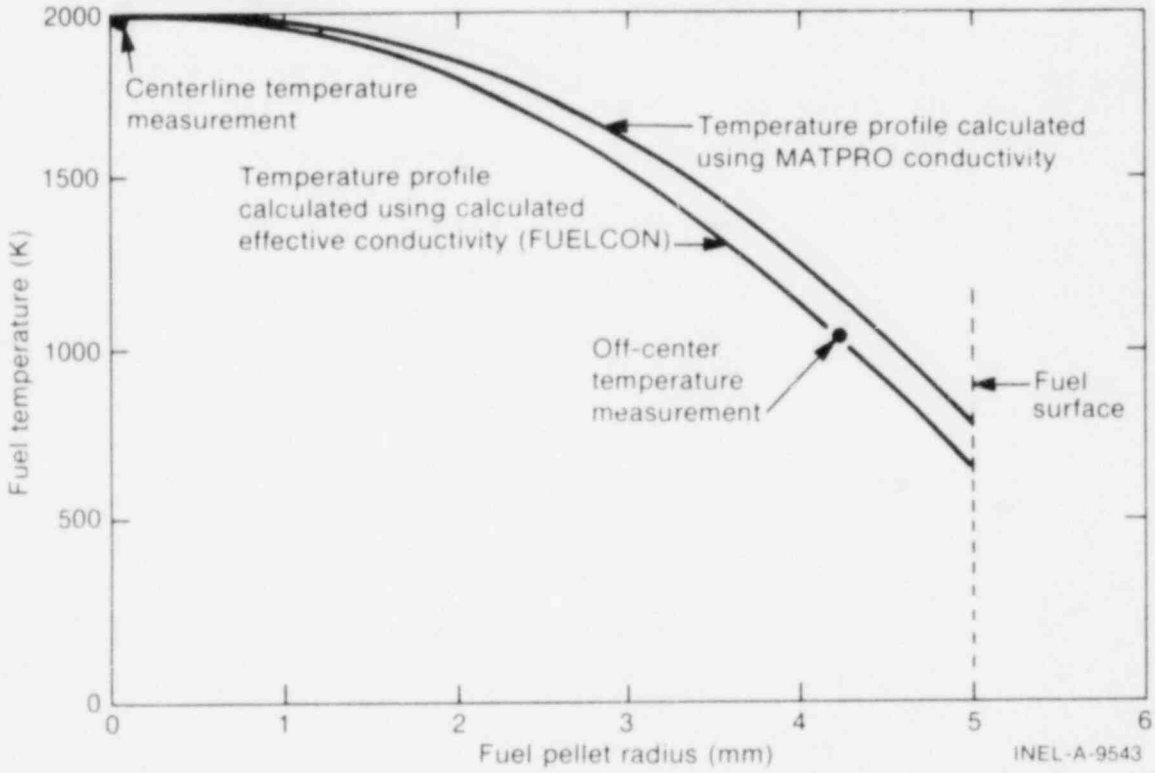

Fig. 38 Representative comparison between fuel pellet radial temperature profiles calculated using the MATPRO thermal conductivity correlation and the FUELCON effective thermal conductivity.

Since the pellet-to-cladding gap width at the off-center thermocouple locations and the fuel cracking patterns and relocation effects between the pellet centerline and the three off-center measurement positions in a given rod are not always the same, effective fuel conductivities were calculated for the centerline and each off-center thermocouple in each of the test fuel rods from Tests GC 2-1, GC 2-2, and GC 2-3. Figure 39 shows representative values for the effective fuel thermal conductivity as determined by FUELCON using the measured centerline and each of the measured off-center temperature measurements in Rod GC 503 (He, 2.2% gap) at test rod power densities of 7.4 and 24.4 kW/m. In Figure 39 the unadjusted MATPRO curve is also shown for comparison. The differences between the values at each power level show that significant differences in fuel thermal conductivity (as a function of temperature) occur within a single test rod because of variations in the azimuthal temperature measurements. These variations are apparently due to differences in crack patterns and crack areas between the pellet centerline and the location of the various

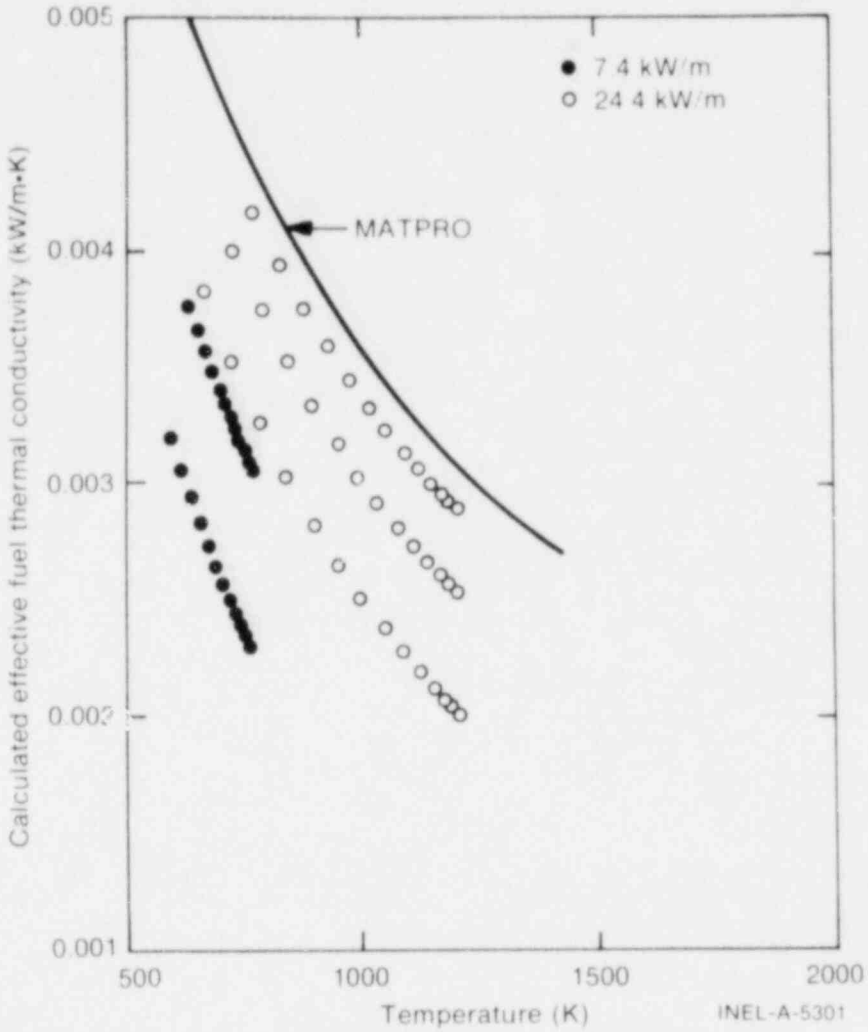

Fig. 39 Calculated effective fuel thermal conductivity in Rod GC 503 (He, 2.2% gap) at power levels of 7.4 and 24.4 kW/m.

off-center temperature measurements. The different crack patterns also contribute to differences in the pellet-to-cladding gap width at the azimuthal orientation of each off-center temperature measurement. Figure 39 also indicates that actual, cracked pellet thermal conductivities are a function of rod power.

The first step in attempting to obtain a correlation for effective fuel thermal conductivity for use in predicting effective thermal conductivities in other LWR design rods, was to plot FUELCON-calculated effective conductivities as a function of the measured variables of test rod power and fuel temperature. The effective conductivities deduced from the off-center temperature measurements at zero degrees in Rod GC 503 of Test GC 2-1 are presented in Figure 40. Conductivities deduced from Rod GC 503 off-center temperature data at 240 degrees are presented in Figure 41. Rod GC 503 was helium filled and contained 95% TD fuel and a 2.2% pellet-to-cladding gap. In Figure 41 the fuel thermal conductivity at low powers is shown to be considerably lower than it is at high powers. This effect is especially noticeable at low temperatures. The same tendency for somewhat lower effective

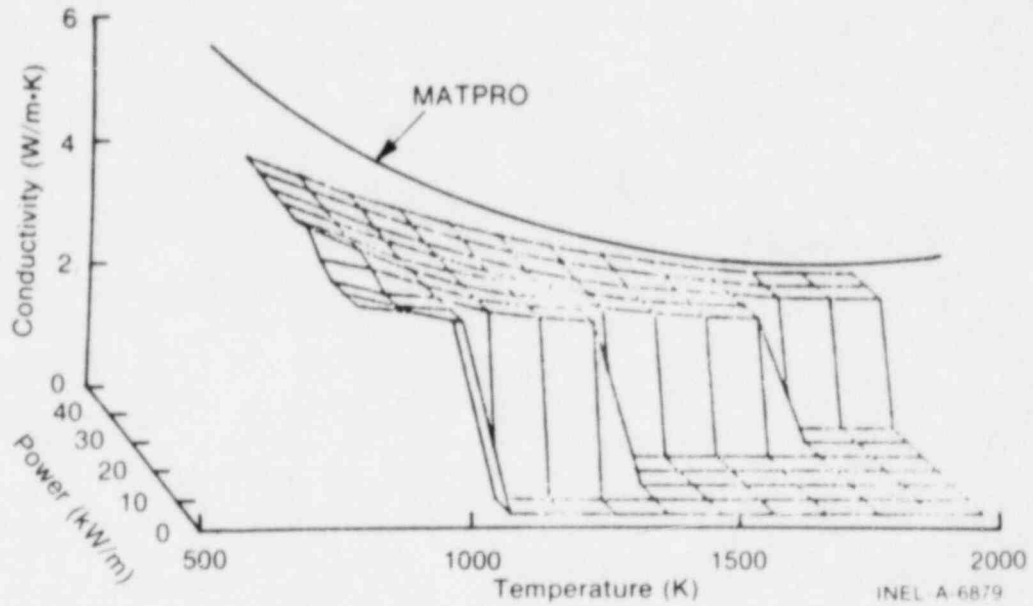

Fig. 40 Effective fuel thermal conductivity as a function of temperature and rod power for test Rod GC 503 (He, 2.2% gap, 95% TD), zero-degree off-center thermocouple.

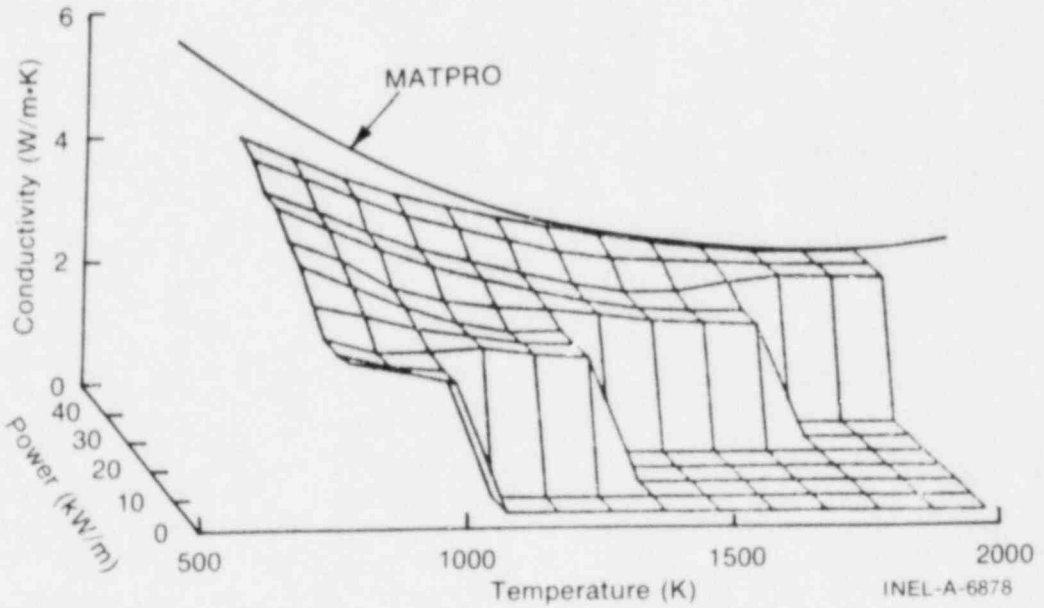

Fig. 41 Effective fuel thermal conductivity as a function of temperature and rod power for test Rod GC 503 (He, 2.2% gap, 95% TD), 240-degree off-center thermocouple.

thermal conductivities at low powers is apparent in Figure 40; however, the effect is much less pronounced. The effective thermal conductivities calculated using the data from the measurements at 120 degrees in Rod GC 503 (not shown) tend to fall between the values shown in Figures 40 and 41 for the measurements at zero and 240 degrees. (The thermal conductivity data are shown in Figures 40 and 41 as the upper surface only. The lines drawn down to and on the zero conductivity floor are shown to provide a perspective and are not data).

Closing or opening of fuel pellet cracks, as the power is increased or decreased, is postulated to be the cause of the effects shown in Figures 39, 40, and 41. The differences in the power dependence of the effective thermal conductivities shown in Figures 40 and 41 are postulated to be due to stochastic variations in the crack patterns within Rod GC 503, and to the differences in pellet-to-cladding gap width at the off-center temperature measurement locations. These postulations are supported by the effective fuel thermal conductivity data from Rods GC 522-3 and GC 522-4 of Test GC 2-2, plotted also as functions of power and temperature in Figures 42 and 43, respectively. MATPRO-calculated thermal conductivities for the same rods are also shown for comparison. The effective thermal conductivities from the small gap, helium filled rod, Rod GC 522-3 (Figure 42), tend to rise sharply as the gap closes with power and then level off. The effective thermal conductivities from the large gap, helium filled rod, Rod GC 522-4, tend to remain relatively low at low temperatures, probably because there was little gap closure in this rod (Figure 43).

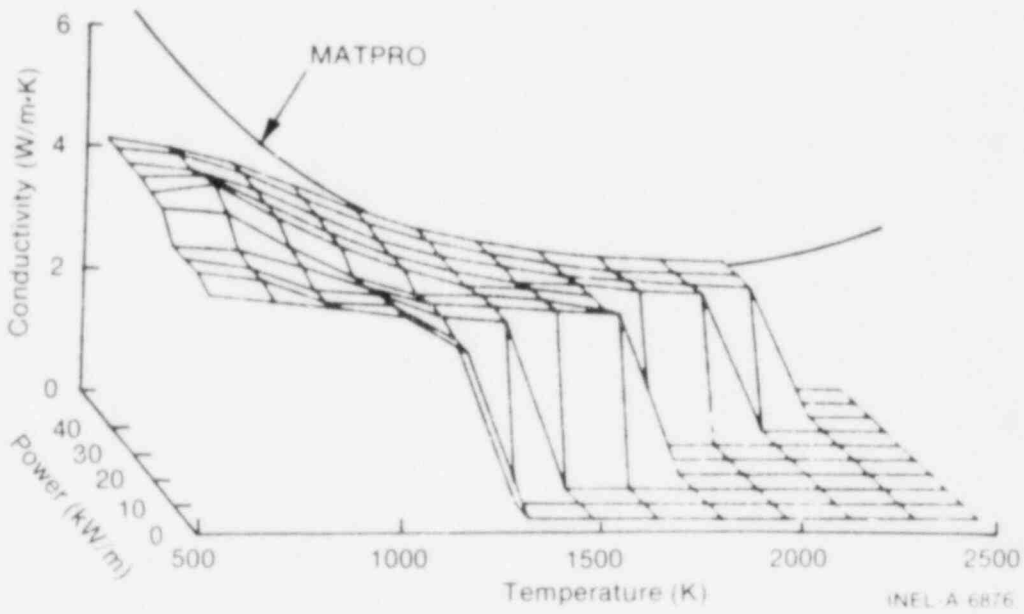

Fig. 42 Effective fuel thermal conductivity as a function of temperature and rod power for test Rod GC 522-3 (He, 0.94% gap, 95% TD), 120-degree off-center thermocouple.

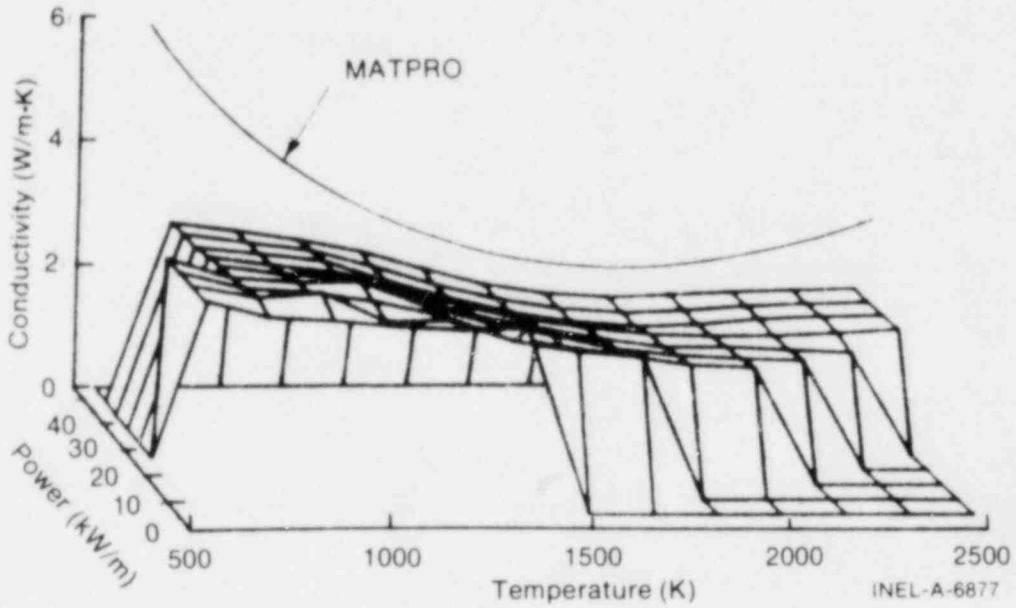

Fig. 43 Effective fuel thermal conductivity as a function of temperature and rod power for test Rod GC 522-4 (He, 3.4% gap, 95% TD), 240-degree off-center thermocouple.

Data similar to those shown in Figures 40 through 43 from the power calibration period of the PBF tests (first power ramp) were compared with the data obtained from the preconditioning and power oscillation periods of the tests (later power ramps). There were no apparent differences between the effective fuel thermal conductivity versus power and temperature relationships measured early in the tests and those observed later in the tests. This lack of difference suggests that pellet cracking and relocation occurred very early in the tests, probably during the first power ramp.

The data shown in Figures 40 through 43 indicate that the thermal conductivity of cracked UO_2 fuel pellets is (a) a strong function of power in moderate gap fuel rods; (b) a weak function of power, and relatively low, in fuel rods with large initial pellet-to-cladding gaps; and (c) a function of power only at low powers in small gap rods. It is suggested that the opening and closing of fuel cracks as the power is decreased or increased may have caused the observed effects. One parameter that can be related to power and pellet crack area is a "nominal hot gap width," defined as the gap between a cylindrical cladding and a solid pellet surface at a given power density, as determined by calculating only fuel and cladding thermal expansions and elastic deflections (for an idealized solid fuel pellet with radial cracks only). As this nominal hot gap closes and opens with increasing or decreasing power, so should the pellet cracks.

1.1 Effect of Nominal Hot Gap Width

A two-dimensional steady state heat transfer computer model called TOODEE[7] [a] was used to calculate the relationship between nominal hot radial gap width and power for each of the PBF test rods. Figure 44 shows the calculated hot radial gap widths as a function of test rod power density for the six helium rods of Tests GC 2-1, GC 2-2, and GC 2-3. Gap closure is predicted to occur for each rod at various power levels which are directly proportional to the initial gap width. The curves in Figure 44 were calculated using the measured initial gap widths (References 3, 4, and 5) and pellet-to-cladding gap conductance values determined using the MATPRO fuel thermal conductivity correlation and the measured fuel centerline temperatures.

On the basis of the FUELCON-calculated effective fuel thermal conductivities for the same six fuel rods, conductivity corrections (difference between MATPRO and FUELCON thermal conductivities) were obtained and are plotted as a function of hot radial gap width in Figure 45. The point at which each curve intersects the zero-correction line corresponds to the power level at which changes in power (and, therefore, pellet geometry) no longer influence the cracked pellet thermal conductivity. In the large and medium gap rods, the curves in Figure 45 intersect the zero-correction line at relatively large nominal hot gaps, as calculated by TOODEE.

The fuel thermal conductivity correction factor data shown in Figure 45, and in the following figures, represent an average of the data from the three off-center temperature measurements for each PBF test rod. Therefore, variations due to the stochastic nature of the pellet cracking process and the differences in pellet-to-cladding gap width near each off-center thermocouple location are averaged out, and the comparisons of the effects of the key design variables on the thermal performance of these test rods are simplified.

1.2 Effect of Initial Cold Gap Width

The plots of the cracked pellet thermal conductivity correction factors versus nominal hot gap width shown in Figure 45 suggest that cracked pellet thermal conductivity cannot be modeled simply as a function of nominal hot gap. Apparently, the initial, cold pellet-to-cladding gap width strongly influenced the subsequent thermal performance of the PBF test rods. Specifically, pellet fragment relocation early in the test apparently influenced the subsequent relationship between increasing and decreasing power and the closing and opening of the pellet-to-cladding gap and the fuel cracks. Therefore, an attempt was made to obtain a single correlation for the helium rods in Tests GC 2-1, GC 2-2, and GC 2-3 by factoring in a "relocation factor" to account for the fact that initial pellet cracking and pellet fragment relocation influence gap closure, and, consequently, the true hot gap width.

---

[a] EG&G Idaho, Inc., Configuration Control Number H003261B.

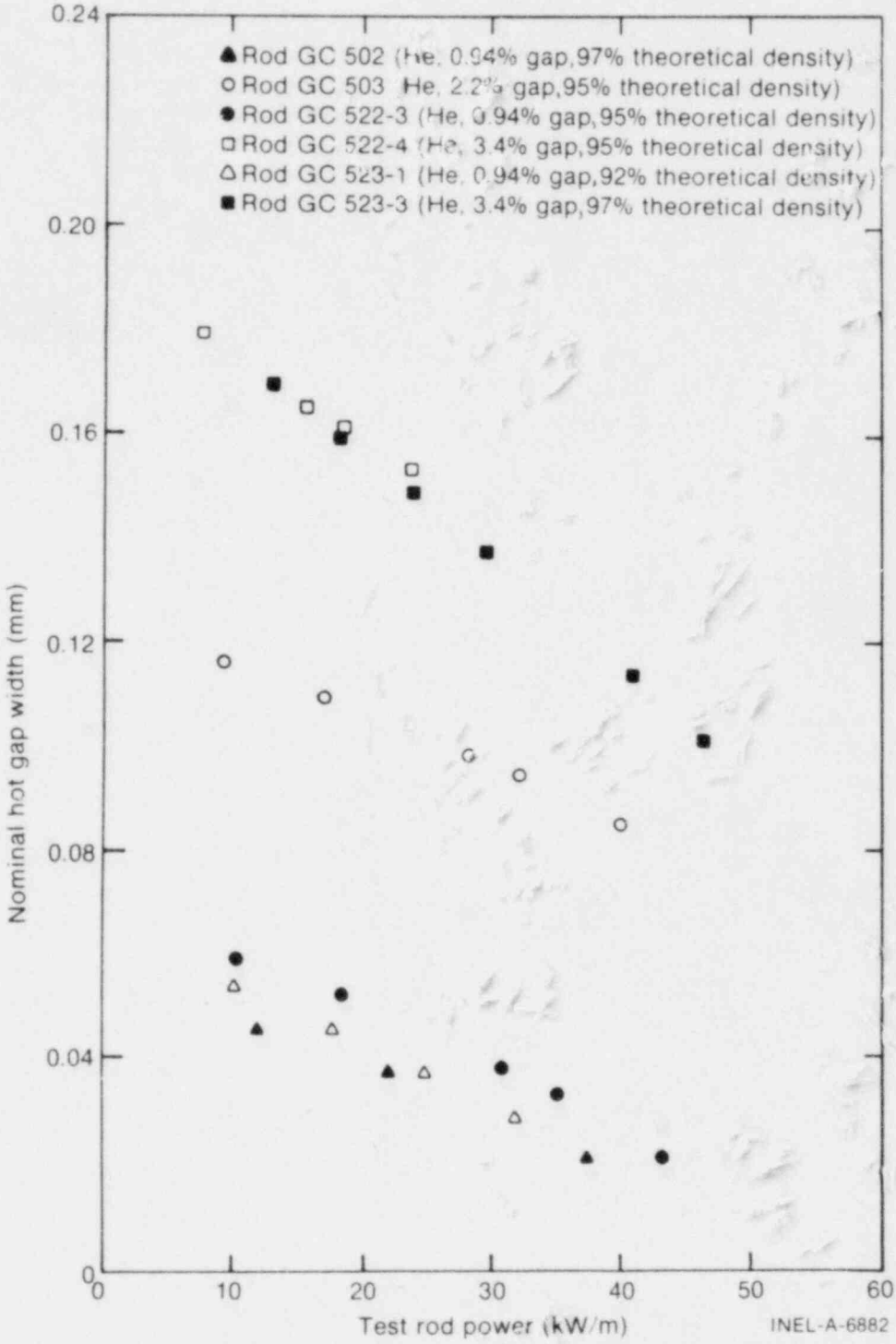

Fig. 44 Calculated nominal hot gap width as a function of test rod power for helium rods in Tests GC 2-1, GC 2-2, and GC 2-3.

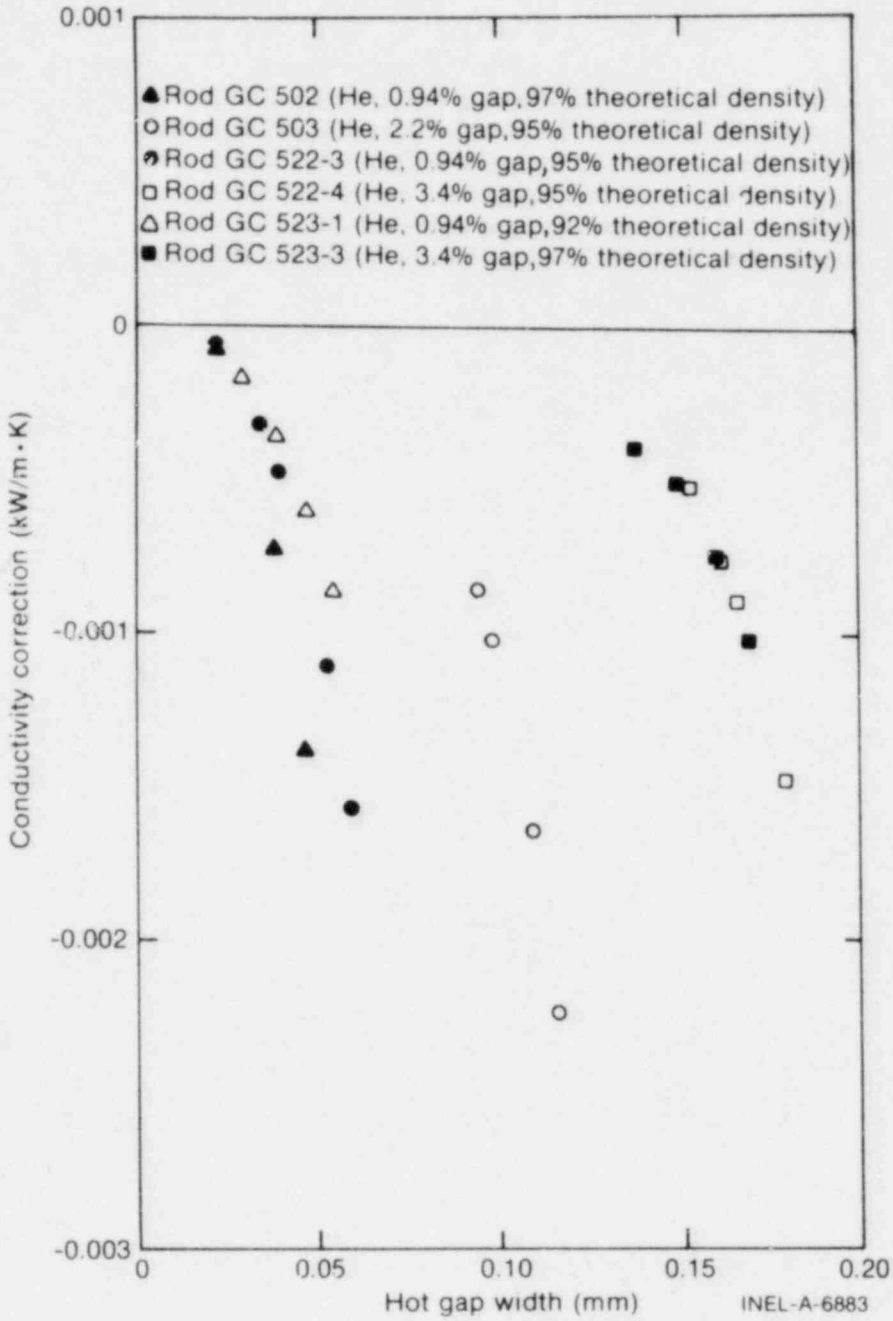

Fig. 45 Calculated fuel thermal conductivity correction factor as a function of calculated hot gap width for helium filled rods in Tests GC 2-1, GC 2-2, and GC 2-3.

The relocation factor was obtained in the following manner. For each fuel rod, the difference between the MATPRO fuel thermal conductivity and the FUELCON-calculated fuel thermal conductivity (conductivity correction) was evaluated as described previously. The power level at which the conductivity correction was zero was the estimated power for gap closure, including relocation effects. The relocation factor was then defined as the nominal hot gap width at this power level (shown in Figure 45), as calculated by the TOODEE solid pellet expansion model. Figure 46 is a composite plot of the "relocated" hot

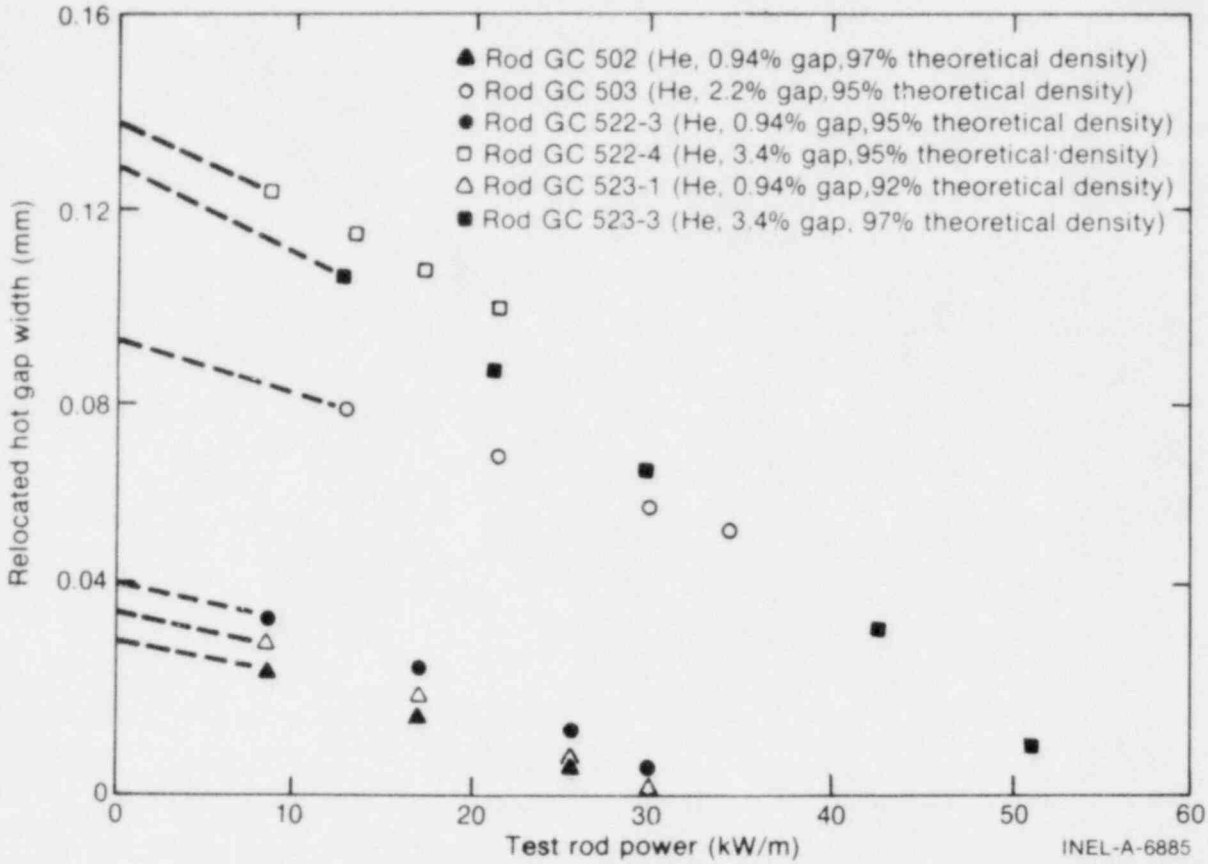

Fig. 46 Relocated hot gap width and estimated zero-power gap width as functions of rod power for the helium rods in Tests GC 2-1, GC 2-2, and GC 2-3.

gap width as a function of test rod power for the six helium rods. The relocated hot gap is the nominal TOODEE hot gap at any power level, less the relocation factor.

Figure 46 also shows the TOODEE-calculated hot gap width curves extrapolated to zero power. This zero-power gap width is less than the initial gap width determined from pretest characterization data. The difference in the zero-power gap widths and the initial gap widths is considered to be due to the fact that when the rods cool down after having experienced high powers and temperatures, the cracks in the fuel do not close, resulting in a redistribution of part of the initial gap toward the center of the fuel pellets.

The relocation factor for a given rod design would be expected to be a strong function of the initial cold gap width, but probably not influenced to any great extent by fill gas composition and fuel density. Figure 47 shows that a strong linear relationship does indeed exist between the calculated relocation factor and the measured initial gap width for most of the rods in Tests GC 2-1, GC 2-2, and GC 2-3, including some xenon and argon filled rods and a wide range of fuel densities. Some of the rods that did not show a good correlation between relocation factor and initial gap width (for example, Rod GC 501) may have been influenced by high fuel temperatures resulting in extensive fuel relocation and a reaction between the fuel and the centerline thermocouple sheath, as previously discussed. Figure 47

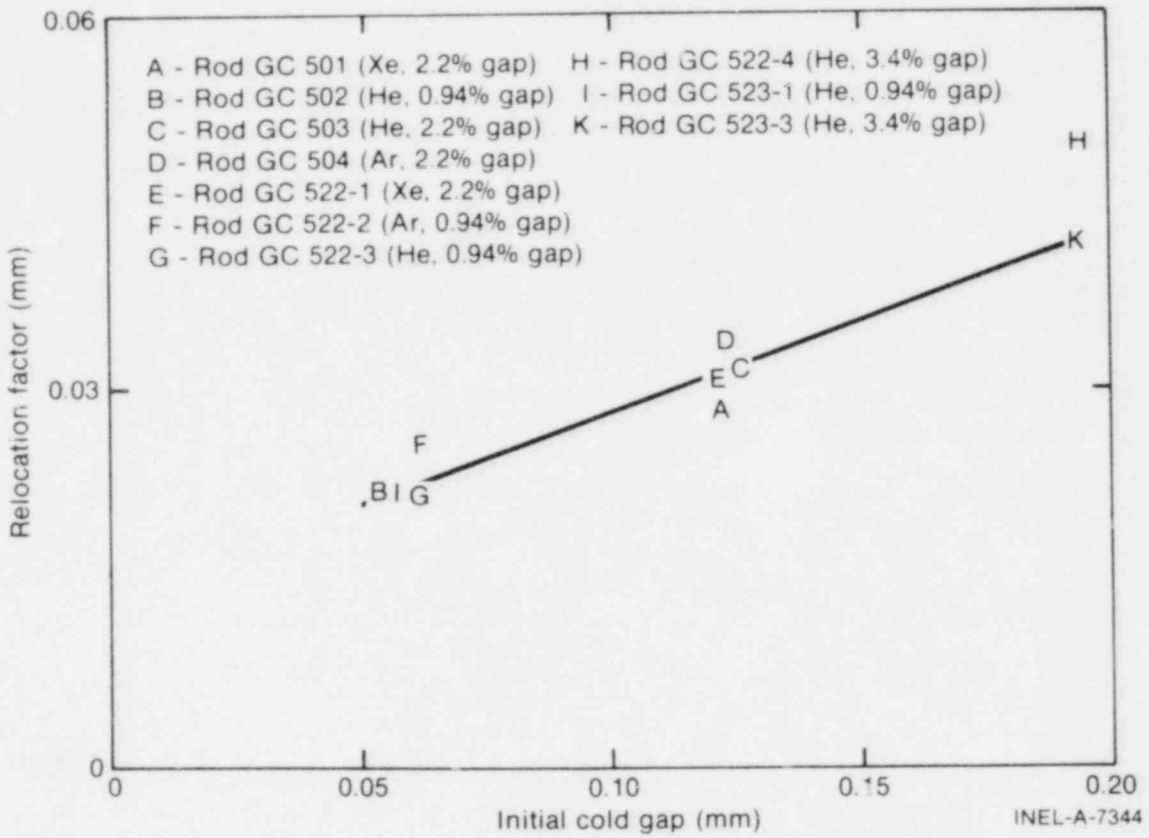

Fig. 47 Relationship between the calculated relocation factor and the initial cold gap width for rods in Tests GC 2-1, GC 2-2, and GC 2-3.

provides a convenient means for estimating the relocation factor of any LWR design fuel rod. Through use of a least squares fitting routine, the relationship between the relocation factor (RF) and initial cold gap shown in Figure 47 can be expressed as

$$RF = 0.014 + 0.14\ CG\ (mm)$$

where CG is the initial cold radial pellet-to-cladding gap in millimeters.

When the conductivity corrections for the helium rods are plotted as a function of the relocated hot gap, the curves in Figure 48 are obtained. Figure 48 does not provide a single curve for all the helium rods; however, the differences between the curves are now much smaller than shown in Figure 45. The remaining differences in the curves of Figure 48 again appear to be related to the initial gap widths. The relocation factor incorporated into the relationship shown in Figure 48 accounts for the fact that in large initial pellet-to-cladding gap rods the pellet fragments move much farther out during the first power ramp and are thereafter pushed in and out at much larger nominal hot gap widths than in the small gap rods. However, when the pellet fragments initially move farther, they do not fit back together as well. Therefore, the slope of the conductivity correction factor versus relocated hot gap width data shown in Figure 48 is much steeper for the small gap rods (where the fragments fit together better) than for the large initial gap rods.

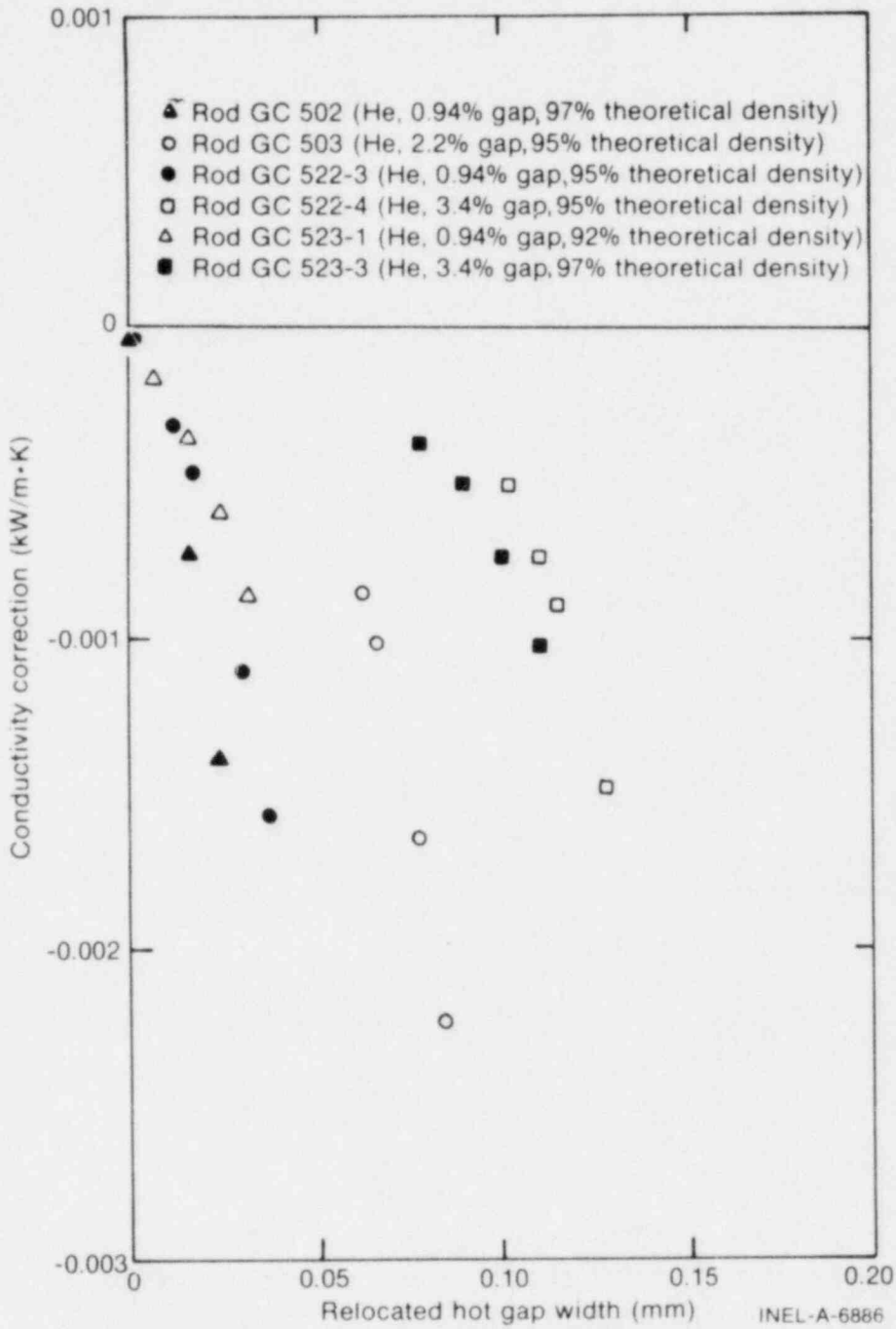

Fig. 48 Calculated fuel thermal conductivity correction factor as a function of calculated hot gap width for helium filled rods in Tests GC 2-1, GC 2-2, and GC 2-3.

Using the rod with the smallest measured gap width (Rod GC 502; 0.94% diametral or 0.0545-mm radial) as a basis for normalization, each curve in Figure 48 was multiplied by the ratio: (0.0545 mm/ initial radial gap width of rod in question, mm). The resulting curves are shown in Figure 49. These curves also do not provide a single curve for all the helium rods, but the differences are no greater than might be expected, considering the amount of scatter in the original data. Also, there does not appear to be any systematic influence of the

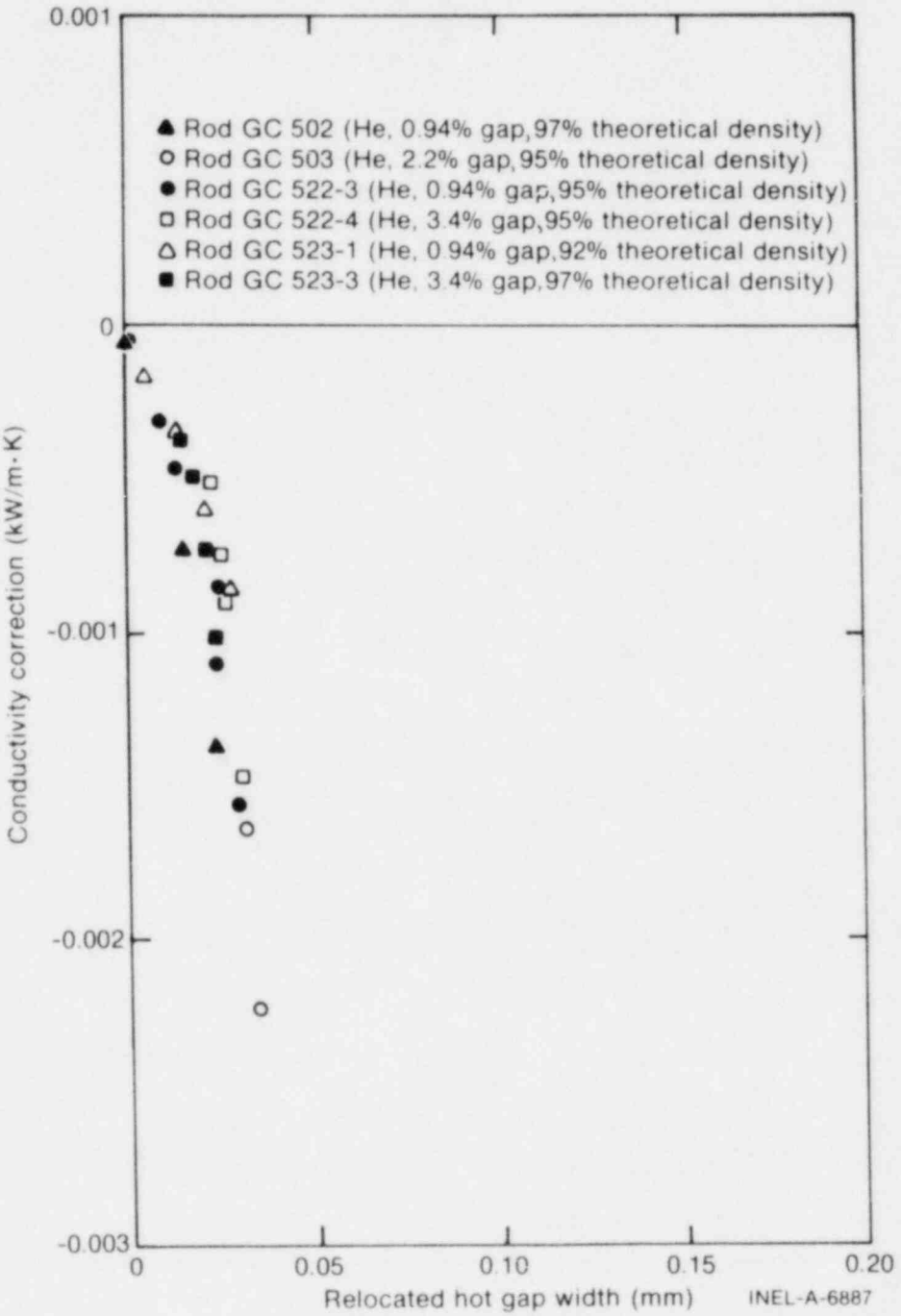

Fig. 49 Calculated fuel thermal conductivity correction factor as a function of calculated hot gap width, including the effects of initial gap width, for the 0.94% initial gap rods in Tests GC 2-1, GC 2-2, and GC 2-3.

initial cold gap left in the relationship shown in Figure 49 between the thermal conductivity correction factor data and the adjusted and relocated hot gap widths.

1.3 Effect of Fuel Density

Low density uranium dioxide fuel generally cracks somewhat more easily (at slightly lower stress levels) than higher density fuel[6]. In addition, the crack surfaces might be expected to be slightly more irregular and pellet fragments might be expected not to fit back together at higher power levels quite so easily in the low density PBF test rods. The curves of UO_2 thermal conductivity correction factor versus adjusted and relocated hot gap width for the three 0.94% helium filled rods shown in Figure 49 are plotted separately in Figure 50. It is apparent that the relationship between conductivity correction factor and the adjusted and relocated hot gap width is steeper in the high density rods, suggesting that

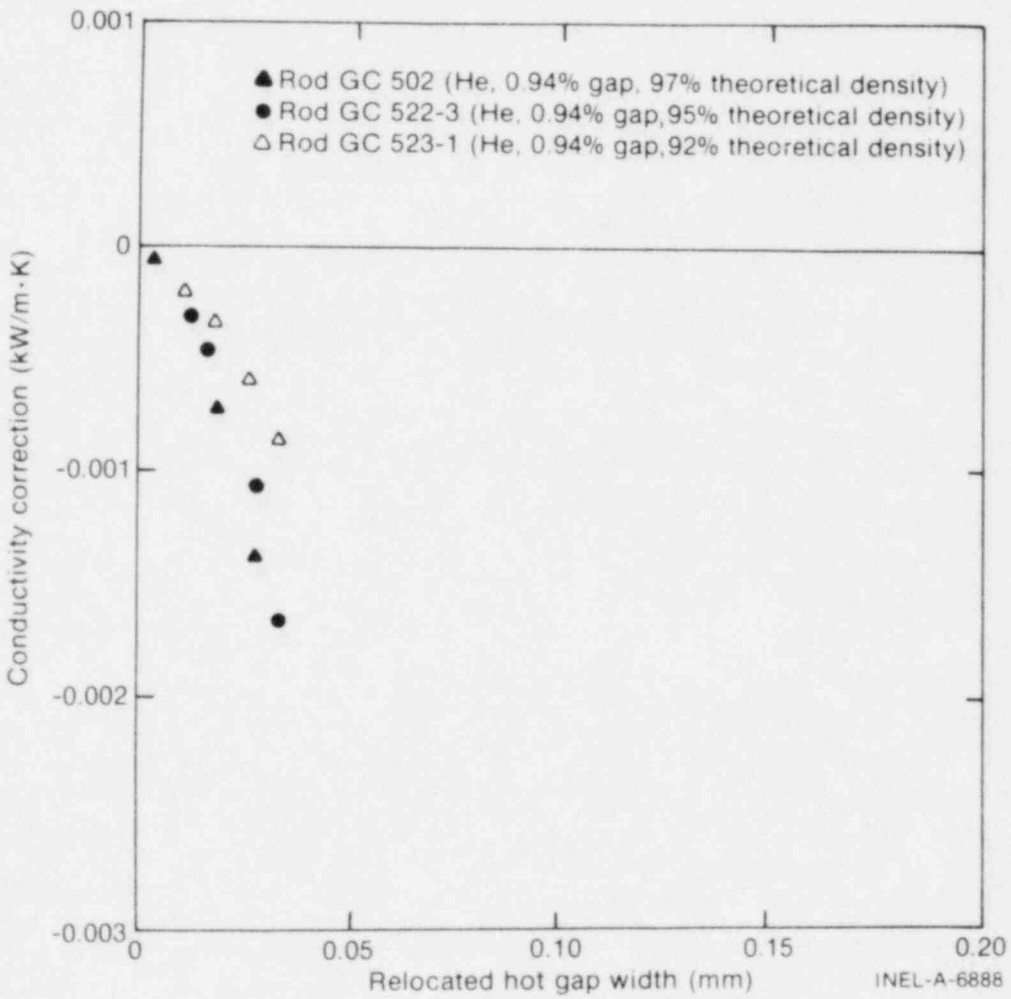

Fig. 50 Calculated fuel thermal conductivity correction factor as a function of relocated hot gap width, including the effects of initial gap width, for the 0.94% initial gap rods in Tests GC 2-1, GC 2-2, and GC 2-3.

the pellet fragments do fit together better as the power is cycled or that there are fewer cracks in the high density rods. By multiplying each curve of Figure 50 by the percent of theoretical density to the eighth power (% TD)^8, an arbitrary empirical factor, the curves were made to essentially coincide as shown in Figure 51. Applying this same density correction to all the helium rods results in the curves shown in Figure 52. These curves do not coincide exactly, but the differences are small and are reduced from those shown in Figure 49 by the fuel density correction.

1.4 Empirical Correlation for Thermal Conductivity of Cracked UO_2 Fuel Pellets

The relationship between the nominal thermal conductivity of a solid uranium dioxide pellet (MATPRO conductivity) and the thermal conductivity of a typical fresh, helium filled LWR fuel rod with cracked and broken fuel pellets and pellet fragments which have moved

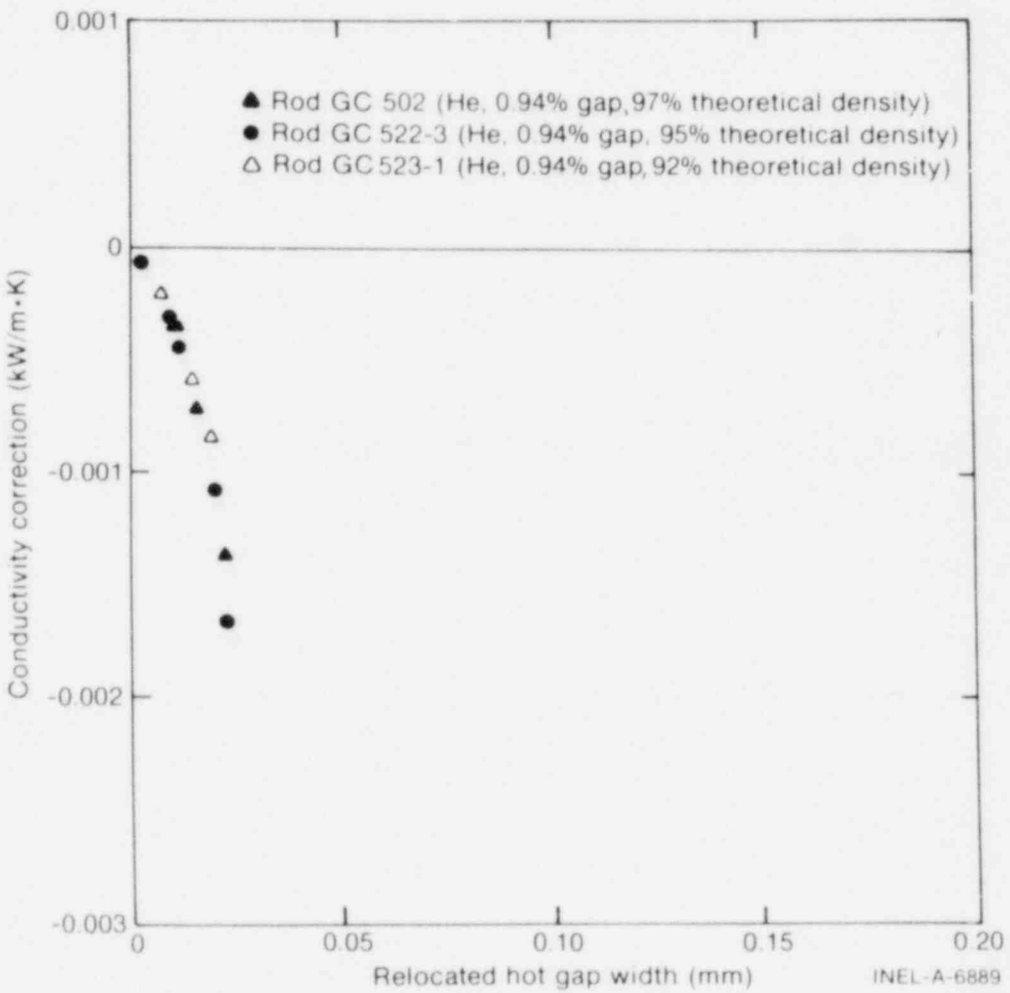

Fig. 51 Calculated fuel thermal conductivity correction factor as a function of relocated hot gap width, including the effects of initial gap width and density, for the 0.94% initial gap rods in Tests GC 2-1, GC 2-2, and GC 2-3.

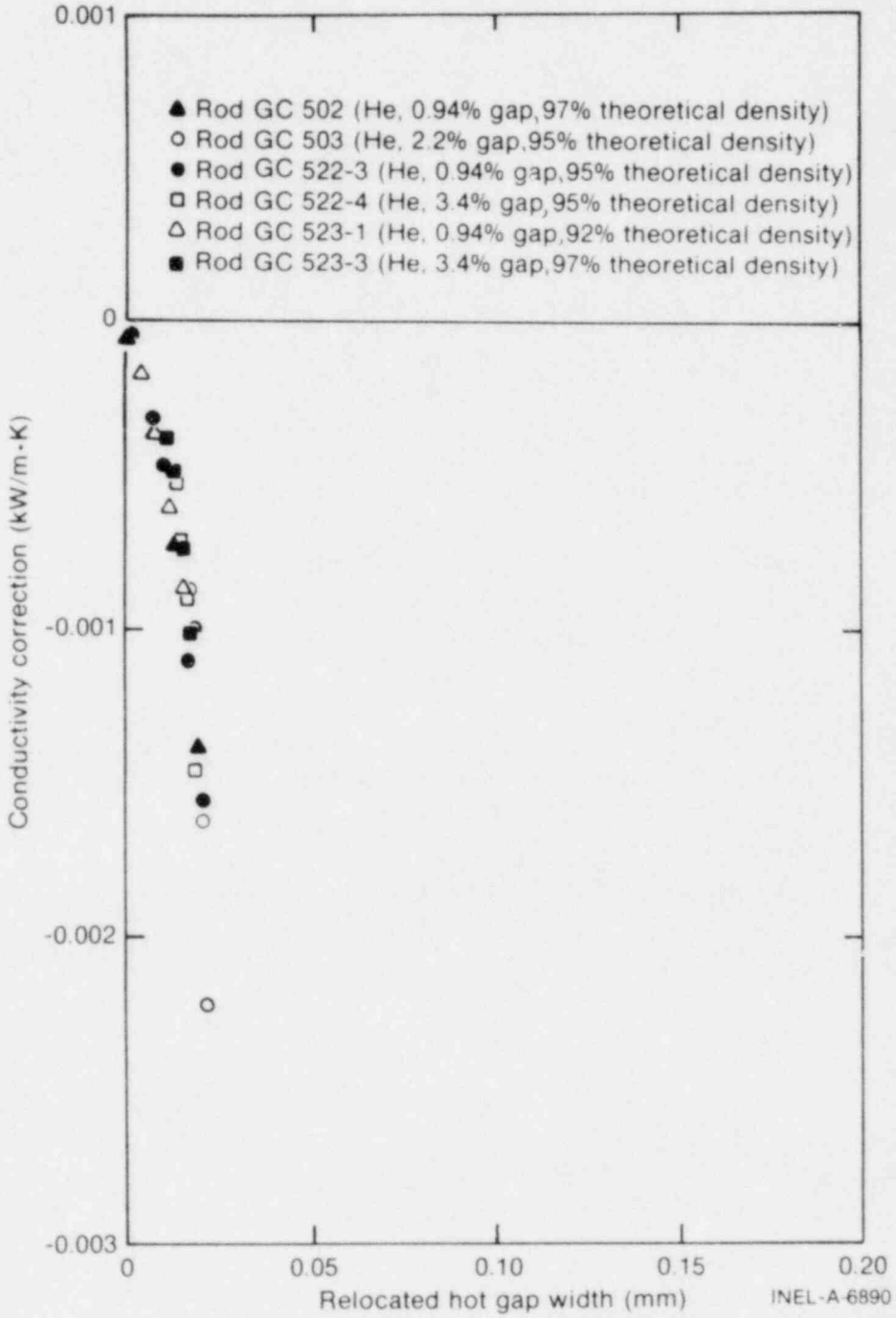

Fig. 52 Calculated fuel thermal conductivity correction factor as a function of relocated hot gap width, including the effects of initial gap width and fuel density, for all helium filled rods in Test GC 2-1, GC 2-2, and GC 2-3.

about and do not necessarily fit well together is shown in Figure 52. This relationship can be expressed in mathematical form as follows:

$$k_{eff} = k_{MATPRO} \cdot (0.0002189 - 0.050867\,\chi + 5.6578\,\chi^{2})$$

where

k_{MATPRO} = the temperature-dependent fuel thermal conductivity of a solid pellet[6]

χ = $(HG - 0.014 - 0.14\,CG)\,(0.0545/CG)\,(\%\,TD)^{8}$,

and

HG = a hot pellet-to-cladding radial gap in millimeters, calculated assuming only radial cracking, thermal expansion, and elastic deflection of an idealized solid pellet and cylindrical cladding

CG = the initial cold radial pellet-to-cladding gap in millimeters

% TD = the theoretical density of the fuel in percent.

1.5 Estimated Uncertainties in Calculated Effective Fuel Thermal Conductivities

Estimated uncertainties in the calculated effective fuel thermal conductivity correlation were determined from the uncertainties calculated by the FUELCON code for each conductivity correction calculated. Parameters which contribute significantly to the uncertainty in the correlation and the sources of the uncertainties are listed in Table III. The uncertainties in the conductivity corrections as a function of power for each helium filled rod of Tests GC 2-1, GC 2-2, and GC 2-3 were calculated and the root-mean-square (RMS) values for each design gap width (0.94, 2.2, and 3.4%) were determined. Because of the small differences in the uncertainties between the different design rods, less than 3%, an uncertainty for all helium rods combined was determined. Figure 53 shows this uncertainty as a function of power as calculated by the relationship

$$\sigma_{k_{eff}}^{TOTAL} = 0.488169 \times 10^{-3} + 0.134487 \times 10^{-4}\,(POWER) - 0.821495 \times 10^{-6}\,(POWER)^{2} + 0.104021 \times 10^{-7}\,(POWER)^{3}.$$

TABLE III

PARAMETERS CONTRIBUTING SIGNIFICANTLY TO THE UNCERTAINTY IN THE EFFECTIVE FUEL THERMAL CONDUCTIVITY CORRELATION AND THE SOURCE OF THE UNCERTAINTY IN THE PARAMETER

Parameter	Source(s) of Uncertainty
Fuel off-center temperature measurement	Fuel pellet off-center thermocouple perturbation analysis (Appendix C) and TOODEE analysis to determine uncertainty due to fuel pellet skewing inside cladding.
Fuel centerline temperature measurement	TOODEE analysis to determine uncertainty due to fuel pellet skewing inside cladding. Accuracy of thermocouple. Accuracy of recording system.
Power	Appendix C of this document.
MATPRO fuel thermal conductivity	Reference 6.
Radial location of off-center Fuel thermocouples	Uncertainty in radial location was set equal to the zero power fuel-to-cladding hot gap width.

The effective fuel thermal conductivity correlation for helium filled rods is then given by

$$k_{eff} = k_{MATPRO} - (0.0002189 - 0.050867x + 5.6578x^2) \pm \sigma^{TOTAL}_{k_{eff}} .$$

Representative calculations for the effective fuel thermal conductivities with estimated uncertainties, for a helium filled rod with an initial gap width of 2.2%, are shown in Figures 54 and 55 at test rod power densities of 8.58 and 39.26 kW/m, respectively. MATPRO thermal conductivities are also shown for comparison, but uncertainties in the MATPRO values are not shown.

The calculations shown in Figures 54 and 55 show that at low power levels the uncertainty in the conductivity correction is small relative to the magnitude of the correction itself; however, at medium power levels the conductivity correction itself is small, and the uncertainty essentially overlaps the expected uncertainty in the MATPRO values. At higher power levels the conductivity correction is even less, and cannot be shown to be statistically different from the MATPRO values. For a 2.2% initial gap helium filled rod, the conductivity correction would be essentially zero at a power level of approximately 57 kW/m.

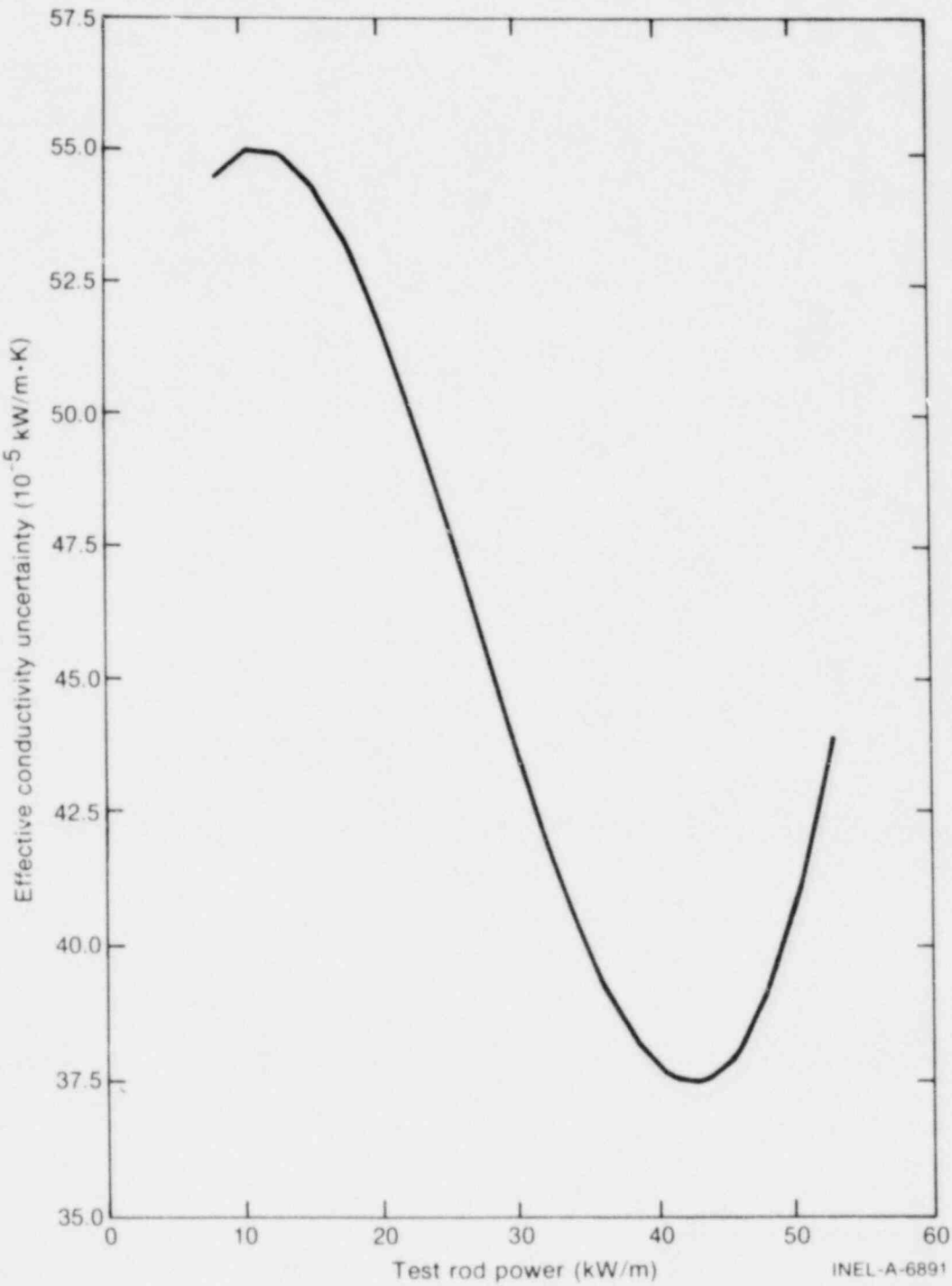

Fig. 53 Estimated uncertainty in effective fuel thermal conductivity as a function of test rod power for helium filled rods in Tests GC 2-1, GC 2-2, and GC 2-3.

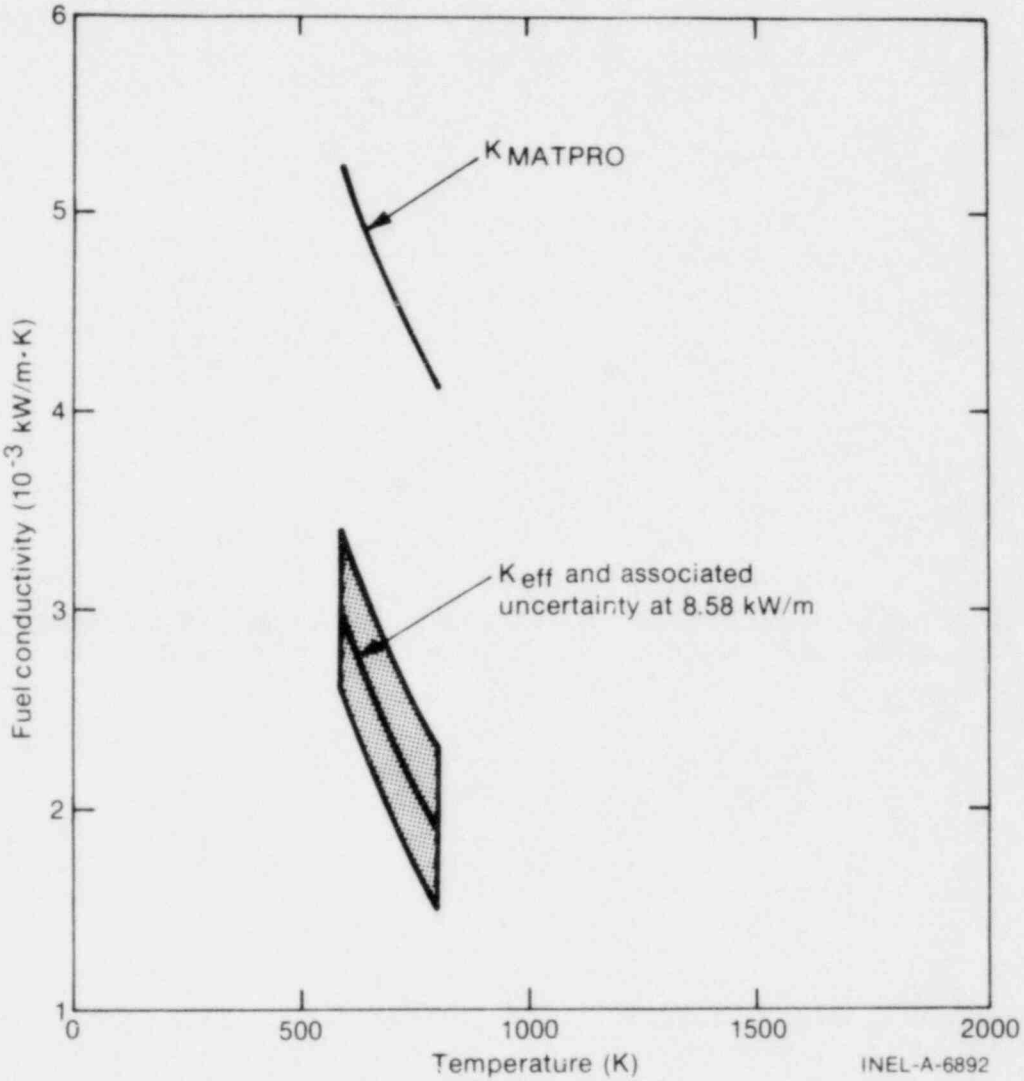

Fig. 54 Representative comparison of MATPRO fuel thermal conductivity with calculated effective fuel thermal conductivity, with estimated uncertainty, for 2.2% initial gap helium filled rods at a power of 8.58 kW/m.

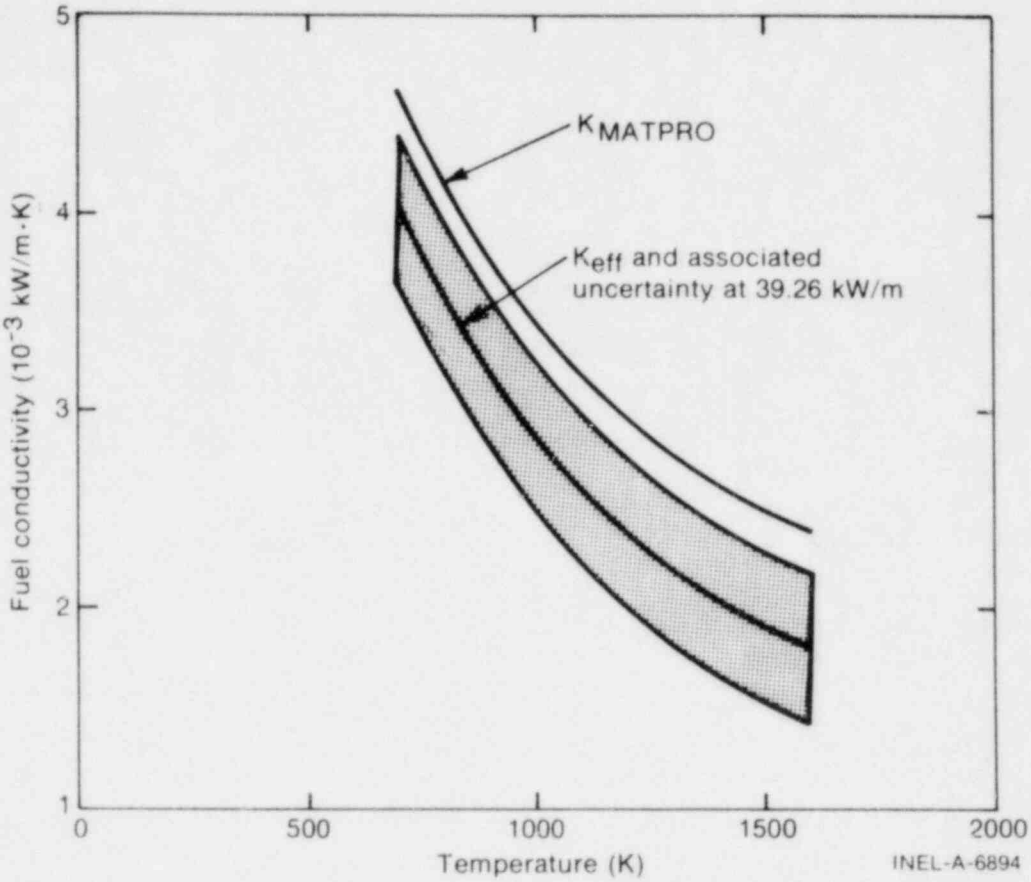

Fig. 55 Representative comparison of MATPRO fuel thermal conductivity with calculated effective fuel thermal conductivity, with estimated uncertainty, for 2.2% initial gap helium filled rods at a power of 39.26 kW/m.

2. EVALUATION OF STEADY STATE GAP CONDUCTANCE VALUES

Steady state pellet-to-cladding gap conductance values are obtained from the relationship

$$h_{gap} = \frac{Q}{A(T_S - T_C)}$$

where

Q = test rod power density (kW/m) over a unit length of fuel

A = pellet surface area for a solid pellet

T_S = pellet surface temperature, and

T_C = cladding inside surface temperature.

In applying this relationship, test rod power densities were evaluated from thermal-hydraulic and neutron flux measurements (obtained from self-powered neutron detector measurements as described in Appendix C). The surface area was calculated on the basis of fuel

pellet measurements at the axial temperature measurement locations. The fuel pellet surface temperatures were calculated using the measured fuel centerline and off-center temperature measurements and the FUELCON code, as described in the previous section. The cladding inside surface temperatures were calculated from the measured cladding outside surface temperatures by the SKDT code, described in Appendix C.

Steady state gap conductance values were calculated for each azimuthal orientation for each test rod in Tests GC 2-1, GC 2-2, and GC 2-3 by the methods described above. The azimuthal gap conductance values were also averaged for each rod to obtain average gap conductance as a function of test rod power density. Plots of the calculated gap conductance as a function of test rod power density for each test rod are presented in Section V-2.1.

Since the pellet-to-cladding gap conductance is inversely proportional to the temperature drop across the gap (T_S-T_C), the fuel design characteristics and thermal properties that are responsible for the observed fuel thermal responses, as described in Section IV, are also responsible for the observed gap conductance behavior. For example, wide gap rods characteristically have higher fuel temperatures than narrow gap rods, resulting in large temperature drops across the gap and lower gap conductances in the wide gap rods than in narrow gap rods. Likewise, fuel rods with low thermal conductivity fill gases generally have higher fuel temperatures than rods with higher thermal conductivity fill gases; therefore, the low conductivity gas rods will have lower gap conductances than the high conductivity gas rods. However, the effects of fuel pellet cracking and fragment relocation may alter these general charactistics, as discussed in Section V-1.

2.1 Development of a Correlation for Gap Conductance in LWR Fuel Rods

Utilization of the gap conductance information obtained from the PBF testing program can be greatly increased if the information is used as a basis for development of a correlation that will permit meaningful predictions of expected gap conductance values in fuel rods that have not been tested. The data from all twelve test rods in Tests GC 2-1, GC 2-2, and GC 2-3 were analyzed and used in the development of a correlation for predicting gap conductance values in other light water reactor fuel rods.

The first step in the development of a correlation was to evaluate existing correlations against experimental results. The most widely accepted existing correlation is the Ross and Stoute[8] correlation that was developed on the basis of solid pellet thermal expansion, and is described by the relationship

$$h_{gap} = \frac{k_{gas}}{GW + C(R_1 + R_2) + J_T}$$

where

k_{gas}	=	MATPRO-calculated thermal conductivity of the fill gas as a function of temperature (kW/m·K)
GW	=	pellet-to-cladding gap width as a function of rod power (m)
$C(R_1 + R_2)$	=	pellet and cladding roughness term (m)
J_T	=	temperature jump distance (m).

In the Ross and Stoute relationship, at cold zero power the pellet-to-cladding gap width is the same as the pretest, as-built gap width, GAB, and the change in gap width as a function of rod power is that predicted for uniform thermal expansion of a solid fuel pellet by a thermal expansion code such as TOODEE.

However, posttest examination and analysis of the test rod thermal response for Tests GC 2-1, GC 2-2, and GC 2-3 indicate that pellet cracking and pellet fragment relocation occur very early in the operating life of a fuel rod. The posttest photomicrographs, as described in Section IV, show that a cold zero power (CZP) gap width exists that is different from the as-built gap width. This relocated gap width, RGW (CZP), is the result of pellet cracking and pellet fragment relocation during operation. Upon cooldown, the pellet fragments do not fit together exactly as a solid pellet, resulting in a relocated gap width.

In addition, when the fuel rods are heated from cold zero power to power conditions, the effects of pellet fragment relocation on gap closure during thermal expansion must be considered. The methods developed to evaluate these relocating effects are described subsequently.

The correlation developed here provides a method for calculating an average relocated gap width at power, which, when used with the existing Ross and Stoute gap conductance correlation, will provide predictive estimates of LWR fuel rod relocated gap conductances.

The average relocated gap width is calculated in two steps. The first step uses a method for estimating the posttest measured relocation expected for a given manufactured fuel rod. The second step provides a means for extrapolating this relocated gap width over the anticipated range of test rod powers to be examined.

2.1.1 Development of Relationship Linking Pretest and Relocated Gap Widths. Pretest (as-built) and posttest (relocated) cold zero power gap width measurements from Tests GC 2-1, GC 2-2, and GC 2-3 were compared to provide a means for predicting relocation at cold zero power. A least squares fit of measured radial average posttest gap

width, RGW (CZP), as a function of measured radial average pretest gap width in mm, GAB, assuming symmetrical positioning of the pellets in the cladding, provided the following relationship:

$$RGW(CZP) = 1.665 \times 10^{-2} + 0.868\ (GAB) - 13.435\ (GAB)^2 + 71.682\ (GAB)^3.$$

Because of limited experimental data for the large, 0.38-mm diametral, gap rods (only the first power up ramp exists, during which the relocation characteristics may not be complete), the preceding correlation is fit so that the estimated relocated radial gap width equals GAB, when GAB $\gtrsim$ 0.19 mm.

This relocated gap width, in conjunction with a model for calculating cracked pellet thermal expansion, is proposed for use in the Ross and Stoute correlation for rods with initial pellet-to-cladding diametral gaps between 0.109 and 0.386 mm.

This definition for relocated gap width (RGW) differs from the relocated hot gap width used in the correlation for effective fuel thermal conductivity in Section V-1 in that it involves posttest measurements of the RGW (CZP), whereas the RGW (CZP) for the conductivity correlation was estimated by extrapolating TOODEE-calculated RGW at predicted gap closure to a zero-power condition. For use in empirical correlations, these definitions are not inconsistent, but they also are not equivalent. The relationship between the two definitions for predicted relocated gap width at cold zero power is illustrated graphically in Figure 56. This relationship assumes minimal pellet-cladding interaction and permanent cladding deformation. Where cladding deformation occurs, corrections are necessary.

2.1.2 Development of Cracked Pellet Thermal Expansion Model. Using the previously developed relationship between the initial gap widths and relocated gap widths, two general fuel pellet expansion models were examined and the resultant predictions were compared with gap conductance values determined from experimental measurements from Tests GC 2-1, GC 2-2, and GC 2-3. The expansion models examined were:

(1) A uniform, radial thermal expansion model, as provided in the TOODEE code

(2) A nonuniform thermal expansion model in which a fractional radial thermal expansion is assumed until the integrated radial thermal expansion, with power, fills the inner pellet relocation-induced cracks and voids.

From the trends found in the comparisons of predicted with measured gap conductance values using the two expansion models, the following were observed:

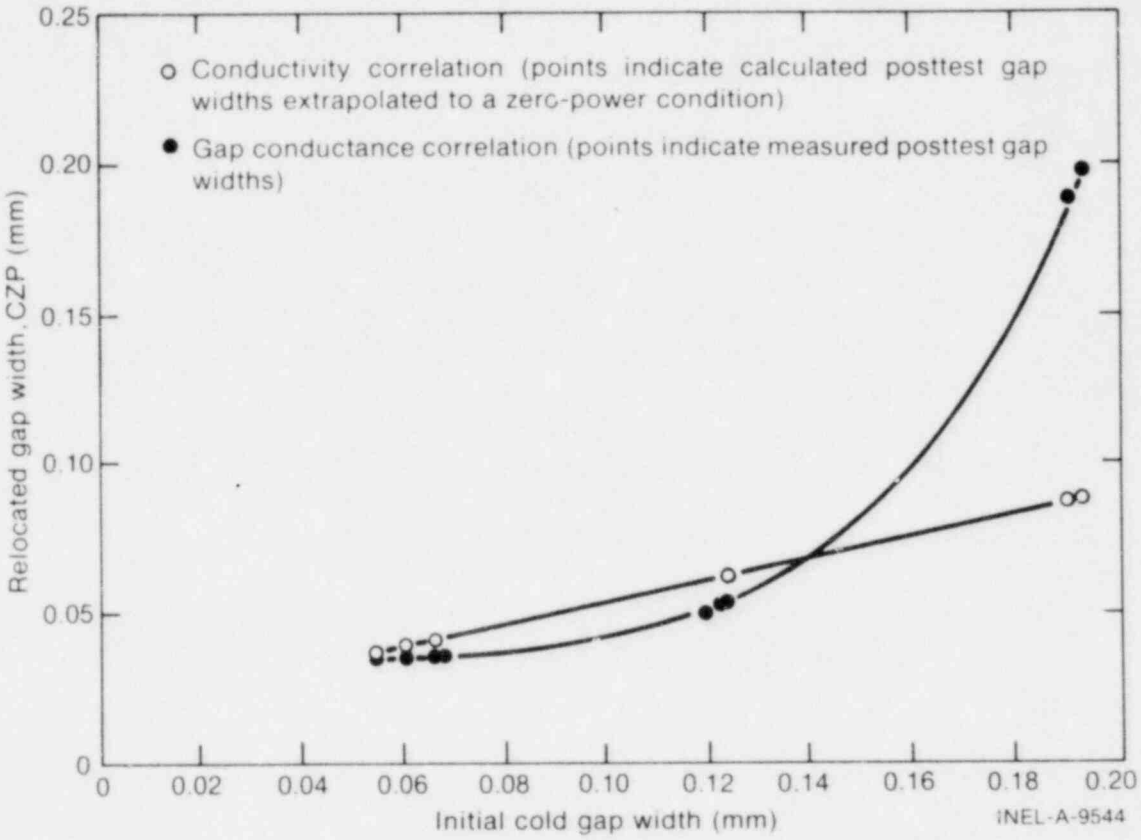

Fig. 56 Plot showing relationship between relocated gap widths, as defined for the effective thermal conductivity correlation, and as defined for the steady state gap conductance correlation.

(1) The assumption of free expansion best fit only the measured gap conductance data from the narrowest as-built gap rods from each backfill gas composition (that is, Rods GC 502, GC 522-2, GC 523-2)

(2) The nonuniform thermal expansion model fit the measured gap conductances from the other nine test rods better, because the change in fill gas conductivity with power alone accounts for most of the change in measured gap conductance with power.

2.1.3 Evaluation of a Thermal Expansion-Gap Closure Model. Additional analyses for rods other than Rods GC 502, GC 522-2, and GC 523-2 showed that a nonuniform thermal expansion model allowing 30% of the integrated fuel pellet radial thermal expansion to be communicated to the relocated pellet-to-cladding gap was found to fit all of the data best.

Therefore, for the smallest gap rod with uniform thermal expansions

$$RGW = RGW(CZP) - \Delta GW$$

where ΔGW is the integrated solid pellet gap width change in mm predicted from thermal code calculations from cold zero power to any given test power. RGW(CZP) is the relocated gap width in mm at cold zero power.

And for the remaining rods with nonuniform thermal expansions

$$RGW(mm) = RGW(CZP) - 0.3\ \Delta GW.$$

Because of the narrow gap widths in Rods GC 502, GC 522-2, and GC 523-2, and the high operating temperatures in Rods GC 522-2 and GC 523-2, the pellet-to-cladding gaps would be expected to close at relatively low test rod powers, resulting in little fuel pellet relocation and narrow internal pellet cracks. Posttest photomicrographs of these test fuel rods do indeed show diffuse crack networks of many narrow cracks. The neighboring pellet fragment faces are thought to interlock, providing a degree of cohesiveness that permits thermal expansion and contraction similar to the uniform thermal expansion for a solid pellet.

For the wider gap rods, photomicrographs show wider, more distinct relocated cracks across which there may be no intimate contact of the pellet fragment faces. Upon cooldown, the pellet fragments do not usually fit together well enough to close the relocated cracks. Therefore, upon reheating by a power increase, the relocated cracks must be filled before all of the thermal expansion can contribute to pellet-to-cladding gap closure.

On the basis of comparisons of gap conductance predictions with experimental measurements for the fuel rods of Tests GC 2-1, GC 2-2, and GC 2-3, the following conclusions were reached:

(1) For narrow gap argon and xenon rods with manufactured diametral gap widths <0.14 mm, thermal expansions are uniform. For rods with gaps ≥ 0.14 mm, thermal expansions are nonuniform, with only 30% of the thermal energy contributing to closure of the pellet-to-cladding gap.

(2) For very narrow gap helium rods with gaps <0.12 mm, the thermal expansions are uniform. For rods with gaps ≥ 0.12 mm, the expansion is nonuniform.

2.2 Comparisons of Correlation-Predicted Gap Conductances with Gap Conductances Obtained From Experimental Data

Figures 57 through 68 show comparisons of the individual test rod gap conductance values obtained from experimental measurements with the predicted gap conductances using the unadjusted Ross and Stoute correlation, and the Ross and Stoute correlation modified to account for relocation effects, for the range of rod powers tested. The data points shown on the plots are azimuthal averages for each test rod.

As noted previously, Rods GC 502, GC 522-2, and GC 523-2 have all been assumed to expand uniformly. Rod GC 523-2 (Xe, 0.94% gap, 95% TD) apparently also underwent plastic deformation of the cladding, and the actual posttest measured gap width was used

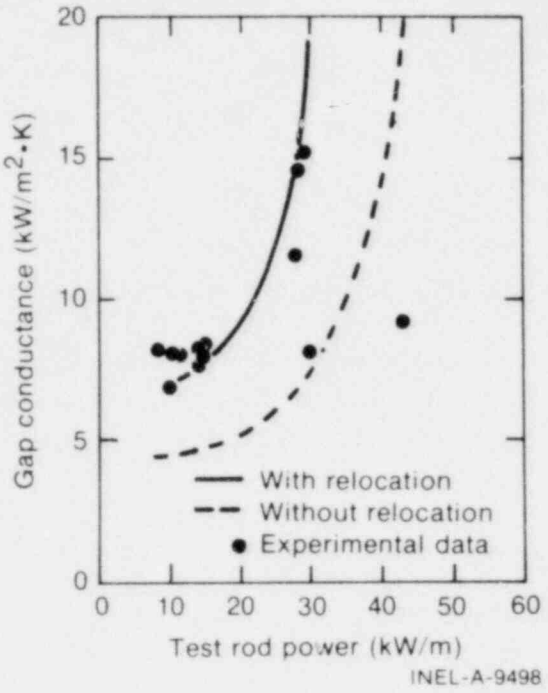

Fig. 57 Comparison of correlation-predicted gap conductance with values based on experimental data from Rod GC 502, Test GC 2-1 (He, 0.94% gap, 97% TD).

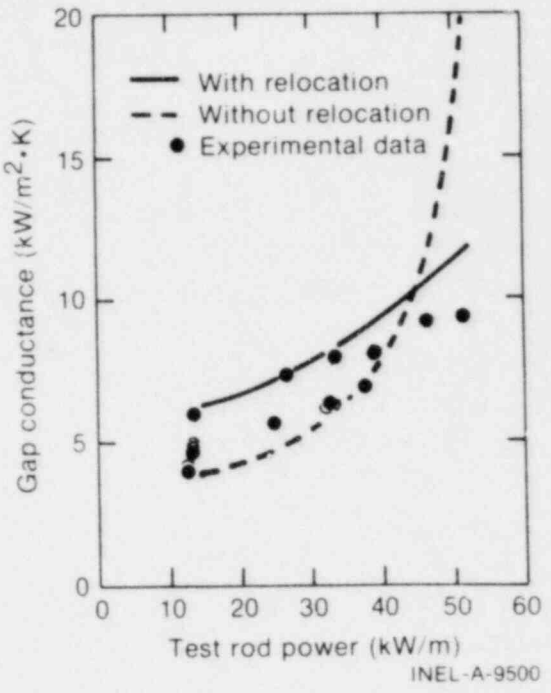

Fig. 58 Comparison of correlation-predicted gap conductance with values based on experimental data from Rod GC 522-3, Test GC 2-2 (He, 0.94% gap, 95% TD).

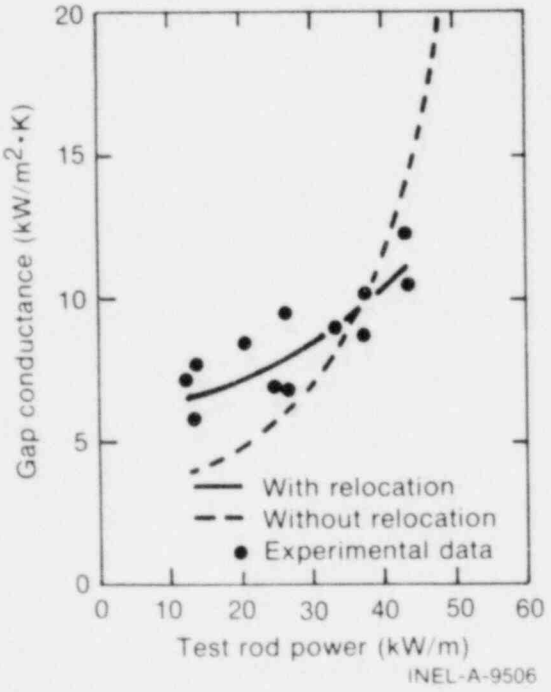

Fig. 59 Comparison of correlation-predicted gap conductance with values based on experimental data from Rod GC 523-1, Test GC 2-3 (He, 0.94% gap, 92% TD).

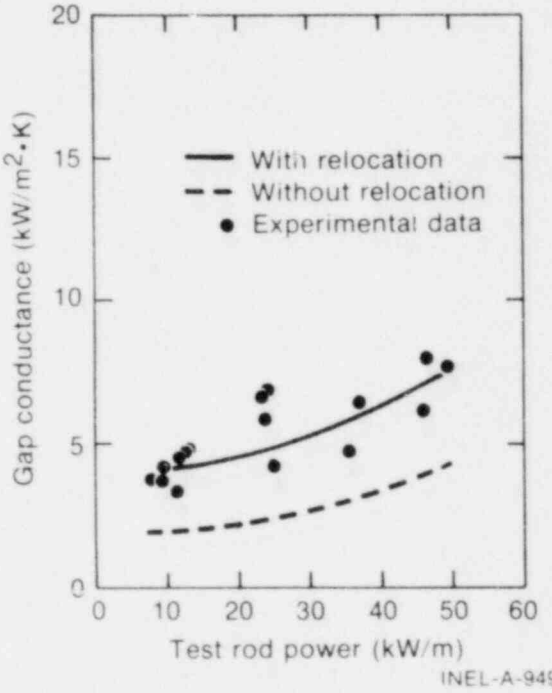

Fig. 60 Comparison of correlation-predicted gap conductance with values based on experimental data from Rod GC 503, Test GC 2-1 (He, 2.2% gap, 95% TD).

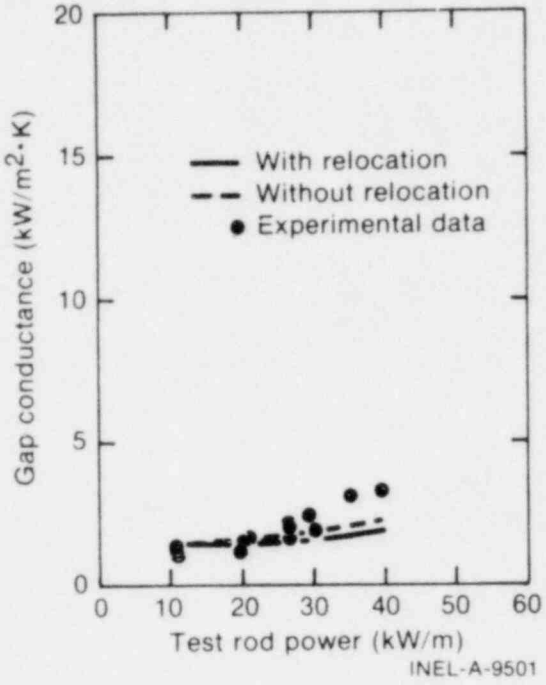

Fig. 61 Comparison of correlation-predicted gap conductance with values based on experimental data from Rod GC 522-4, Test GC 2-2 (He, 3.4% gap, 95% TD).

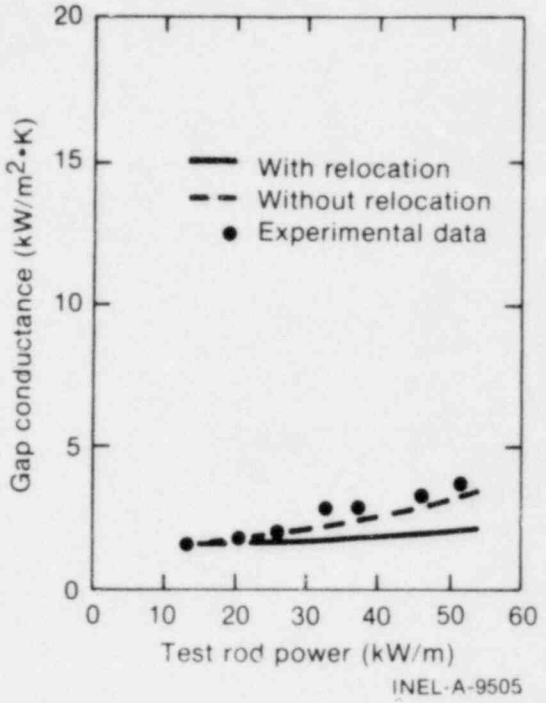

Fig. 62 Comparison of correlation-predicted gap conductance with values based on experimental data from Rod GC 523-3, Test GC 2-3 (He, 3.4% gap, 97% TD).

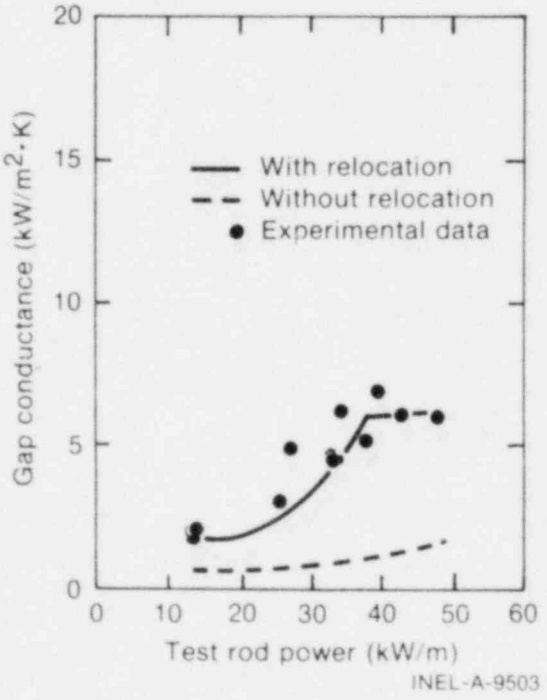

Fig. 63 Comparison of correlation-predicted gap conductance with values based on experimental data from Rod GC 522-2, Test GC 2-2 (Ar, 0.94% gap, 95% TD).

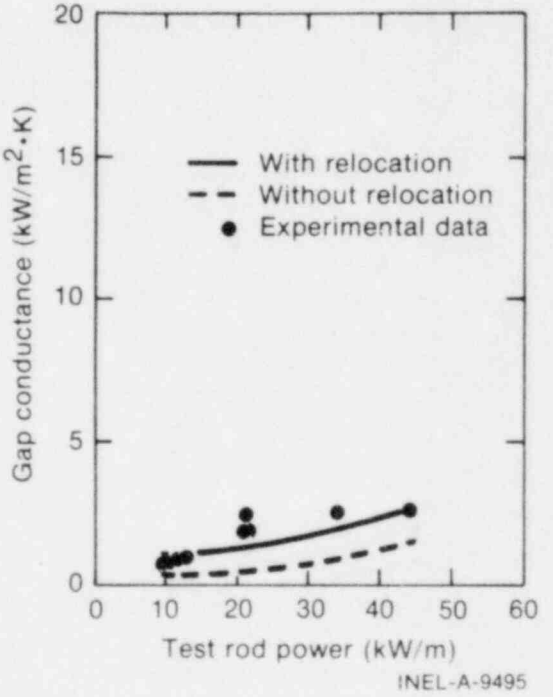

Fig. 64 Comparison of correlation-predicted gap conductance with values based on experimental data from Rod GC 504, Test GC 2-1 (Ar, 2.2% gap, 95% TD).

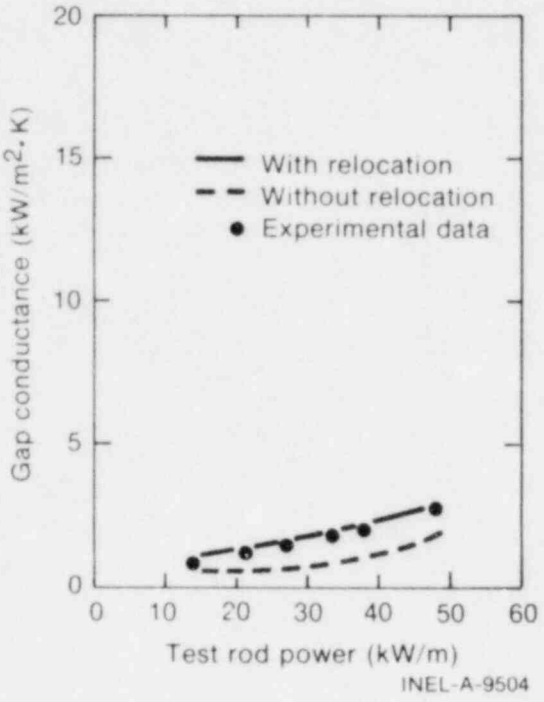

Fig. 65 Comparison of correlation-predicted gap conductance with values based on experimental data from Rod GC 523-4, Test GC 2-3 (Ar, 2.2% gap, 92% TD).

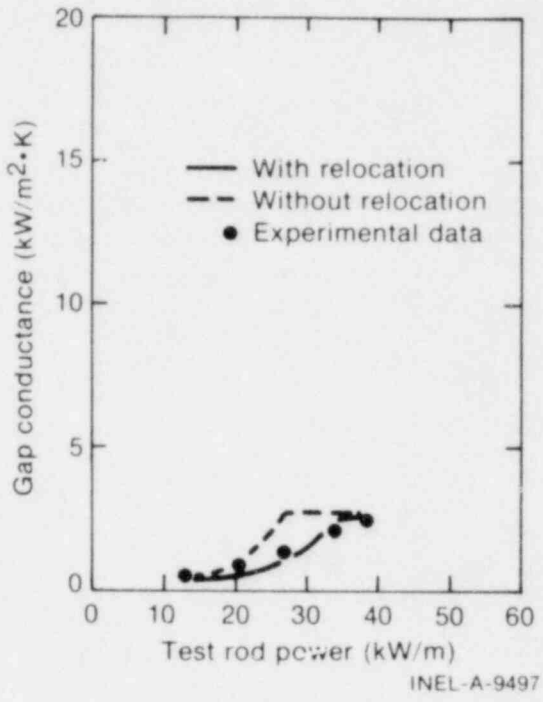

Fig. 66 Comparison of correlation-predicted gap conductance with values based on experimental data from Rod GC 523-2, Test GC 2-3 (Xe, 0.94% gap, 95% TD).

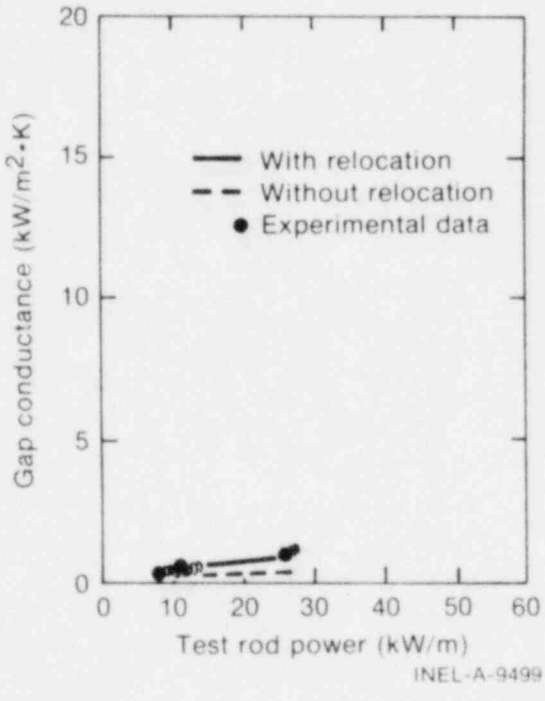

Fig. 67 Comparison of correlation-predicted gap conductance with values based on experimental data from Rod GC 501, Test GC 2-1 (Xe, 2.2% gap, 97% TD).

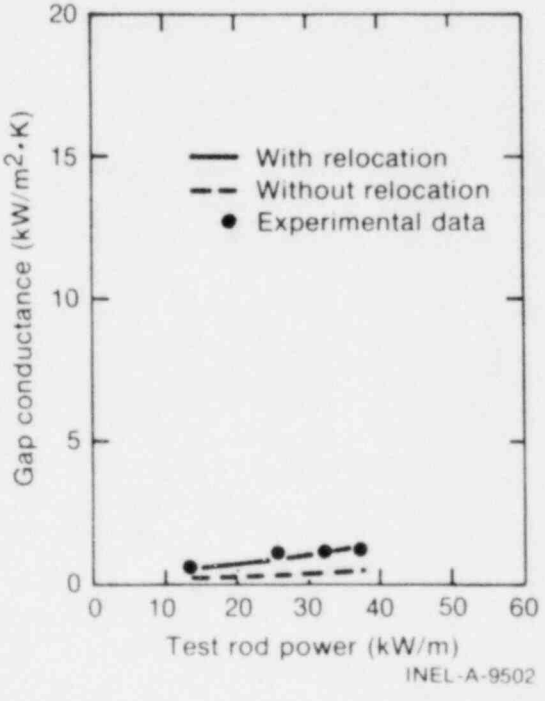

Fig. 68 Comparison of correlation-predicted gap conductance with values based on experimental data from Rod GC 522-1, Test GC 2-2 (Xe, 2.2% gap, 92% TD).

for the cold zero power gap width rather than the predicted value (Subsection 2.1.1), which is based on minimal cladding deformation.

Table IV provides a listing of the standard deviations between test-evaluated gap conductances and predictions by the modified Ross and Stoute correlation for all three tests. Figures 69 through 72 provide an indication of the correlations goodness of fit. For the three individual tests, Figures 69 through 71, and the combination of all three tests, Figure 72, the histograms of the frequency distribution of $(H_{correlation}-H_{measurement})$ are near normal with an absolute one-sigma standard deviation of ± 0.9154 kW/m^2-K and a relative one-sigma standard deviation of ± 25.38%, including 67.72% of the data comparisons.

The apparent result that a uniform thermal expansion model should be used for predicting gap conductance in very narrow gap rods and a nonuniform model should be used for wider gap rods is not totally satisfactory. The need for more than one model implies a discontinuity in fuel thermal response as a function of initial gap width that was not identified in the effective fuel thermal conductivity analyses.

Of the twelve rods tested, only three (Rods GC 502, GC 522-2, and GC 523-2) were better predicted by the uniform expansion model than by the nonuniform model. Close examination of the data shown in Figure 58 for the narrow gap helium rod (Rod GC 502) show three low-lying points that could be interpreted as identifying a different response curve for this rod that would best be fit by the nonuniform expansion model. These three low-lying points were obtained at steady state conditions during the power oscillation portion of Test GC 2-1, and could be an indication that the thermal response of the fuel had indeed changed after several ramps. However, other data (Appendix B, Figure B-11) show that the fuel off-center temperature measurement at the zero-degree orientation indicated an approximately 50 K lower temperature response during the oscillation period than during the power calibration and preconditioning periods at the same power levels, which would result in higher gap conductance values. The same behavior was observed by the off-center temperature measurement at 240 degrees, as shown in Appendix B, Figure B-13. For gap conductance analyses, the narrow gap helium rods are extremely sensitive to small changes in the fuel surface temperature because the ΔT across the gap is small; therefore, it is not unreasonable to expect that the uncertainty in the narrow gap helium rod, Rod GC 502, gap conductance values would be large enough to permit the results to be predicted by either the uniform or the nonuniform expansion models. For the thermal conductivity analysis, only data obtained during the power calibration period were used because the centerline thermocouple failed during the initial part of the oscillation period. Test GC 2-5 will provide additional narrow gap helium filled test rod data that will aid in evaluating the thermal response of the narrow gap rods.

With respect to test Rods GC 522-2 and GC 523-2, the argon and xenon filled narrow gap rods, respectively, the low conductivity fill gases in these rods was observed to cause high fuel temperatures at very low power levels, resulting in early gap closure between fuel and cladding. Since the gap is essentially closed at low powers in these rods, subsequent thermal expansion would also be expected to be essentially the same as for a solid pellet

TABLE IV

STANDARD DEVIATIONS OF FIT BETWEEN PREDICTIONS OF GAP CONDUCTANCE AND VALUES BASED ON EXPERIMENTAL MEASUREMENTS

Test Rod	Number of Data Points-n	Standard Deviation ($kW/m^2 \cdot K$)	Relative Standard Deviation[a] (dimensionless)
GC 502(He, 0.94% gap, 97% TD)	11[b]	0.9606	0.1066
GC 522-3(He,0.94% gap, 95% TD)	17	1.7573	0.3039
GC 523-1(He,0.94% gap, 92% TD)	12	0..9693	0.1160
GC 503(He, 2.2% gap, 95% TD)	16	1.0036	0.1870
GC 522-4(He, 3.4% gap, 95% TD)	16	0.7037	0.2577
GC 523-3(He, 3.4% gap, 97% TD)	7	1.1973	0.3765
GC 522-2(Ar, 0.94% gap, 95% TD)	14	0.8715	0.1833
GC 504(Ar, 2.2% gap, 95% TD)	9	0.6093	0.3260
GC 523-4(Ar, 2.2% gap, 92% TD)	6	0.2691	0.2761
GC 523-2(Xe, 0.94% gap, 95% TD)	5	0.4390	0.3400
GC 501(Xe, 2.2% gap, 97% TD)	10	0.1794	0.4492
GC 522-1(Xe, 2.2% gap, 92% TD)	4	0.1623	0.1454
	127	0.9154	0.2538

[a] (absolute) = $H_{prediction} - H_{measurement}$

(relative) = $\frac{H_{prediction} - H_{measurement}}{H_{measurement}}$

[b] Two points have been excluded from this listing: 30.0 kW/m, 8.18 $kW/m^2 \cdot K$ and 43.38 kW/m, 9.27 $kW/m^2 \cdot K$.

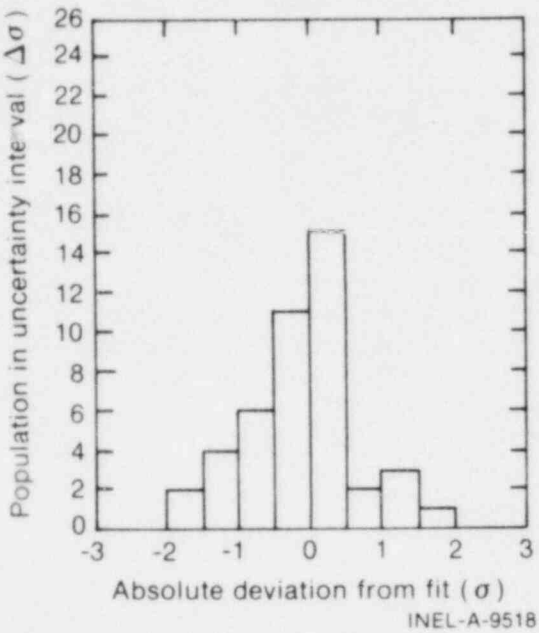

Fig. 69 Histogram of fitting uncertainty of the correlation for gap conductance for all rods in Test GC 2-1.

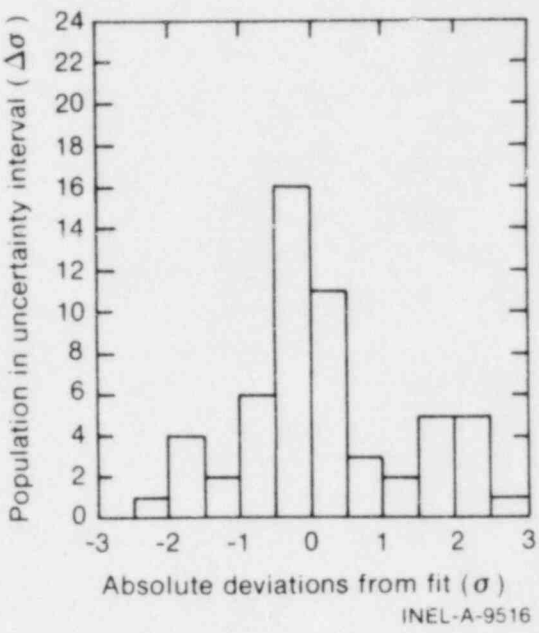

Fig. 70 Histogram of fitting uncertainty of the correlation for gap conductance for all rods in Test GC 2-2.

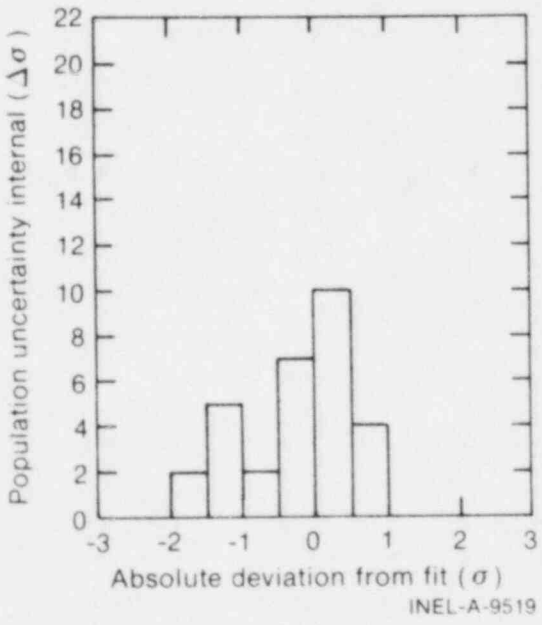

Fig. 71 Histogram of fitting uncertainty of the correlation for gap conductance for all rods in Test GC 2-3.

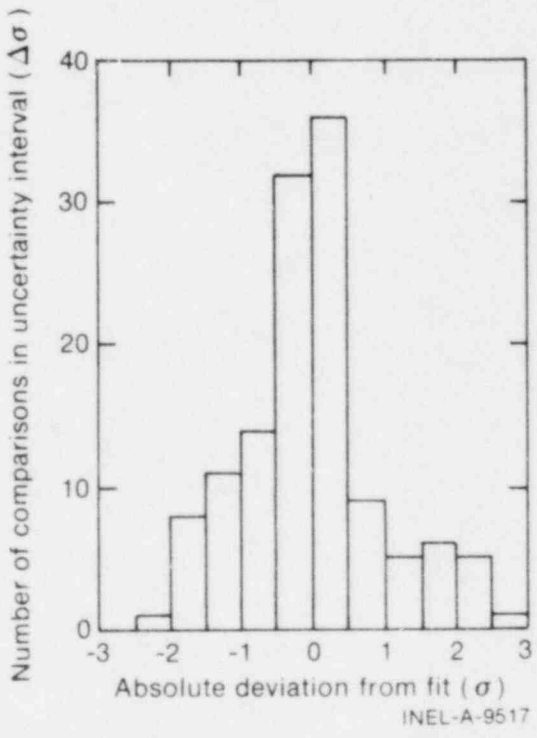

Fig. 72 Histogram of fitting uncertainty of the correlation for gap conductance for all rods in Tests GC 2-1, GC 2-2, and GC 2-3.

(that is, uniform thermal expansion), even after the pellets have cracked. In addition, because of the high fuel temperatures, the ΔT across the gap is large and the gap conductance is much less sensitive to small pellet surface temperature variations than it is in the narrow gap helium filled test rods.

2.3 Estimated Uncertainties in Evaluated Gap Conductances

The fitting or correlational uncertainty, σ_f, was calculated in the previous section. The fitting uncertainty is a measure of how well the existing xenon, argon, and helium test rod gap conductance data are fit by the described gap conductance correlation.

To predict how well the correlation will fit new data, an estimate of the data acquisition process uncertainties must be made. The identified data acquisition uncertainties can be lumped together and called the measured gap conductance uncertainty, σ_m.

To obtain an estimate of the total uncertainty, σ_p, in the prediction σ_m and σ_f are combined. In the combination, σ_m is assumed to be independent of σ_f (that is, correlation coefficients are ~zero), or at least that the following combination overpredicts the uncertainty:

$$\left(\sigma_p\right)^2 = \left(\sigma_m\right)^2 + \left(\sigma_f\right)^2$$

Evaluation of σ_m is based on the assumption that the testing technology that was used to acquire data for Tests GC 2-1, GC 2-2, and GC 2-3 will apply for future tests.

2.3.1 Calculation of the Measured Gap Conductance Uncertainty (σ_m).

Since

$$h_g\,(\text{Meas}) = Q/A(T_S - T_C),$$

$$\sigma_m = f(\sigma_Q,\ \sigma_A,\ \sigma_{T_S},\ \sigma_{T_C})$$

where

σ_Q = uncertainty in the pellet surface heat flux

σ_A = uncertainty in the pellet surface heat transfer area.

The average gap surface temperature difference uncertainty is assumed to include the following components:

σ_{T_S} = f (fuel conductivity and measured temperature uncertainties)

σ_{T_C} = f (cladding conductivity and measured temperature uncertainties)

so that

$$\sigma_{T_S} = f(\sigma_R, \sigma_{ACC}, \sigma_{AS}, \sigma_{LOC}, \sigma_{KFUEL}, \sigma_Q, \sigma_A)$$

$$\sigma_{T_C} = f(\sigma_R, \sigma_{ACC}, \sigma_{KCLAD}, \sigma_Q)$$

where

(1) σ_{LOC} is the off-center temperature measurement uncertainty extrapolated to the fuel pellet surface due to the uncertainty in the off-center thermocouple radial location within its hole. Analyses for evaluating the perturbation effects of off-center thermocouples are described in Appendix C.

(2) σ_{AS} reflects the temperature measurement uncertainty extrapolated to the pellet surface which exists if a solid fuel pellet is allowed to move around in the cladding. TOODEE half-pellet studies indicate that movement away from a symmetric fuel-cladding orientation may induce, within a tested fuel pellet, diametral temperature profile changes and temperature upsets at the azimuthally located off-center temperature measurement locations. Analyses for evaluating the effects of fuel pellet eccentricity are described in Appendix C.

(3) σ_{KFUEL} and σ_{KCLAD} are the fuel and cladding thermal conductivity uncertainties (from MATPRO) and account for the fact that the pellet-to-cladding gap temperatures are inferred rather than directly measured. T_S and T_C are obtained by extrapolating measured cladding and fuel off-center temperatures.

(4) σ_Q reflects the local test rod power level uncertainties. When three equally spaced off-center thermocouples are operating within a test pellet, the contribution from the uncertainty in the azimuthal pellet surface heat flux is approximately zero. When only one or two off-center thermocouples exist, this uncertainty may be significant. To obtain a first estimate of the total uncertainty, this effect will be neglected. Other contributions to this uncertainty arise from the uncertainty in calculating the precise relative axial power level within the test fuel rod while simultaneously calculating the proper calorimetric integrated power of the test power level. These two uncertainties are assumed at a one-sigma level to be a ± 3% uncertainty in calorimetrics and a ± 2.5% axial power level calculational uncertainty. Assuming independence and linearity at an inferred one-sigma level, the combined local test power level uncertainty is <3.9%.

(5) σ_A reflects the uncertainty in the pellet surface heat transfer area. Because of radial thermal expansion and pellet relocations, the area of pellet heat transfer is unknown. Error propagation analyses, however, indicate the effect of the uncertainty in pellet surface area on the measured gap conductance is negligible.

(6) σ_R and σ_{ACC}, the recording system and thermocouple measurement accuracies, are discussed in Appendix A.

An indication of the variability in fuel pellet surface temperatures, possibly due to assymetrics in pellet-cladding orientation and relocation, may be inferred from the data shown in Figures 73, 74, and 75. These plots represent three samples of the test data that illustrate azimuthal variations in measured off-center temperatures. It is easily seen how the failure of a single off-center thermocouple may bias the evaluated average off-center temperature measurement.

2.3.2 Evaluation of σ_P from σ_m and σ_f. Evaluations of σ_m and σ_f have been performed for six representative test fuel rods from Tests GC 2-1, GC 2-2, and GC 2-3. Estimates of the total uncertainty in a prediction, σ_P, for Rods GC 502, GC 503, GC 522-4, GC 504, GC 522-2, and GC 523-3 have been made and are shown as a function of test rod power density in Figures 76 through 81, respectively.

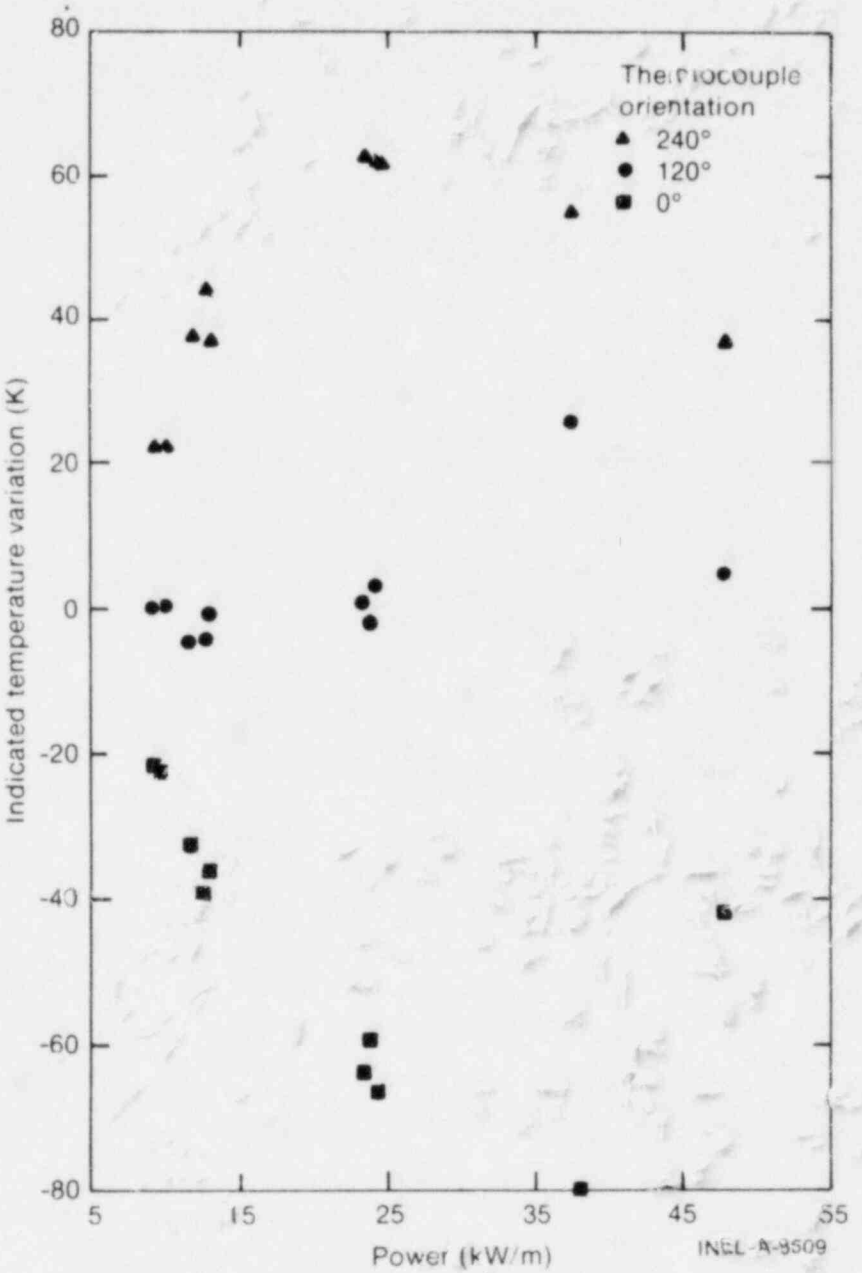

Fig. 73 Representative azimuthal variations from the mean of measured fuel off-center temperatures in Rod GC 503, Test GC 2-1.

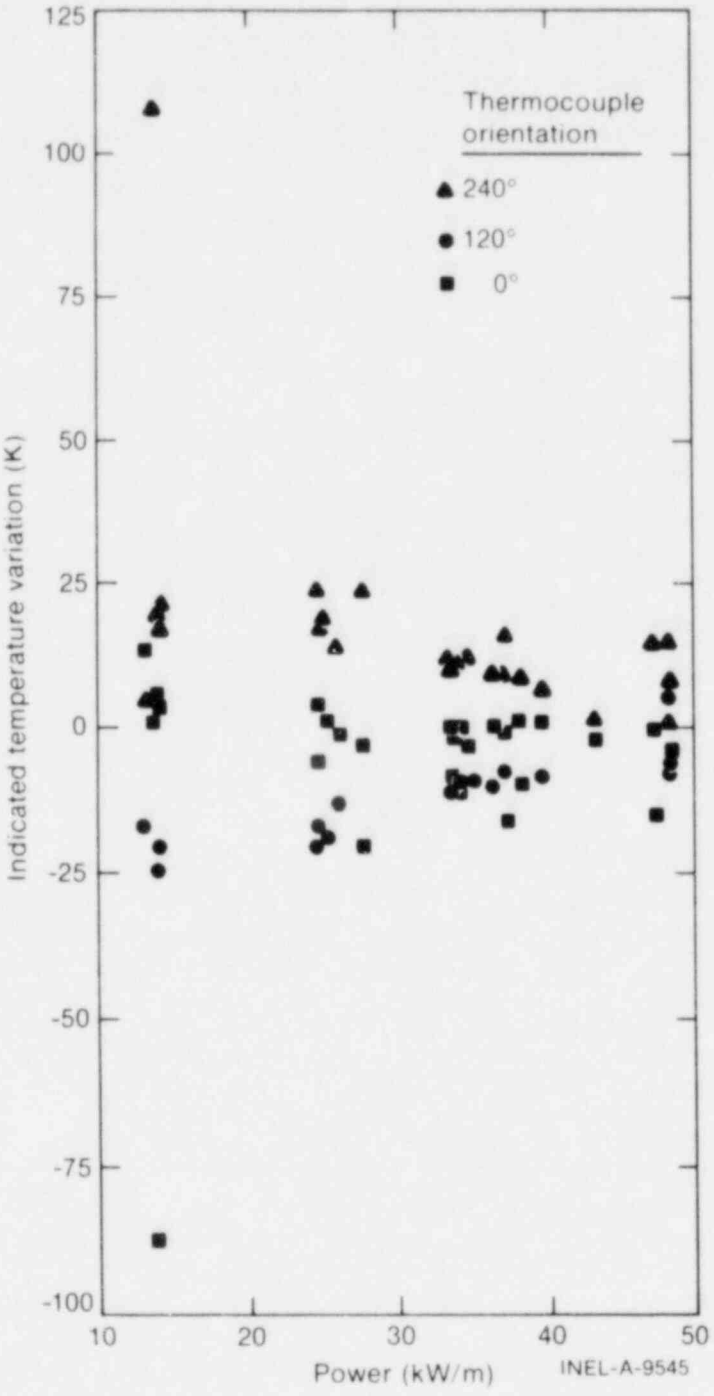

Fig. 74 Representative azimuthal variations from the mean of measured fuel off-center temperatures in Rod GC 522-2, Test GC 2-2.

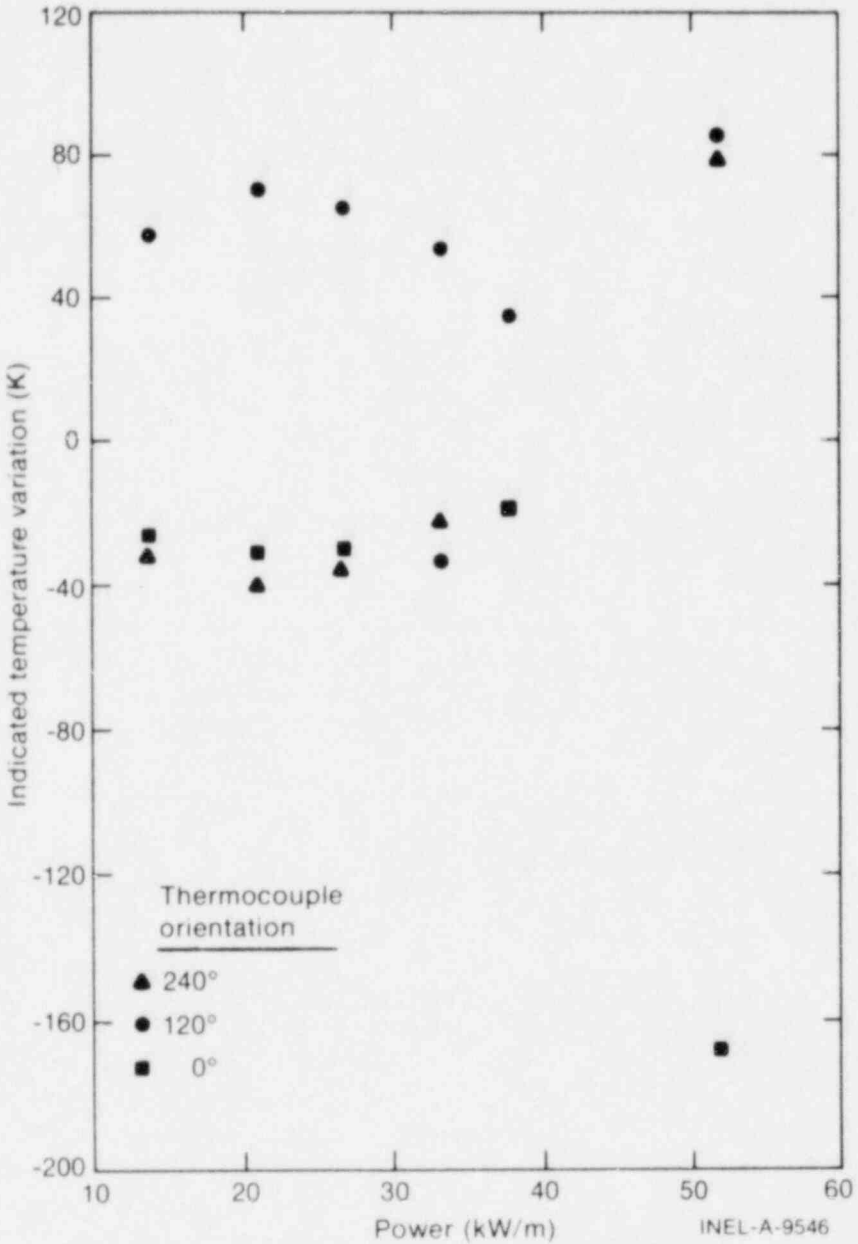

Fig. 75 Representative azimuthal variations from the mean of measured fuel off-center temperatures in Rod GC 523-3, Test GC 2-3.

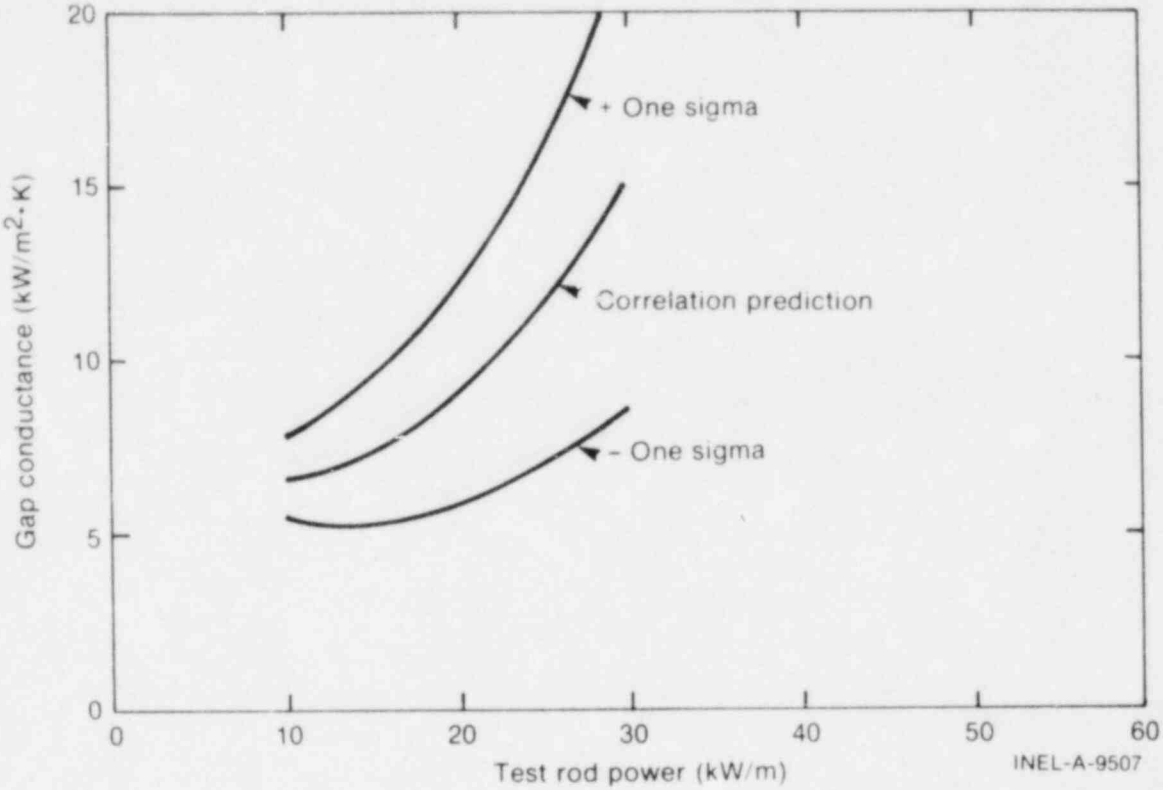

Fig. 76 Estimated one-sigma uncertainty error bounds on the correlation prediction for Rod GC 502, Test GC 2-1, with two operational off-center thermocouples.

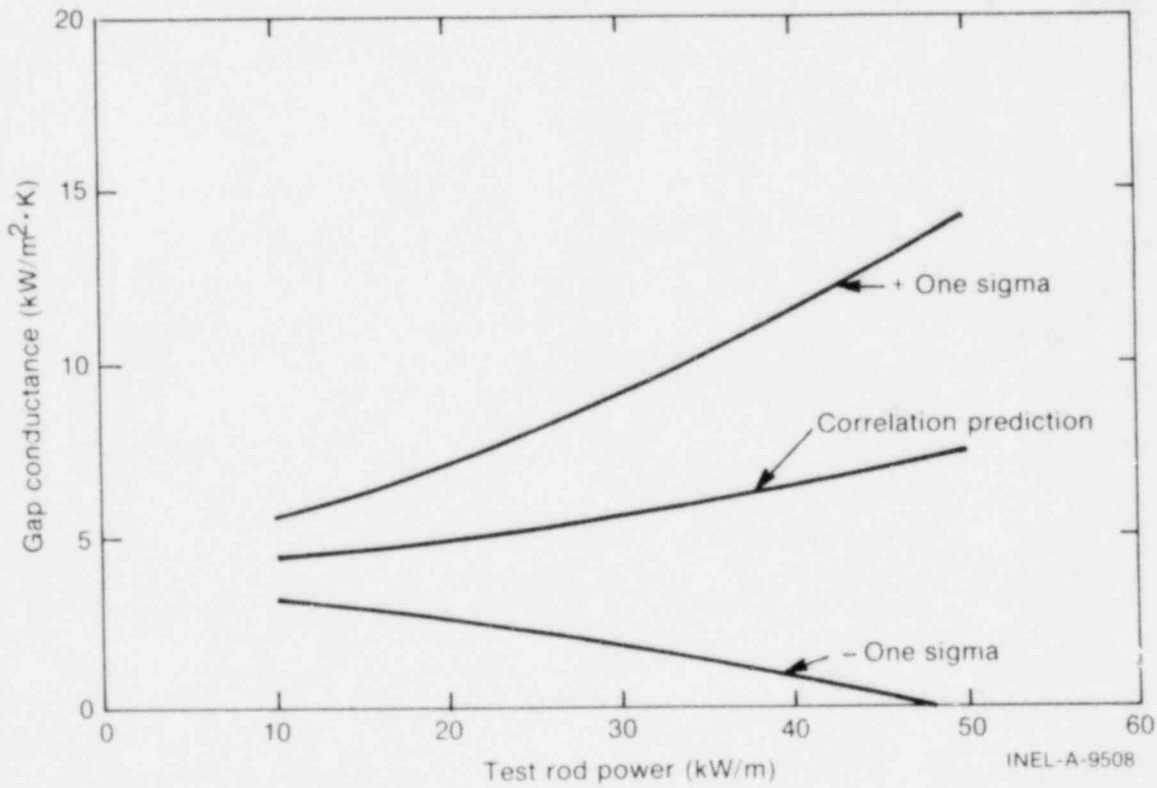

Fig. 77 Estimated one-sigma uncertainty error bounds on the correlation prediction for Rod GC 503, Test GC 2-1, with three off-center thermocouples.

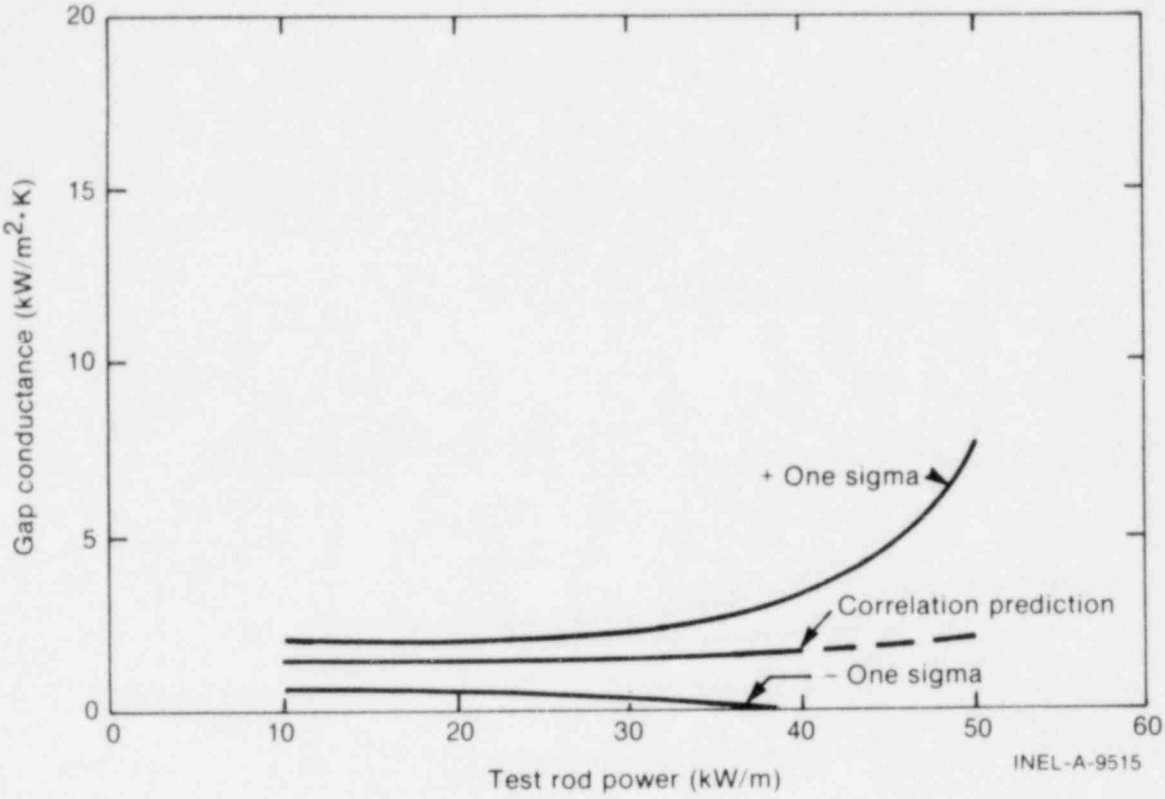

Fig. 78 Estimated one-sigma uncertainty error bounds on the correlation prediction for Rod GC 504, Test GC 2-2, with one off-center thermocouple.

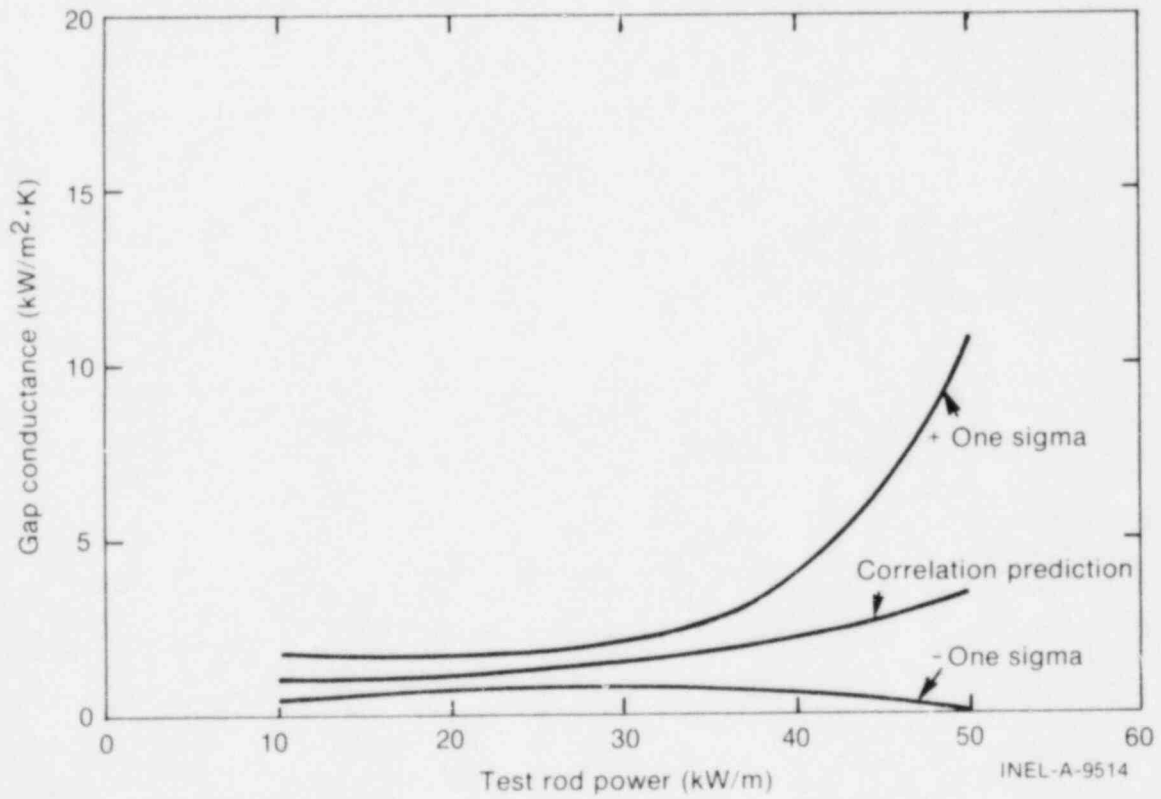

Fig. 79 Estimated one-sigma uncertainty error bounds on the correlation prediction for Rod GC 504, Test GC 2-1, with one off-center thermocouple.

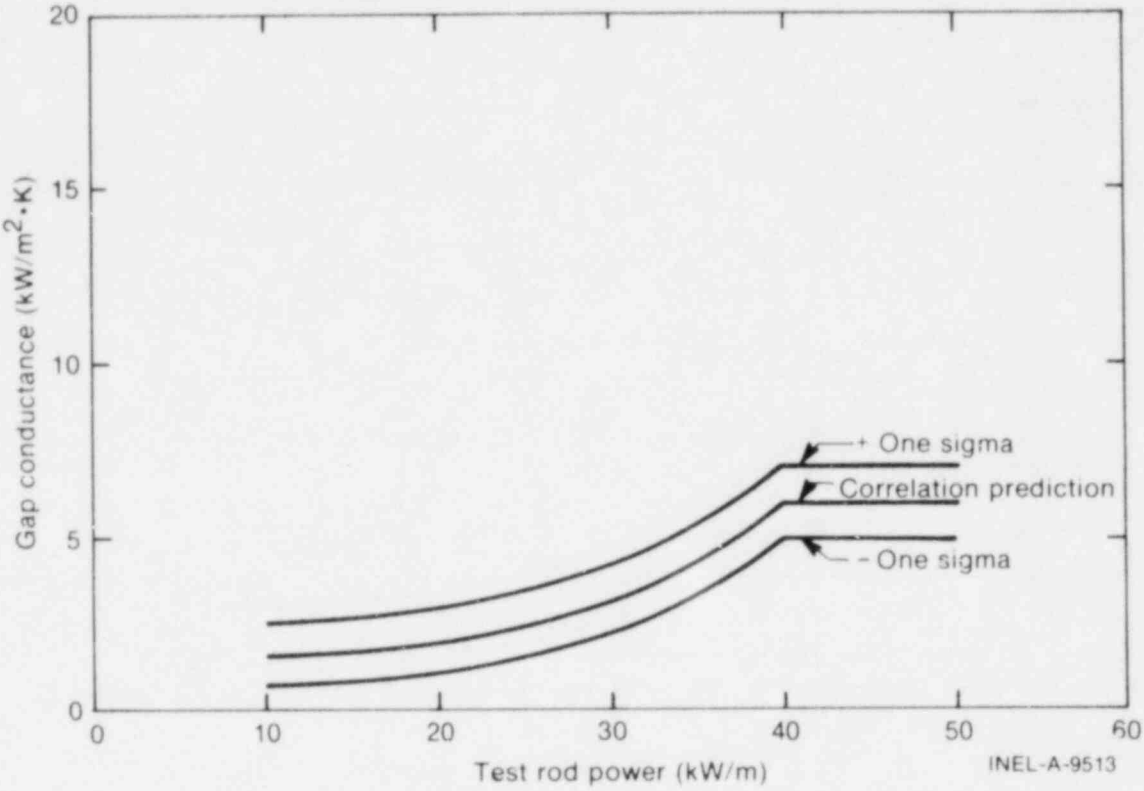

Fig. 80 Estimated one-sigma uncertainty error bounds on the correlation prediction for Rod GC 522-2, Test GC 2-2, with three off-center thermocouples.

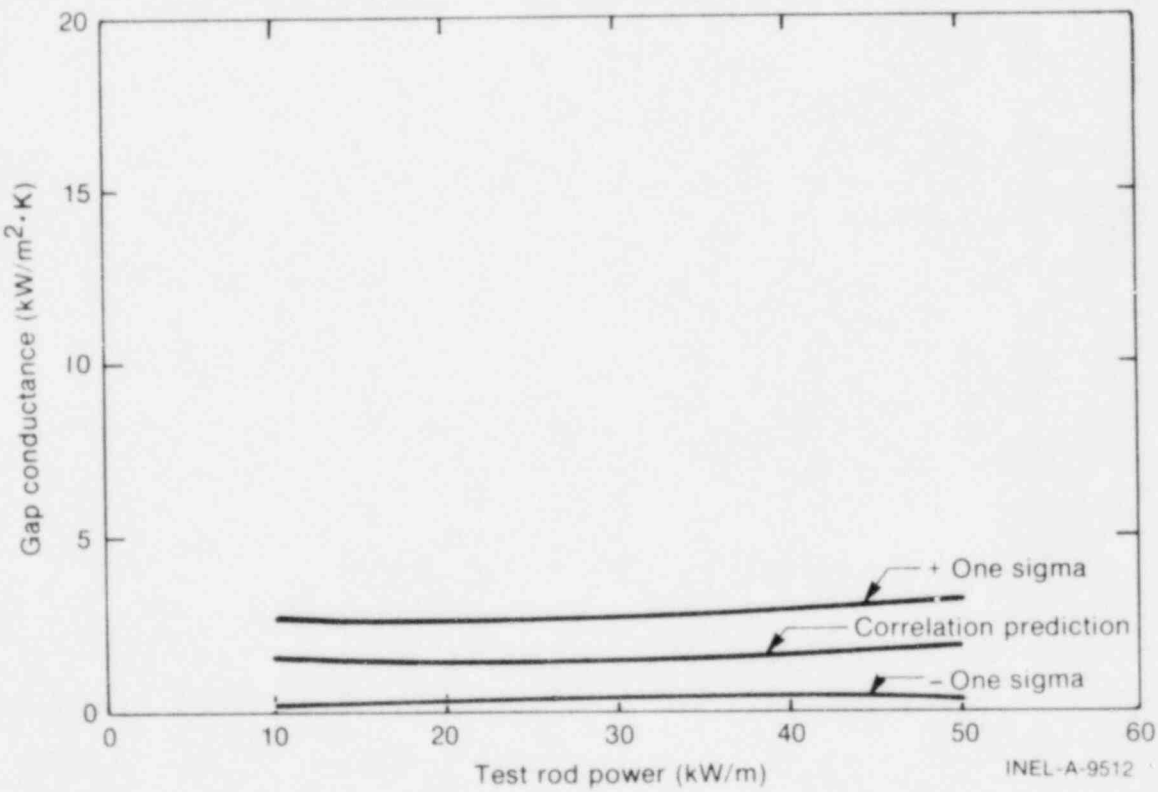

Fig. 81 Estimated one-sigma uncertainty error bounds on the correlation prediction for Rod GC 523-3, Test GC 2-3, with three off-center thermocouples.

VI. ANALYSIS OF EXPERIMENT POWER OSCILLATION RESULTS

The power oscillation (or thermal oscillator) method for estimating gap conductance relates the fuel-to-cladding gap conductance to the phase relationship between a sinusoidal fuel rod power oscillation and the corresponding cladding surface temperature response. During a power oscillation, the two signals will oscillate at the same frequency, but with a phase lag between the power signal and the cladding surface temperature signal. The gap conductance can theoretically be determined from analytical relationships between the measured phase lag and the gap conductance. The impetus for evaluating the power oscillation method stems from the need to evaluate gap conductance in irradiated fuel rods. By this method, only the relative cladding surface temperature response and the fuel rod power density need be measured to obtain sufficient data for evaluating the fuel-to-cladding gap conductance. The method, if practicable, would allow determination of gap conductances in irradiated fuel rods without the need for fuel temperature measurements. The power oscillation method is described in detail in Appendix C.

1. COMPARISON OF POWER OSCILLATION AND STEADY STATE GAP CONDUCTANCE VALUES

Power oscillation gap conductance values were determined for each fuel rod at the locations of the cladding surface thermocouples over a wide range of test rod powers. The power oscillation gap conductance values determined from thermocouples located at the peak of the axial flux profile were compared with steady state gap conductance values determined from the corresponding off-center fuel temperature measurements over the same range of test rod powers. Figures 82, 83 and 84 show representative comparisons between steady state and power oscillation gap conductance values. The oscillation data shown are for a power oscillation amplitude of ± 20% at an oscillation period of 20 s. The vertical boxes in Figures 82, 83 and 84 indicate the range of azimuthal variation in gap conductance determined by both methods (steady state and power oscillation) at a specified test rod power density. The figures show that, in general, the oscillation values are higher than the steady state values, and tend to exhibit a large amount of azimuthal variation, especially at the higher power densities, but also considerable randomness in the amount of azimuthal variations. At lower power densities, agreement between values determined by the two methods is much better.

More specifically, the comparisons shown in Figure 82 indicate that within the range of scatter shown, the power oscillation and steady state values for the narrow and medium gap rods are generally in agreement, but the power oscillation values for the wide gap rods are significantly larger than the steady state values. An interpretation of this effect of hot gap width on the power oscillation results is that during the power oscillations, the pellet-to-cladding gap may be closed, or nearly closed, during the power increase, and open during the power decrease. This effect would be more pronounced in the wide gap rods than in narrow or medium gap rods because the change in the temperature drop across the gap

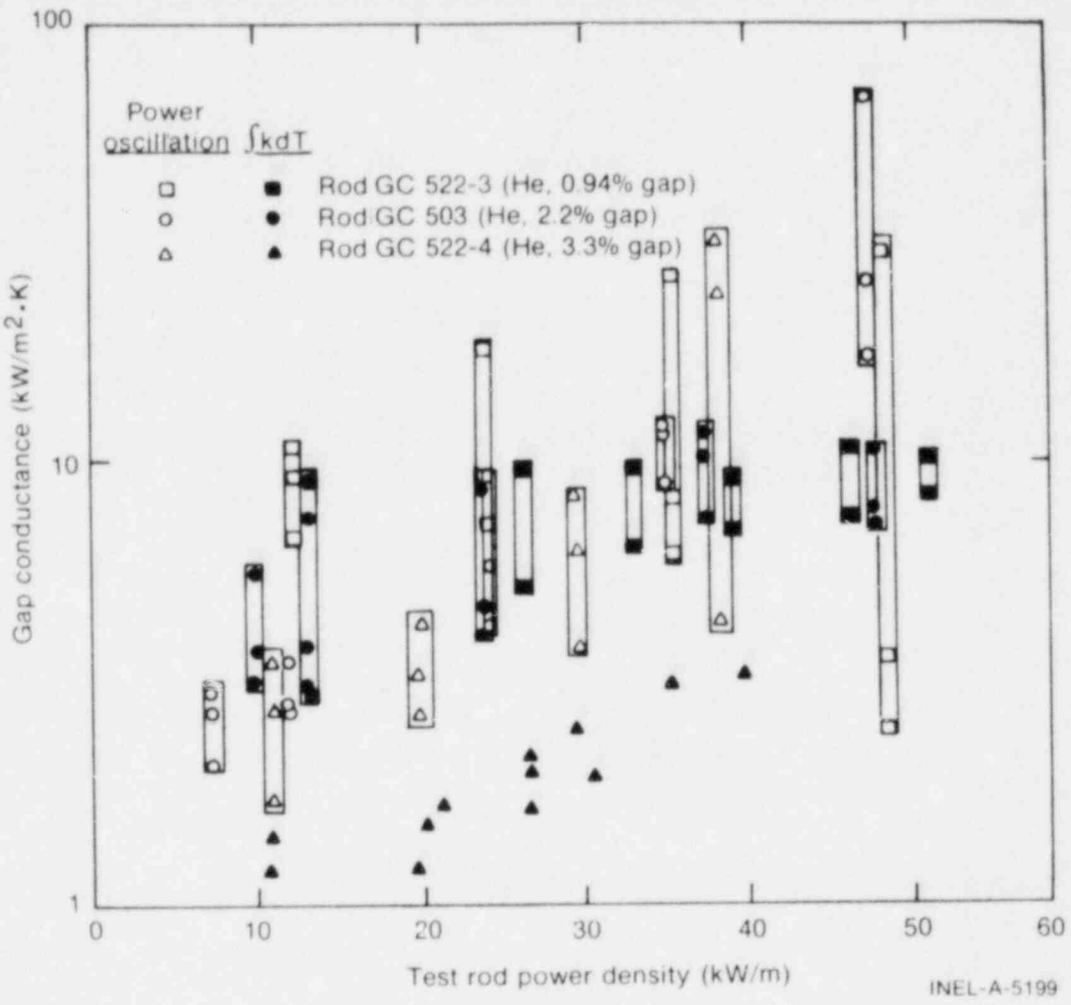

Fig. 82 Comparison of gap conductance values obtained by steady state and power oscillation methods for three helium filled test rods.

would be greater in the wide gap rods. The random nature of scatter in the power oscillation data indicate that random pellet-to-cladding contact is occurring during power oscillations when the hot gap is small. Pellet-to-cladding contact during a portion of a power cycle would be expected to result in a distorted output signal, which, when analyzed at the fundamental frequency by the MACRAN-III computer code, would yield an unrealistic power to cladding temperature phase relationship. Probable causes of pellet-to-cladding contact at power levels below the predicted gap closure regime are (a) fuel pellet thermal expansion, (b) pellet cracking and fragment relocation, and (c) pellet motion during power oscillations.

Figure 83 shows an example of the effect of fill gas composition on the comparison between power oscillation and steady state gap conductance values in narrow gap rods. The oscillation data again show trends that are consistent with the steady state results, but are generally higher and have a significantly larger amount of scatter. The distinction between the power oscillation results for the different rods is much less clear than it is for the steady state results.

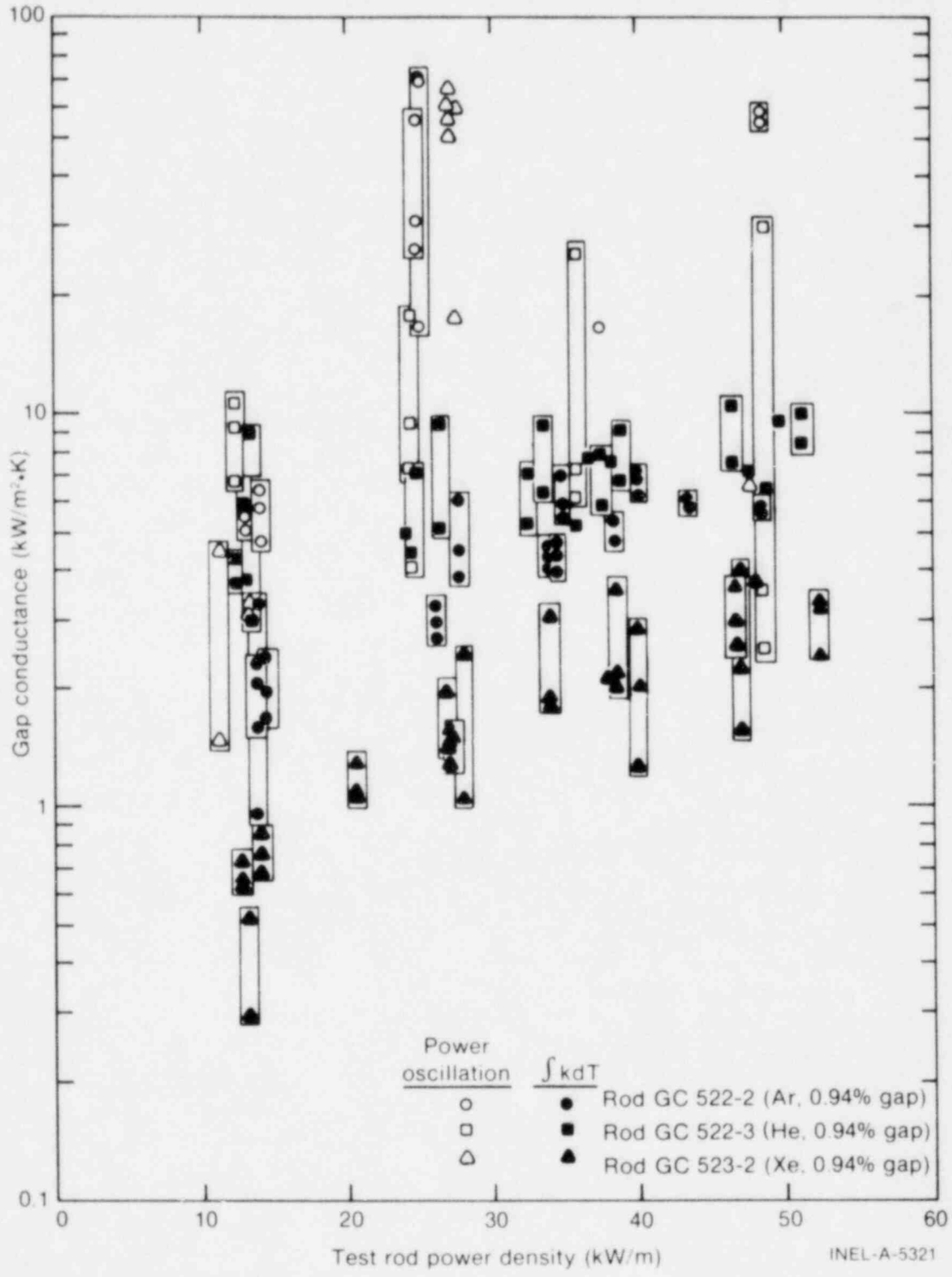

Fig. 83 Comparison of gap conductance values obtained by steady state and power oscillation methods for 0.94% initial diametral gap rods.

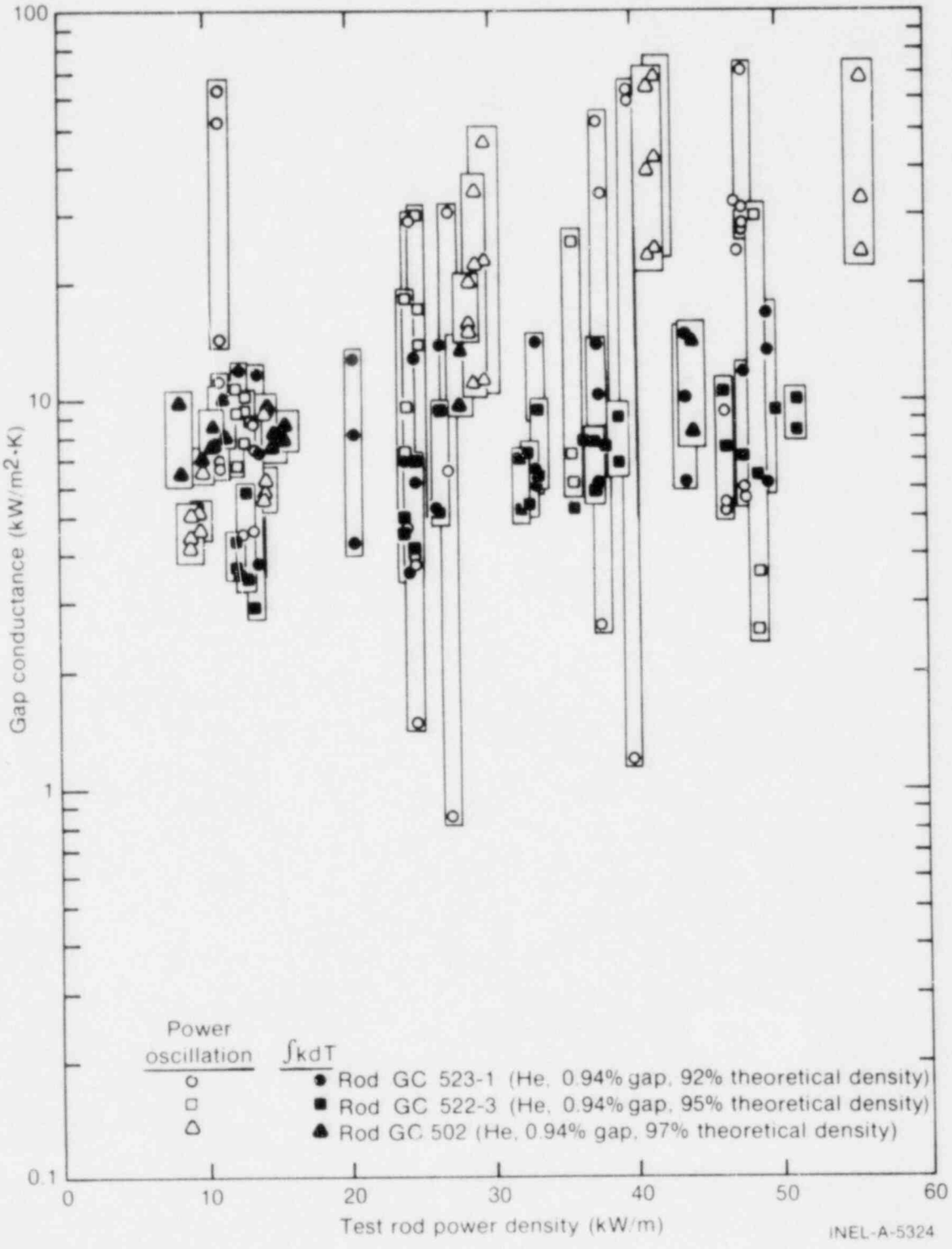

Fig. 84 Comparison of gap conductance values obtained by steady state and power oscillation methods for 0.94% initial diametral gap helium rods.

Comparisons between power oscillation and steady state gap conductance values that show the effect of fuel density are shown in Figure 84. Again, the trend is for the power oscillation results to be slightly larger than the steady state values and to exhibit much more scatter in the results, especially at power levels above which pellet-to-cladding gap closure would be expected to occur. Taking the scatter in the azimuthal variations into account, however, the power oscillation results also indicate very little effect from variations in fuel density.

The relatively poor agreement between the power oscillation and steady state evaluated gap conductances, as shown by the representative comparisons in Figures 82, 83, and 84, was unexpected. Power oscillations results obtained with pressurized water reactor (PWR) design test fuel rods are, generally, in much better agreement with the steady state results. (The design details of some of the PWR tests are presented in Appendix D.) Observation of the BWR rod cladding and off-center temperature response waveforms during oscillation revealed significant nonlinearities in the signals at higher power levels, and indicated a need for additional analyses to provide an appropriate basis for evaluating the power oscillation method. These additional analyses were performed on the specific waveforms of the individual detector responses. To provide additional comparisons between BWR and PWR rod design results, the additional waveform analyses were also performed on the PWR test results, as described in the following section.

2. POWER OSCILLATION WAVEFORM ANALYSIS

Inherent in the oscillation method is the assumption that the amplitude of the driving function (power) is sufficiently small that nonlinearities in the fuel rod system are negligible. Potential sources of nonlinearities during an oscillation are changes in fuel thermal conductivity and gap width. The effects of nonlinearities in the fuel rod response can be exhibited in two forms: (a) asymmetry in the phase shift between the minimum and maximum in the power oscillation waveform and the minimum and maximum in the cladding temperature oscillation waveform, and (b) distortion in the shape of the cladding surface temperature waveform as exhibited by deviations from a smooth function. Cladding surface temperature waveforms were analyzed at several different power levels to determine if significant waveform distortion or asymmetry was occurring, and to quantitatively determine the effect of the observed nonlinearities on the results obtained by the oscillation experimental method.

2.1 Analytical Methods

An eighth-order recursive Fourier-fit routine was developed for the CDC 7600 computer to analyze the digitized oscillation data. The data were time averaged over 20 cycles of power oscillations in increments of 1 s to obtain a statistically valid oscillation cycle. The Fourier-fit of the data was then plotted with the time averaged data points to observe whether the fit was a reasonable approximation to the data. If the fit was adequate, the function was then plotted over ten cycles of the original data set to verify the time

averaged cycle approximation. Additional verification of the single cycle approximation was accomplished by comparing phase angles between the cladding thermocouples and power signals determined from a first-order Fourier-fit of the time averaged data with cycle averaged phase angles from the MACRAN-III[9] analysis.

2.2 BWR Design Test Rods

To investigate the cladding surface temperature waveform nonlinearities, the eighth-order Fourier-fit function was used to determine the relative times corresponding to cladding temperature oscillation minimum and maximum. These times were related to the sinusoidal driving function (power oscillation) to determine a minimum and maximum phase angle. The minimum and maximum phase angles determined by this method, and the comparison between the first-order Fourier-fit and the MACRAN-III phase angles, are listed in Table V for the power levels investigated. Within the uncertainty in determining the first-order fit minimum and maximum (± 1.8 degrees), the fit and the MACRAN-III phase angles agree very well. This agreement indicates that in most cases the Fourier-fit to the time averaged single cycle is a good approximation to the entire oscillation data set at a specific power level.

Table V also shows that a significant variation exists between the minimum and maximum phase angles determined from the eighth-order Fourier-fit to the data. This variation indicates that the oscillation waveforms are significantly asymmetric. To identify the amount of asymmetry, the mean phase difference between the minimum and maximum for each fuel rod (average from all cladding thermocouples at the same axial position on each rod) at individual power levels was calculated. The results of these calculations are listed in Table VI.

Although the uncertainty in the mean phase difference is greater than 2.5 degrees, the data in Table VI suggest that the degree of asymmetry in the cladding surface temperature waveforms for a ± 20% power oscillation is dependent on the fuel rod design and test rod power density. Limited time for analysis precluded quantitive evaluation of the test rod design parameter and power density effects on the oscillation waveform asymmetry.

To observe possible oscillation waveform distortion, the averaged cladding temperature response was plotted along with the time averaged data points. The power driving function and its first-order Fourier-fit were plotted on the same relative time scale to provide a basis for comparison. Figures 85(a-f) through 88(a-f) are representative plots of the time averaged data points and the appropriate Fourier-fits at four power levels. All of the data for these plots were obtained at an oscillation amplitude of ± 20% and oscillation period of 20 s, from Test GC 2-3. The reference signal for all Figures 85 through 88 (b) and (c) at all power levels is shifted in time from the reference signal for Figures 85 through 88 (e) and (f) due to a time shift during the digitizing process. In Figures 85 through 88, the eighth-order Fourier-fit sufficiently reproduced the experimental data so the data points are not shown on the plots.

TABLE V

COMPARISONS BETWEEN FOURIER-FIT WAVEFORM ANALYSIS PHASE ANGLES AND PHASE ANGLES DETERMINED BY MACRAN-III FOR TEST GC 2-3

Transducer Identifier[a]	Test Rod Power[b] = 13.0 kW/m				Test Rod Power[b] = 26.7 kW/m				Test Rod Power[b] = 37.5 kW/m				Test Rod Power[b] = 47.0 kW/m			
	Eighth-Order Fit (degrees)		First-Order Fit (degrees)	MACRAN-III Phase (degrees)	Eighth-Order Fit (degrees)		First-Order Fit (degrees)	MACRAN-III Phase (degrees)	Eighth-Order Fit (degrees)		First-Order Fit (degrees)	MACRAN-III Phase (degrees)	Eighth-Order Fit (degrees)		First-Order Fit (degrees)	MACRAN-III Phase (degrees)
	Minimum	Maximum			Minimum	Maximum			Minimum	Maximum			Minimum	Maximum		
CLDTEMP 11	-45.9	-40.5	-45.9	-46.6	-49.5	-45.9	-47.7	-47.60	-60.3	-42.3	-67.5	-66.96	-51.3	-8.1	-38.7	-37.12
15	-42.3	-36.9	-42.3	-42.8	-44.1	-42.3	-40.5	-40.22	-42.3	-33.3	-35.1	-35.16	-54.9	-47.7	-40.5	-39.95
21	-45.0	-45.0	-50.4	-50.84	-36.0	-37.8	-39.6	-38.75	N/A	N/A	N/A	N/A	N/A	N/A	N/A	N/A
25	-67.5	-65.7	-63.9	-64.64	-33.3	-31.5	-33.3	-32.45	-31.5	-29.7	-27.9	-28.58	-20.7	-27.9	-24.3	-24.10
31	-54.0	-55.8	-50.4	-51.09	-50.4	-48.6	-50.4	-50.96	-45.0	-28.8	-43.2	-44.14	-32.4	-30.6	-27.0	-44.50
33	-59.4	-50.4	-54.0	-54.93	-54.0	-54.0	-50.4	-61.39	-50.4	-43.2	-48.6	-48.35	N/A	N/A	N/A	N/A
35	-55.8	-66.6	-61.2	-61.67	-54.0	-45.0	-50.4	-50.21	-45.0	-54.0	-48.6	-48.36	-43.2	-43.2	-45.0	-44.34
41	-65.7	-105.3	-103.5	-105.73	-76.5	-60.3	-51.3	-47.45	-45.9	-26.1	-31.5	-32.35	-27.9	-29.7	-29.7	-30.21
43	-31.5	-29.7	-40.5	-38.74	-35.1	-45.9	-42.3	-43.21	-33.3	-38.7	-38.7	-37.25	-33.3	-31.5	-33.3	-31.66
45	-62.1	-74.7	-71.1	-69.51	-56.7	-33.3	-44.1	-43.64	-27.9	-33.3	-33.3	-33.15	-17.1	-17.1	-29.7	-39.32

[a] Transducer Identifier is interpreted as: cladding surface temperature measurement (CLDTEMP), rod designation number (1, 2, 3 or 4), and azimuthal orientation (1 = 60°, 3 = 180°, 5 = 300°) at 0.452-m elevation.

[b] Test rod power is the average power of the four test rods in Test GC 2-3 at an elevation of 0.452 m.

TABLE VI

WAVEFORM ASYMMETRY AT VARIOUS POWER LEVELS (BWR Test Rods)

Test Rod	Individual Test Rod Power Density (kW/m)	Mean Phase[a] Difference (degrees)	Number of[b] Data Points Used to Calculate Mean
GC 523-1	13.55	5.4	2
(He, 0.94%	27.25	2.7	2
gap, 92% TD)	39.84	13.5	2
	48.60	25.2	2
GC 523-2	13.22	0.9	2
(Xe, 0.94%	26.89	1.8	2
gap, 95% TD)	37.73	1.8	1
	47.49	7.2	1
GC 523-3	12.57	7.2	3
(He, 3.6%	25.67	5.4	2
gap, 97% TD)	35.81	10.8	3
	44.34	0.0	1
GC 523-4	12.58	7.2	2
(Ar, 2.2%	27.06	7.2	2
gap, 92% TD)	36.72	10.2	3
	47.43	1.8	2

[a] Average of all available cladding temperature sensors on a given test fuel rod.

[b] Data point not used if value was outside the range of uncertainty in first-order Fourier-fit when compared to MACRAN-III phase angles ($\pm$ 1.8).

In all cases, the plots of Figures 85 through 88 show increasing waveform distortion from the lower to higher power levels analyzed. The amount of distortion is also seen to be dependent on the fuel rod design parameters. For example, the small gap (0.94%) xenon rod, Figure 88(e), and the medium gap (2.2%) argon rod, Figure 88(c), exhibit noticeably more waveform distortion than the small gap (0.94%) helium rod, Figure 88(b) at the highest power level analyzed. At the lowest power level (Figure 85), only the medium gap argon filled test rod, Figure 85(c), exhibits perceptable signal distortion. The data in Tables V and VI suggest that even at low power levels the cladding surface temperature signals are not necessarily symmetrical, even though Figures 85 and 86 show that noticeable signal distortion is not always apparent.

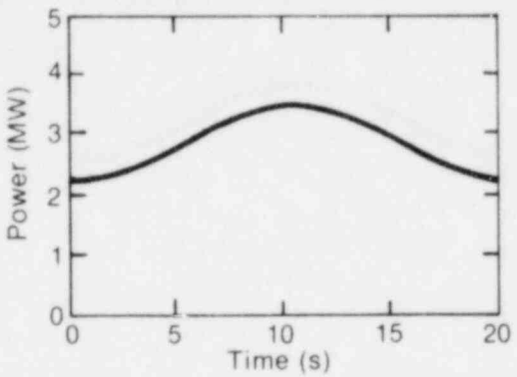

(a) Power driving function for Figures 85 (b) and (c) (first-order Fourier fit).

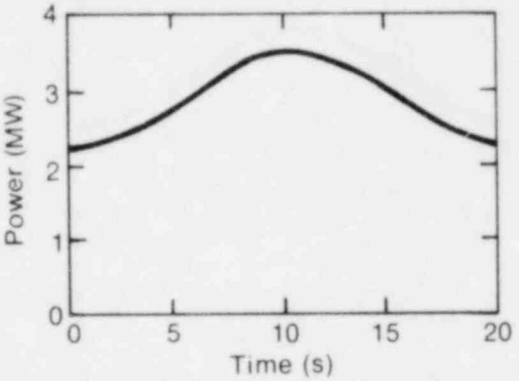

(d) Power driving function for Figures 85 (e) and (f) (first-order Fourier fit).

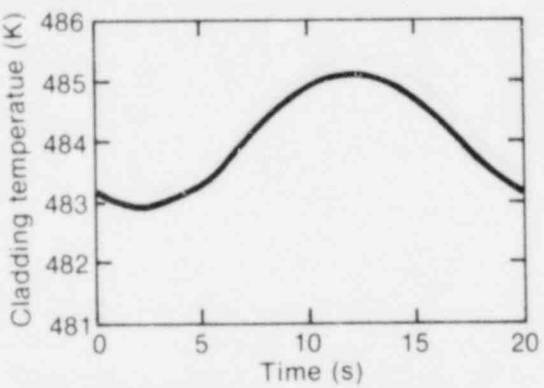

(b) Cladding temperature, Rod GC 523-1, 300° orientation (eighth-order Fourier fit) (He, 0.94% gap, 92% TD).

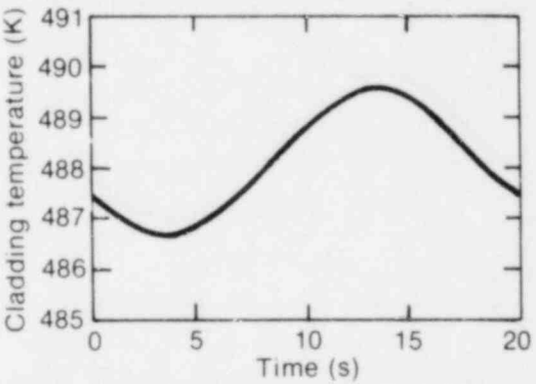

(e) Cladding temperature, Rod GC 523-2, 300° orientation (eighth-order Fourier fit) (Xe, 0.94% gap, 95% TD).

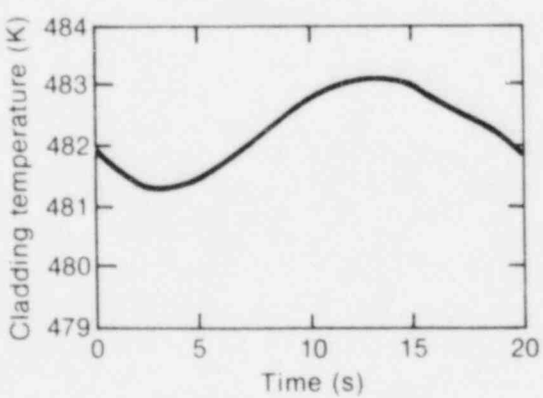

(c) Cladding temperature, Rod GC 523-4, 300° orientation (eighth-order Fourier fit) (Ar, 2.2% gap, 92% TD).

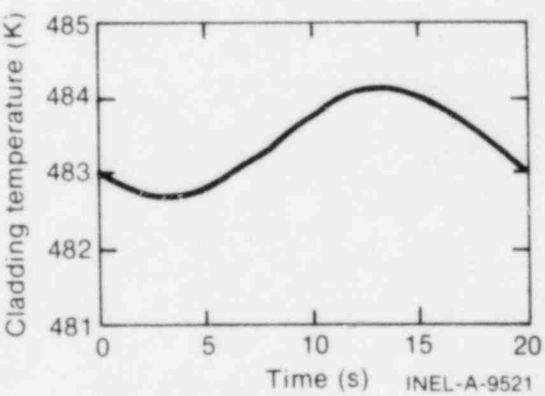

(f) Cladding temperature, Rod GC 523-3, 300° orientation (eighth-order Fourier fit) (He, 3.4% gap, 97% TD).

Fig. 85 Driving function (power) and cladding surface temperature responses at an average nominal power of 13.0 kW/m. Time averaged data points and Fourier fit to data.

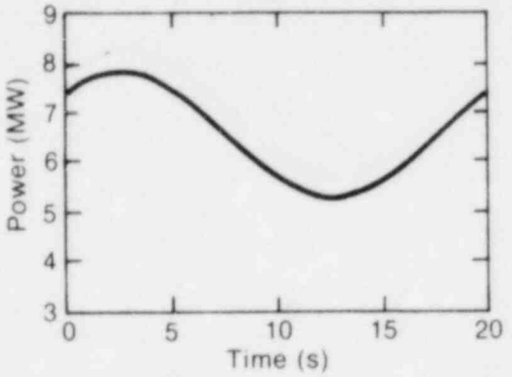

(a) Power driving signal for Figures 86 (b) and (c) (first-order Fourier fit).

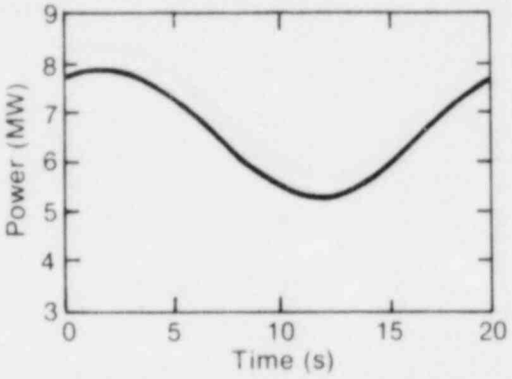

(d) Power driving function for Figures 86 (e) and (f) (first-order Fourier fit).

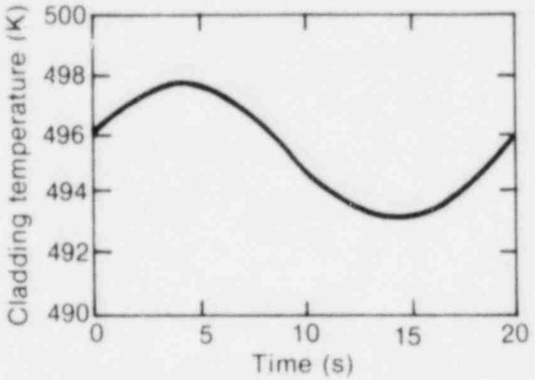

(b) Cladding temperature, Rod GC 523-1, 300° orientation (eighth-order Fourier fit) (He, 0.94% gap, 92% TD).

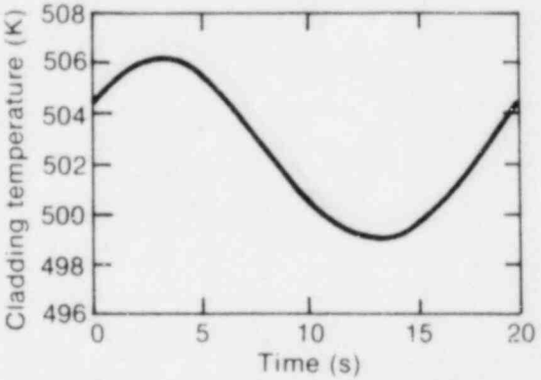

(e) Cladding temperature, Rod GC 523-2, 300° orientation (eighth-order Fourier fit) (Xe, 0.94% gap, 95% TD).

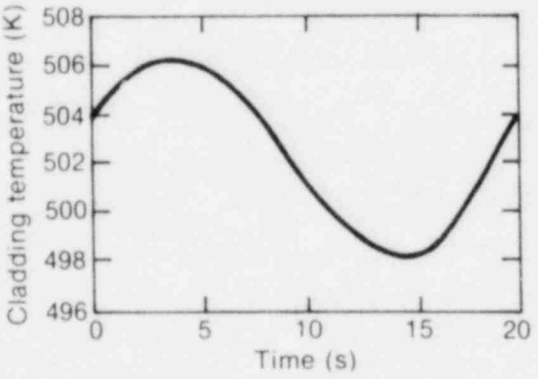

(c) Cladding temperature, Rod GC 523-4, 300° orientation (eighth-order Fourier fit) (Ar, 2.2% gap, 92% TD).

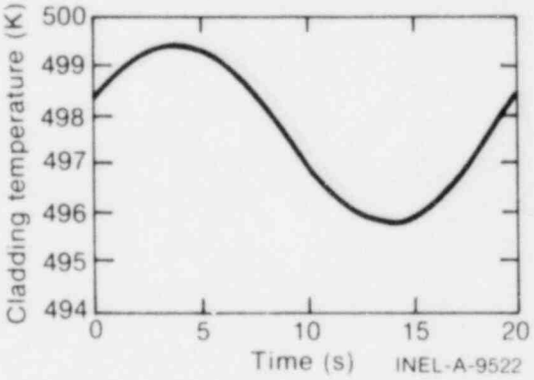

(f) Cladding temperature, Rod GC 523-3, 300° orientation (eighth-order Fourier fit) (He, 3.4% gap, 97% TD).

Fig. 86 Driving function (power) and cladding surface temperature responses at an average nominal power of 26.7 kW/m. Time averaged data points and Fourier fit to data.

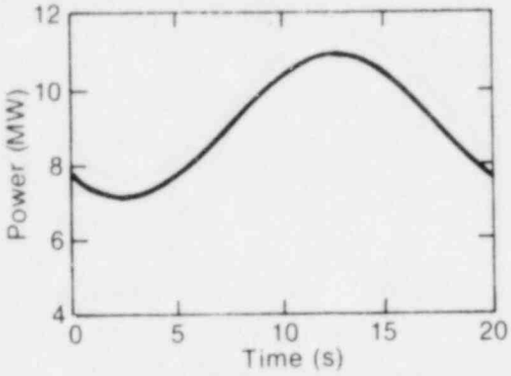

(a) Power driving function for Figures 87 (b) and (c) (first-order Fourier fit).

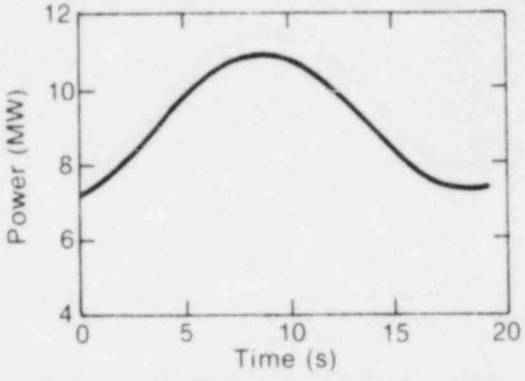

(d) Power driving function for Figures 87 (e) and (f) (first-order Fourier fit).

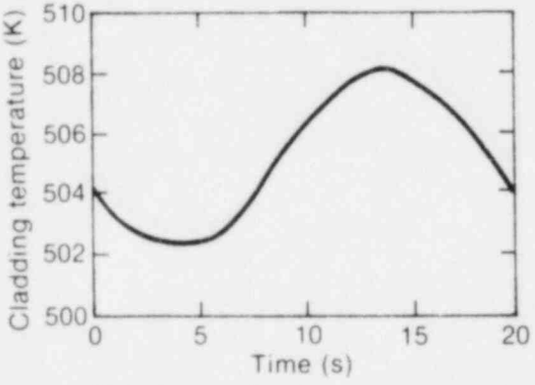

(b) Cladding surface temperature, Rod GC 523-1, 300° orientation (eighth-order Fourier fit) (He, 0.94% gap, 92% TD).

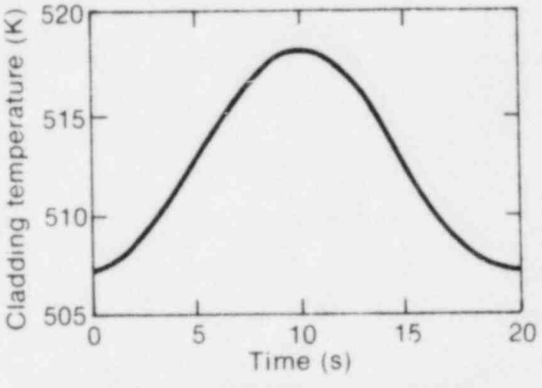

(e) Cladding surface temperature, Rod GC 523-2, 300° orientation (eighth-order Fourier fit) (Xe, 0.94% gap, 95% TD).

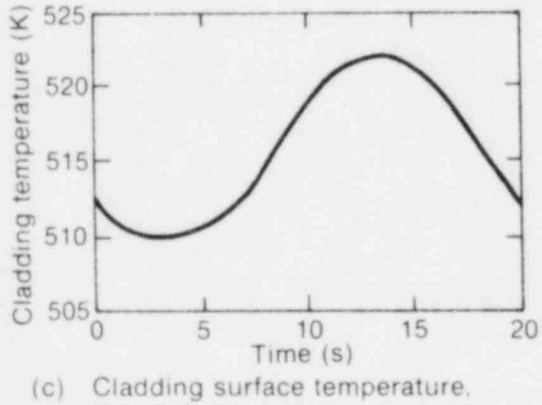

(c) Cladding surface temperature, Rod GC 523-4, 300° orientation (eighth-order Fourier fit) (Ar, 2.2% gap, 92% TD).

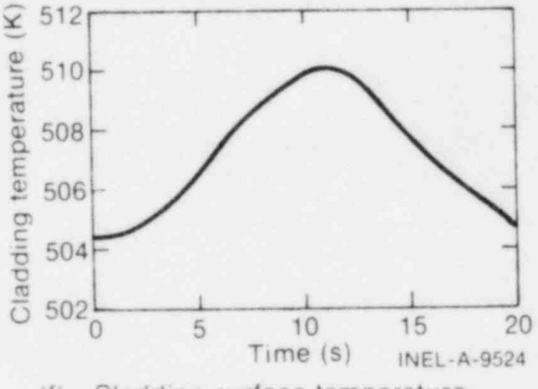

(f) Cladding surface temperature, Rod GC 523-3, 300° orientation (eighth-order Fourier fit) (He, 3.4% gap, 97% TD).

Fig. 87 Driving function (power) and cladding surface temperature responses at an average nominal power of 37.5 kW/m. Time averaged data points and Fourier fit to data.

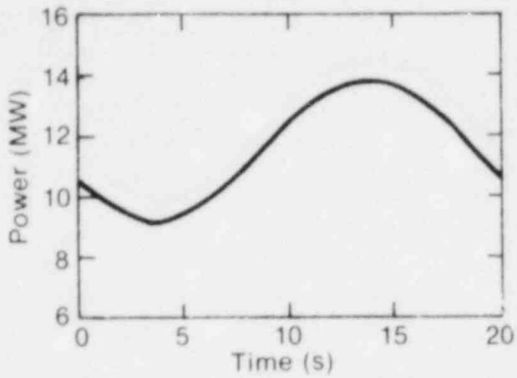

(a) Power driving function for Figures 88 (b) and (c) (first-order Fourier fit).

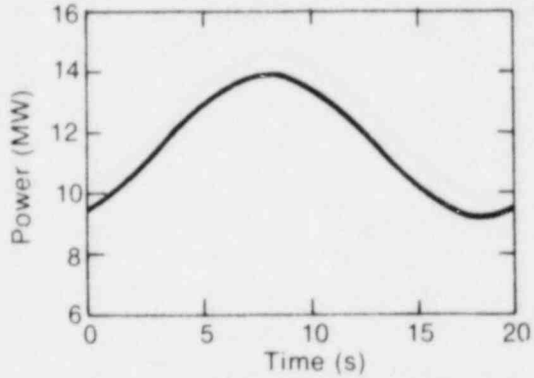

(d) Power driving function for Figures 88 (e) and (f) (first-order Fourier fit).

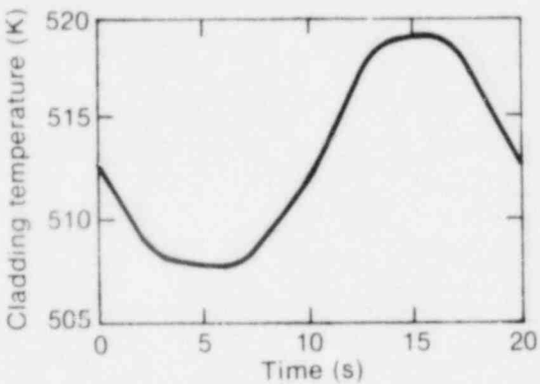

(b) Cladding surface temperature, Rod GC 523-1, 300° orientation (eighth-order Fourier fit) (He, 0.94% gap, 92% TD).

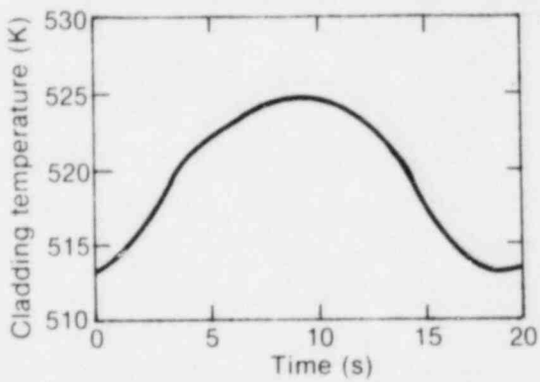

(e) Cladding surface temperature, Rod GC 523-2, 300° orientation (eighth-order Fourier fit) (Xe, 0.94% gap, 95% TD)

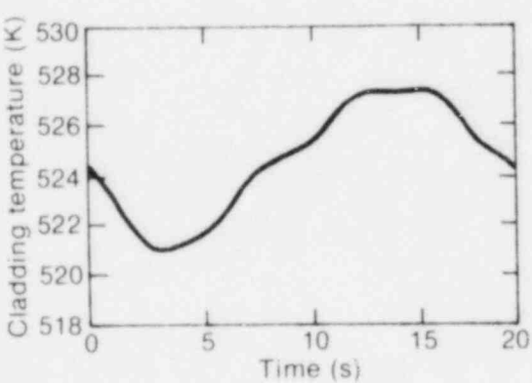

(c) Cladding surface temperature, Rod GC 523-4, 300° orientation (eighth-order Fourier fit) (Ar, 2.2% gap, 92% TD).

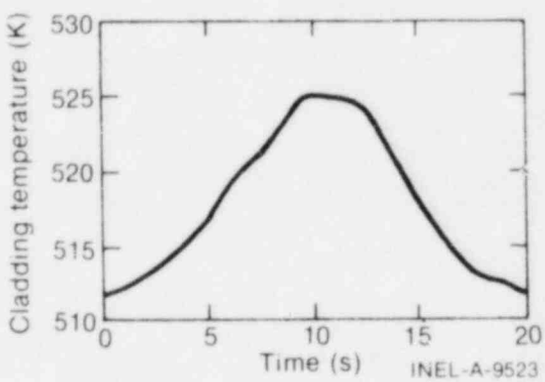

(f) Cladding surface temperature, Rod GC 523-3, 300° orientation (eighth-order Fourier fit) (He, 3.4% gap, 97% TD).

Fig. 88 Driving function (power) and cladding surface temperature responses at an average nominal power of 47.0 kW/m. Time averaged data points and Fourier fit to data.

2.3 PWR Design Test Rods

Gap conductance data taken in conjunction with the PBF PCM-2 and PCM-3[a] tests indicated that reasonable agreement between the steady state and oscillation methods could be obtained. These two tests were conducted with PWR design fuel rods and were operationally similar to the tests conducted with BWR design fuel rods (Tests GC 2-1, GC 2-2 and GC 2-3)[b]. Steady state ($\int$KDT) and power oscillation gap conductance values as a function of test rod power density are shown in Figure 89 for the GC PCM-2 and GC PCM-3 "piggyback" tests. The figure shows that, although the gap conductance values determined by the oscillation method are generally higher than those determined by the steady state method, reasonable agreement between the two values is obtained. Inherent differences between the BWR and PWR fuel rod designs were not anticipated to result in large differences between the two methods since the tests were conducted similarily.

To investigate the apparent inconsistencies between the BWR and PWR test results, a waveform analysis was conducted on a limited sampling of Test GC PCM-3 oscillation data at three power levels. This analysis was essentially identical to that performed on the Test GC 2-3 (BWR) data discussed previously.

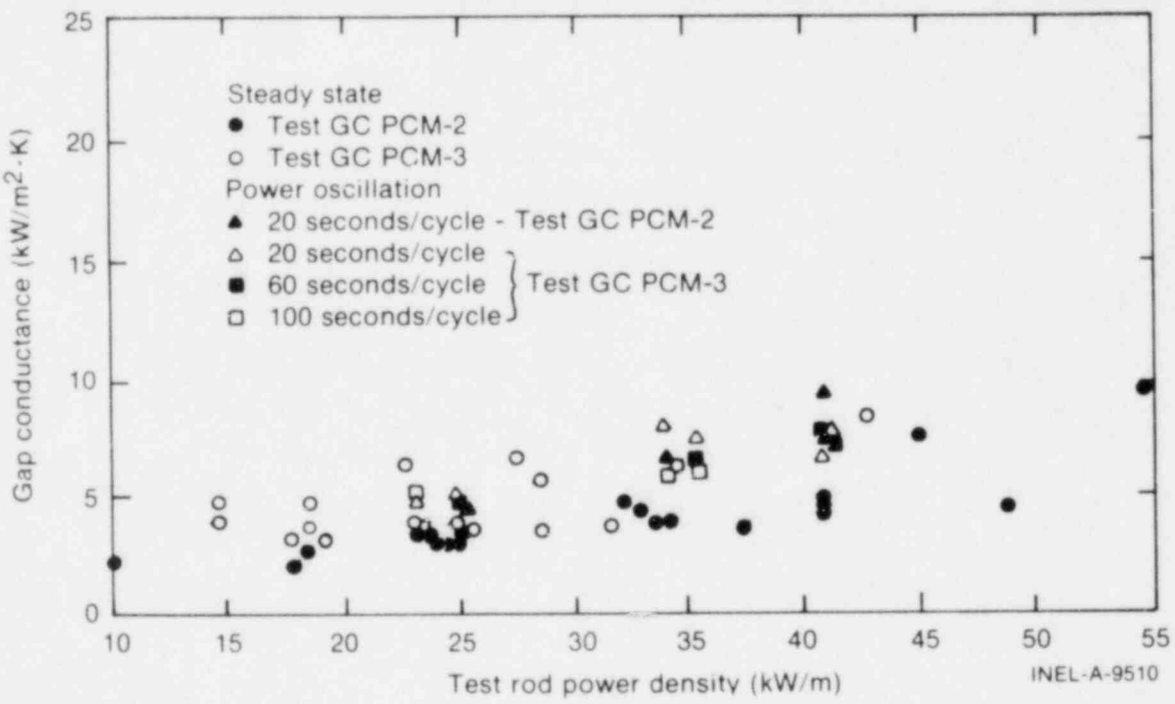

Fig. 89 Comparison of measured steady state and power oscillation gap conductance values for Tests GC PCM-2 and GC PCM-3.

[a] The measured fuel rod cladding temperatures and rod powers will be published in the PCM-2 and PCM-3 Test Results Reports.

[b] Pertinent details of the Tests GC PCM-2 and GC PCM-3 test rod nominal design characteristics and tests conduct are provided in Appendix D.

Results of the PWR symmetry analysis are provided in Table VII. The amount of asymmetry at each power level was estimated by averaging the difference between the minimum and maximum phase angle for each rod investigated. These calculations are summarized in Table VIII. The data from Tables VII and VIII indicate that for the three identical PWR design fuel rods analyzed from Test GC PCM-3, the cladding waveforms do show a noticeable amount of asymmetry, which generally decreases as the power is increased. (The power densities listed in Table VIII correspond to the test rod power at the axial peak location, and, at all thermocouple locations the local power is less than the peak value.)

Figures 90(a-d) through 92(a-d) show the power driving signal at each power level [Figures 90(a) through 92(a)], and representative cladding surface temperature responses [Figures 90(b-d) through 92(b-d)] to the driving function. The data points on the plots correspond to the time averaged data over 20 oscillation cycles. The driving signal (SLP #1) was again fit with a first-order Fourier series; the cladding temperature responses with an eighth-order Fourier series.

Figures 90 through 92 do not reveal an appreciable amount of waveform distortion except on the Rod UTA-0011 cladding temperature oscillations [Figures 90(b) through 92(b)]. The increased incidence of signal distortion apparent in the BWR analysis at progressively higher power levels does not appear to occur in the PWR design rod analysis, although the high powers experienced in Test GC 2-3 were not achieved in Test GC PCM-3.

2.4 Summary of Power Oscillation Analysis Results

The signal analysis for both BWR and PWR fuel rod designs showed that perceptible waveform asymmetry was apparent at all power levels analyzed. For the BWR design test rods, the amount of signal distortion visibly increased as the power increased, and is dependent on fuel rod design parameters. Results from the argon filled test rod (Rod GC 523-4) with 2.2% initial gap width exhibited the greatest degree of distortion, with obvious nonlinearities at even the lowest power investigated (Figure 85). Nonlinearities evident in the results from the small gap helium filled rod (Rod GC 523-1) at the two highest powers (Figures 87 and 88) suggest that the distortion is not only dependent on the temperature of the gap gas, but also on the gap width.

For the PWR design fuel rods, the asymmetry was most significant at low power levels. The amount of distortion apparent at comparable power levels suggests that the PWR design fuel rods maintain a more stable fuel stack geometry during a power oscillation. The larger fuel pellet central expansion is postulated to be compensated by the dished ends in the PWR fuel pellets, but it contributes to an unstable geometry in the flat-ended BWR fuel pellets during a power oscillation. This conclusion is supported by noting that the greatest degree of distortion in the cladding waveforms is apparent in the BWR design rods when the pellet-to-cladding hot gap is small, and when the large gap rods are at high power levels.

TABLE VII

COMPARISONS BETWEEN FOURIER-FIT WAVEFORM ANALYSIS PHASE ANGLES DETERMINED BY MACRAN-III FOR TESTS GC PCM-2 AND GC PCM-3

Transducer Identifier[a]	Test Rod Power[b] = 20.5 kW/m				Test Rod Power[b] = 31.5 kW/m				Test Rod Power[b] = 36.3 kW/m			
	Eighth-Order Fit (degrees)		First-Order Fit (degrees)	MACRAN-III Phase (degrees)	Eighth-Order Fit (degrees)		First-Order Fit (degrees)	MACRAN-III Phase (degrees)	Eighth-Order Fit (degrees)		First-Order Fit (degrees)	MACRAN-III Phase (degrees)
	Minimum	Maximum			Minimum	Maximum			Minimum	Maximum		
CLDTEMP 111	-46.8	-50.4	-48.6	-47.72	-41.4	-55.8	-46.8	-46.68	-41.4	-41.4	-43.2	-46.61
112	-51.3	-42.3	-47.7	-47.03	-44.1	-44.1	-42.3	-42.93	-42.3	-42.3	-44.1	-43.17
113	-77.4	-61.2	-64.8	-64.81	-41.4	-45.0	-41.4	-42.31	-39.6	-41.4	-41.4	-41.99
114	-47.7	-44.1	-47.7	-47.68	-47.7	-53.1	-45.9	-45.91	-44.1	-44.1	-44.1	-43.80
131	-48.6	-43.2	-46.8	-46.34	-45.0	-52.2	-43.2	-44.36	-43.2	-45.0	-43.2	-42.89
132	-49.5	-42.3	-47.7	-45.82	-44.1	-45.9	-44.1	-43.93	-40.5	-38.7	-42.3	-41.44
133	-48.6	-45.0	-46.8	-46.71	-41.4	-45.0	-43.2	-44.72	-43.2	-41.4	-43.2	-41.59
134	-47.7	-42.3	-45.9	-44.15	-42.3	-36.9	-42.3	-42.64	-44.1	-38.7	-42.3	-42.92
211	-58.5	-45.9	-53.1	-52.53	-38.7	-35.1	-36.9	-37.59	-42.3	-31.5	-40.5	-40.36
212	-55.8	-61.2	-54.0	-52.54	-46.8	-45.0	-43.2	-44.09	-45.0	-39.6	-43.2	-41.81
213	-54.9	-62.1	-53.1	-52.28	-40.5	-42.3	-42.3	-41.98	-26.1	-35.1	-35.1	-34.93

[a] Transducer identifier is interpreted as: cladding surface temperature (CLDTEMP), test rod designation (11, 13, or 21), and azimuthal orientation (1 - 0°, 2 - 90°, 3 - 180°, 4 - 270°). For Rod UTA-0011 (CLDTEMP 11x), the angular orientations correspond to elevations of: 0° - 0.68 m, 90° - 0.74 m, 180° - 0.58 m, 270° - 0.64 m. For Rod UTA-0013: 0° - 0.68 m, 90° - 0.48 m, 180° - 0.58 m, 270° - 0.64 m. For Rod A-0021: 0° - 0.68 m, 90° - 0.64 m, 180° - 0.58 m, 270° - 0.89 m.

[b] Test rod power is three-rod average of peak power. Elevation of peak is approximately 0.41 m from bottom of fuel stack.

TABLE VIII

WAVEFORM ASYMMETRY AT VARIOUS POWER LEVELS (PWR Test Rods)

Test Rod	Individual Test Peak[a] Power Density (kW/m)	Mean Phase[b] Difference (degrees)	Number of[c] Data Points Used to Calculate Mean
UTA-0011	20.0	8.1	4
	29.8	5.8	4
	34.7	0.4	4
UTA-0013	20.4	5.7	4
	31.3	4.5	4
	36.3	2.7	4
A-0021	21.2	8.4	3
	33.3	2.4	3
	37.8	7.4	3

[a] Cladding temperature sensors were placed at several axial elevations on each fuel rod. Power density listed is at peak elevation.

[b] Average of difference between minimum and maximum phase for all cladding thermocouples on designated fuel rod.

[c] Data point not used if value was outside range of first-order Fourier-fit when compared to MACRAN-III phase angles ($\pm$ 1.8).

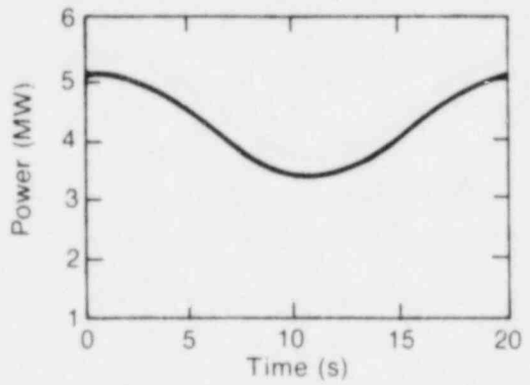

(a) Power driving function (first-order Fourier fit).

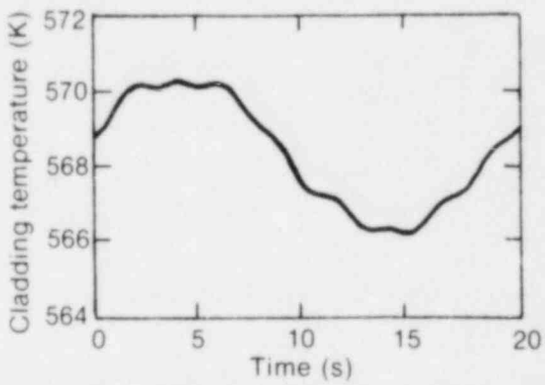

(b) Cladding surface temperature, Rod UTA-0011, 180° orientation, 0.58-m elevation (eighth-order Fourier fit).

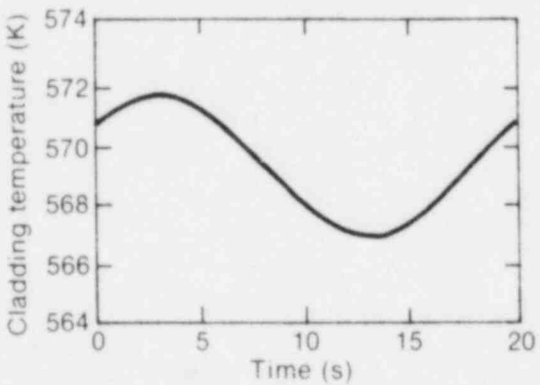

(c) Cladding surface temperature, Rod UTA-0013, 180° orientation, 0.58-m elevation (eighth-order Fourier fit).

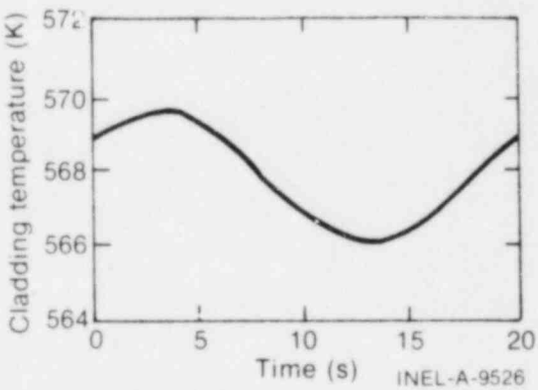

(d) Cladding surface temperature, Rod A-0021, 180° orientation, 0.58-m elevation (eighth-order Fourier fit).

Fig. 90 Driving function (power) and cladding surface temperature responses at an average nominal power of 20.5 kW/m. Time averaged data points and Fourier-fit to data.

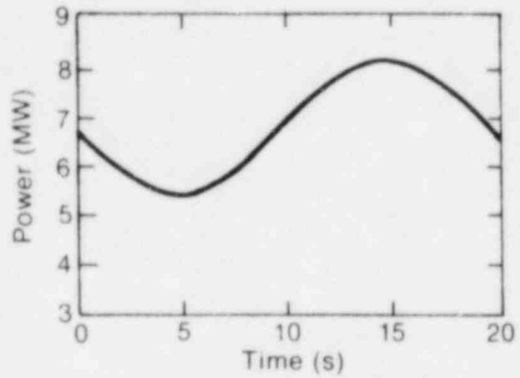

(a) Power driving function (first-order Fourier fit).

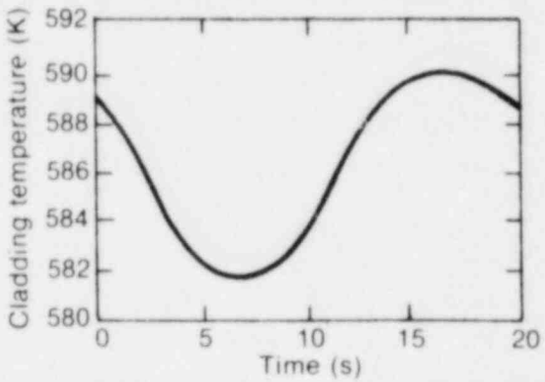

(b) Cladding surface temperature, Rod UTA-0011, 180° orientation, 0.58-m elevation (eighth-order Fourier fit).

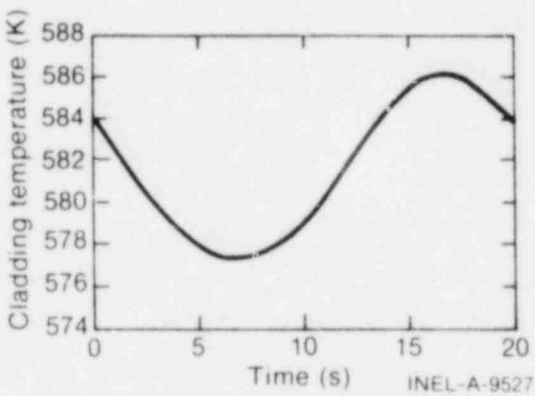

(c) Cladding surface temperature, Rod UTA-0013, 180° orientation, 0.58-m elevation (eighth-order Fourier fit).

Fig. 91 Driving function (power) and cladding surface temperature responses at an average nominal power of 31.5 kW/m. Time averaged data points and Fourier-fit to data.

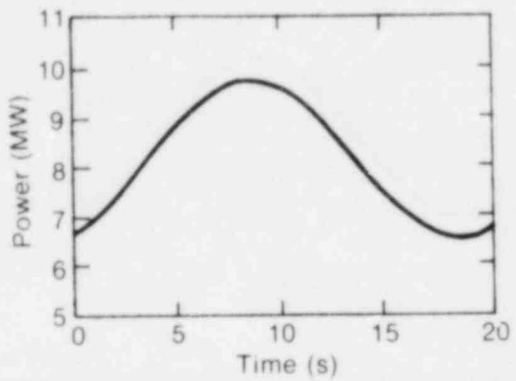

(a) Power driving function (first-order Fourier fit).

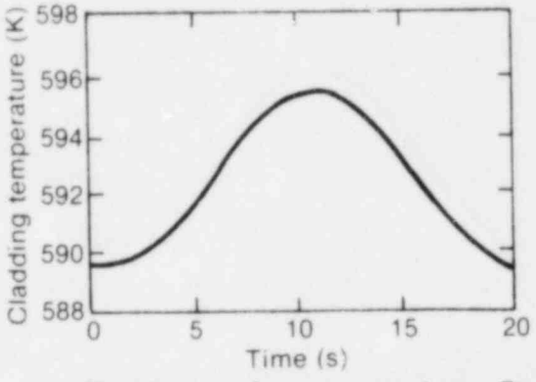

(b) Cladding surface temperature, Rod UTA-0011, 180° orientation, 0.58-m elevation (eighth-order Fourier fit).

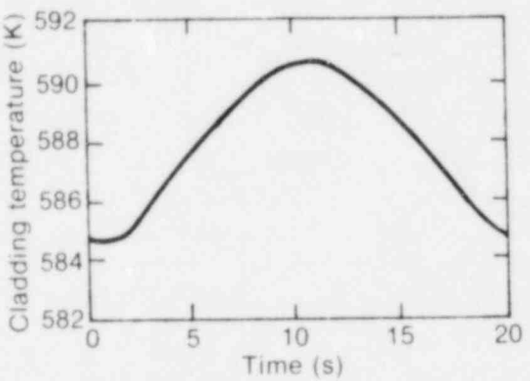

(c) Cladding surface temperature, Rod UTA-0013, 180° orientation, 0.58-m elevation (eighth-order Fourier fit).

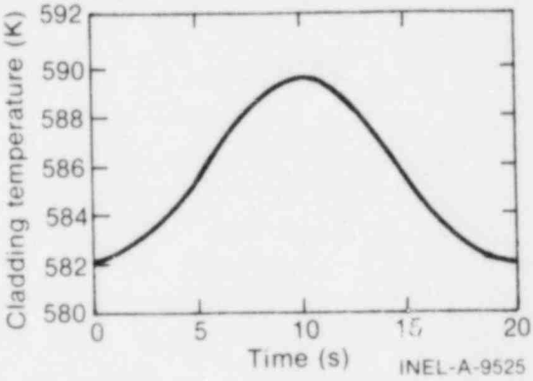

(d) Cladding surface temperature, Rod A-0021, 180° orientation, 0.58-m elevation (eighth-order Fourier fit).

Fig. 92 Driving function (power) and cladding surface temperature responses at an average nominal power of 36.3 kW/m. Time averaged data points and Fourier-fit to data.

3. EVALUATION OF THE POWER OSCILLATION METHOD FOR OBTAINING GAP CONDUCTANCE VALUES

The results of the waveform analysis do not generally support the use of the power oscillation method for estimating gap conductances over the range of power levels and fuel rod design variations of interest. In particular, for ± 20% amplitude power oscillations the method appears to be most applicable at medium power levels in the more stable PWR design fuel rods.

At low power levels, nonlinear changes in fuel thermal conductivity probably contribute to the observed cladding signal asymmetry during a ± 20% power oscillation. Analysis of waveforms from Test GC 2-1 with a ± 10% oscillation amplitude at low power

levels were inconclusive with respect to the effect of oscillation amplitude on the waveform nonlinearities due to the small relative signal-to-noise relationship.

At high power levels, changes in the gap width during a ± 20% oscillation are the probable cause of the large degree of signal distortion observed in the BWR rods. Pellet cracking and relocation, as well as fuel thermal expansion, contribute to the nonlinear gap width changes. An attempt was made to correlate the expected phase angles determined from the SKDT gap conductance values and the linear oscillation model, with the minimum and maximum phase angles determined from the waveform analysis. A functional relationship between the models was not apparent. This result would be expected if the gap width changes were random, as would be the case if pellet motion were evident. Fuel conductivity changes due to pellet relocation and continuously changing radial temperature profiles during power oscillations are probable contributors to the cladding waveform nonlinearities.

The power oscillation method appears to yield reasonable results for PWR design fuel rods at low and medium power levels (that is, below 35 kW/m). At low power levels, the relative changes in gap width and fuel conductivity are small enough that the asymmetric waveform can be approximated by a linear signal of the same frequency. At medium power levels (20 to 35 kW/m) the PWR design fuel rods do not exhibit a significant amount of waveform distortion or asymmetry, indicating a stable fuel stack and relatively small changes in gap width and fuel thermal conductivity. Information on PWR design rods at high power levels (greater than 35 kW/m at the temperature measurement location) was not available.

Power oscillation gap conductance values obtained from BWR design fuel rods appear to be in good agreement with the steady state results for cladding temperature response waveforms which exhibit only a small amount of distortion. The degree of distortion is dependent on the power level and fuel rod design parameters, indicating that the hot gap width, fuel thermal conductivity, and fuel stack stability are important in the applicability of the thermal oscillator technique.

The oscillation waveform analysis has shown that the assumption of negligible nonlinearities is not valid for a ± 20% power oscillation at all power levels of interest. Analysis of ± 10% power oscillation cladding responses has proven inconclusive due to the small signal-to-noise ratio. Possibly, improved signal enhancement capabilities and larger output temperature devices could allow acceptable measurement of gap conductance values at low and medium power levels with very small (± 5%) power oscillations. The small oscillation magnitude is necessary to satisfy the apparent range of applicability of the linear oscillation model. At high powers, the present oscillation method may be unacceptable, even with a low amplitude driving function, due to the assumed unstable behavior of the BWR design fuel stack. Additional oscillation data on PWR design fuel rods at high power levels are necessary before conclusions as to the use of the power oscillation method on PWR rods can be made.

VII. SUMMARY AND CONCLUSIONS

Tests GC 2-1, GC 2-2, and GC 2-3 have provided an extensive and important data base for evaluating LWR design fuel rod thermal response, for evaluating existing analytical models, and for the development of new models. The rod design parameter variations encompass design variations in initial gap width, fuel density, and fill gas composition.

The response of a fuel rod to changes in rod power level is manifest through measured changes in such variables as fuel temperatures, cladding temperatures, cladding elongation, and internal pressure. Generally, at a given power level higher fuel temperatures would be expected to be observed in initially wide gap rods than in initially narrow gap rods, and in low thermal conductivity fill gas rods than in high thermal conductivity fill gas rods. The effect of fuel density would be expected to be small, or even indistinguishable for the small density variations used in the PBF gap conductance tests. The effects of pellet cracking and fill gas inclusion would be expected to alter the thermal response of a fuel rod in possibly opposing ways; cracking would be expected to lower fuel temperatures by reducing the pellet-to-cladding gap, resulting in higher gap conductances, but fill gas inclusion in the cracks would be expected to increase fuel temperatures by effectively reducing the thermal conductivity of the fuel pellet. At high fuel temperatures, fuel restructuring and total gap closure may occur, which would further affect the resulting fuel temperatures, and possibly cause permanent cladding deformation, which would affect subsequent behavior at lower test rod powers.

Further complicating the expected thermal response picture is the fact that the fuel pellets may be eccentrically positioned within the cladding; that is, the pellets may be touching on one side and further away from the other side than normally expected. Analyses have indicated that eccentric positioning of the fuel pellets does not affect the interpretation of the overall thermal behavior of the fuel rod; that is, effective fuel thermal conductivity and average gap conductance, if at least three, equally spaced azimuthal temperature measurements are made. However, if only one or two temperature measurements are made, large uncertainties are inherent in the expected fuel temperatures and interpreted effective fuel thermal conductivities and average gap conductance.

Although additional data will be forthcoming from Tests GC 2-4 and GC 2-5, the data from the three tests performed to date (Tests GC 2-1, GC 2-2, and GC 2-3) have provided a basis for evaluating the effects of fuel design parameter variations on (a) fuel rod thermal response (that is, temperature response), (b) effective fuel thermal conductivity, and (c) pellet-to-cladding gap conductance as a function of rod power density. The data from these three BWR rod tests and the PWR rod piggyback tests also provide a broad basis for evaluation of the power oscillation method for obtaining pellet-to-cladding gap conductance in LWR design rods.

Significant interpretations and conclusions from each aspect of the test results are discussed subsequently.

1. TEST ROD THERMAL RESPONSE

The observed effects of variations in the fuel rod design parameters of initial gap width, fill gas composition, and fuel density on the measured fuel centerline and fuel off-center temperatures as functions of test rod power are summarized in the following subsections. Generally, the test rod steady state thermal responses were as expected, except that the xenon and argon filled rods were hotter at low powers.

1.1 Effect of Initial Gap Width

Initial gap width has a strong effect on the fuel centerline and pellet surface temperatures in helium filled rods when the gap width is increased from 2.2 to 3.4% of the pellet diameter, but only a small effect was observed when the gap width was increased from 0.94 to 2.2%. However, for argon and xenon filled rods, the effect of gap width between 0.94 and 2.2% gap rods was much greater. The stronger effect of gap width in the argon and xenon filled rods than in the helium filled rods is interpreted to be due to the strong effect of pellet cracking and fill gas inclusion on the effective thermal conductivity of the fuel. Inclusion of the low conductivity fill gases of argon and xenon in the fuel cracks strongly inhibits heat conduction across the cracks. At high powers, however, fuel restructuring and contact pressure somewhat offset the effect of cracking and gas inclusion.

In all test rods, the fuel centerline temperatures increased much more than did the off-center (pellet surface) temperatures when the initial gap width was increased. This indicates that when the pellets crack, part of the thermal resistance normally associated with the pellet-to-cladding gap was redistributed within the fuel pellet, especially in moderate and large gap rods. This result further illustrates that pellet cracks and the movement of pellet fragments degrade the fuel thermal conductivity while improving the gap conductance.

1.2 Effect of Fill Gas Composition

As would be expected, the xenon filled rods showed the highest fuel temperatures at a specified power level. However, the differences in the fuel centerline temperatures between xenon and argon rods were much smaller than the differences in the off-center (pellet surface) temperatures for the same rods. This result indicates that the gap thermal resistance and the fuel thermal conductivity are both reduced in both xenon and argon filled rods, but that the reduction in fuel thermal conductivity in the high temperature xenon filled rod was somewhat offset by some other effect, possibly fuel restructuring.

The high fuel temperatures in both the xenon and argon filled medium gap rods caused a chemical reaction between the fuel thermocouple sheath materials and the UO_2. This reaction resulted in a region of material at the center of the pellets that had significantly different thermal properties than UO_2. Consequently, once the xenon and argon medium gap rods had experienced high temperatures, thermocouple failures and changes in the fuel material make use of the experimental data from these rods beyond the first power increase questionable for subsequent analyses.

For the small gap rods, the effect of fill gas composition also caused the xenon rods to exhibit the highest temperatures and the helium filled rods the lowest temperatures. However, at high powers, the fuel centerline temperatures in the xenon filled rods were only slightly higher than those in the argon and helium filled rods, whereas the off-center temperatures in the xenon filled rods were significantly higher (~500 K) than in the argon and helium rods. This result again indicates an apparent improvement in the thermal conductivity of the xenon filled fuel rod as compared with the argon and helium filled rods, and the effect may be due to extensive restructuring or to pellet-to-cladding gap closure in the hotter, xenon filled rod.

1.3 Effect of Fuel Density

The effect of fuel density on the observed thermal response was small for fuel centerline temperatures and was indistinguishable from normal scatter in the data for off-center temperatures.

2. EFFECTIVE FUEL THERMAL CONDUCTIVITY

Under actual operating conditions, pellet cracking, relocation, and fill gas inclusion significantly alter the thermal conductivity of UO_2 fuel pellets. An analytical procedure was developed for evaluating the "effective fuel thermal conductivity" that takes these effects into account. To be of use in predicting fuel rod effective thermal conductivities, an emperical correlation was developed on the basis of evaluated effective thermal conductivities from Tests GC 2-1, GC 2-2, and GC 2-3. The thermal conductivity correlation is briefly summarized.

A correlation was obtained for all of the helium filled test rods in terms of (a) a nominal "hot gap width," (b) the initial cold gap width, and (c) the fuel density. Although the fuel density had a small effect, it did serve as an arbitrary multiplier to fine-tune the relationship for the various helium test rods.

The resulting correlation is given as

$$k_{eff} = k_{MATPRO} - (0.002189 - 0.050867\chi + 5.6578\chi^2)$$

where

$$\chi = (HG - 0.014 - 0.14\,CG)\,(0.0545/CG)\,(\%\,TD)^8$$

and

HG	=	a hot pellet-to-cladding radial gap in millimeters, calculated assuming only radial cracking, thermal expansion, and elastic deflection of an idealized solid pellet and cylindrical cladding
CG	=	the initial cold radial pellet-to-cladding gap in millimeters
% TD	=	the theoretical density of the fuel in percent
k_{MATPRO}	=	the temperature-dependent fuel thermal conductivity of a solid pellet[6].

Analytical models used for predicting fuel rod thermal response should take pellet cracking effects on the thermal conductivity into account.

3. PELLET-TO-CLADDING GAP CONDUCTANCE

Pellet-to-cladding gap conductance was evaluated as a function of test rod power density by steady state ($\int k dT$) and power oscillation experimental methods. The results obtained by both methods are summarized.

3.1 Steady State Method

The steady state values were very consistent between similar rods in the three tests, and showed relatively small azimuthal variations in a given rod. The effect of initial gap width was significant for the helium filled rods between the wide gap and narrow gap rods, but was relatively small between the medium and narrow gap rods. Only medium and narrow gap xenon and argon rods were tested and the effect of gap width was small between the different gap rods for both xenon and argon.

The low thermal conductivities of the xenon and argon fill gases significantly decrease the gap conductance in these rods with respect to the relatively high conductivity helium fill gas rods. However, the effect of fill gas is offset somewhat, but not entirely, by high fuel temperatures which result in greater fuel expansion, pellet cracking, and pellet fragment relocation, all of which increase the gap conductance by decreasing the gap width.

A correlation was developed which provides a simple method for estimating the gap conductance of a specific LWR design fuel rod under a specific set of rod conditions. In the development of the correlation for predicting gap conductance it was observed that all but

three of the test rods in the three tests could be predicted quite well by the Ross and Stoute gap conductance correlation, modified to account for pellet cracking and pellet fragment relocation by assuming a nonuniform thermal expansion of the cracked pellets. The nonuniform thermal expansion model takes into consideration that the pellets have been heated and cracked. Upon cooldown, the pellet fragments do not usually fit together well enough to completely close the relocated cracks. Upon reheating, the relocated cracks must be filled before thermal expansion contributes to closing the existing pellet-to-cladding gap. A nonuniform thermal expansion model that allowed only 30% of the integrated fuel pellet radial thermal expansion to be communicated to the relocated pellet-to-cladding gap was determined to fit the data best. The nonuniform thermal expansion model relocated gap width is given by

$$RGW(mm) = RGW(CZP,mm) - 0.3\ \Delta GW(mm)$$

where

RGW(mm)	=	the relocated gap width to be used in the Ross and Stoute gap conductance correlation at a specific power level
RGW(CZP,mm)	=	the relocated gap width at cold zero power = $1.665 \times 10^{-2} + 0.868\ (GAB) - 13.435\ (GAB)^2 + 71.682\ (GAB)^3$, where GAB is the as-built gap width
ΔGW(mm)	=	the integrated solid pellet gap width change predicted from thermal code calculations to any given test rod power.

For the other three rods (the narrowest initial gap width rods; Rods GC 502, GC 522-2, and GC 523-3), a uniform thermal expansion model provided the best fit with the experimental data. For Rod GC 502, the narrow gap helium filled rod, data were also obtained that would be better fit by a nonuniform expansion model. These data were obtained during the power oscillation portion of the test and may be indicative of a definite change in the thermal response of the rod after the power was cycled several times. The xenon (Rod GC 523-2) and argon (Rod GC 522-2) filled narrow gap rods exhibited high fuel temperatures at low power levels because of the low thermal conductivity fill gases, resulting in early gap closure. With gap closure at low power levels, subsequent thermal expansion

would be expected to be essentially the same as for a solid pellet; that is, uniform thermal expansion. The uniform thermal expansion model relocated gap width is given by

$$RGW(mm) = RGW(CZP,mm) - \Delta GW(mm)$$

with the definition of terms as given previously for the nonuniform expansion model.

3.2 Power Oscillation Method

Gap conductance values determined by the power oscillation method were generally in agreement with the steady state values at low powers, but deviated significantly (much higher values) at high powers. A direct correlation exists between the power levels at which the two methods deviate and the occurrence of waveform changes in the fuel and cladding temperature oscillations. The waveform changes are believed to be due to pellet-to-cladding contact during the oscillations, possibly indicating gap closure during the power increase, and gap reopening during the power decrease.

Azimuthal variations within a rod were much greater for the power oscillation results than for the steady state results. Many of the indicated power oscillation values at high powers were unrealistically high (greater than 40 kW/m^2-K). Pellet-to-cladding contact is postulated to have occurred during the high power oscillations, with possible gap closure during the increase in power, and gap reopening during the decrease in power. Gap closure and reopening during a power oscillation cycle would alter the measured phase lag of the cladding surface temperature oscillation by introducing higher harmonics. The analytical methods used to evaluate gap conductances do not account for higher harmonics, and may result in unrealistic values.

Analyses are described that were performed to identify cladding surface temperature waveform distortions and to quantitively determine the effect of observed nonlinearities on the results obtained by the power oscillation method. Nonlinearities in the waveforms were identified for both PWR and BWR design rods, but the nature of the nonlinearities was different for the two rod designs; that is, for BWR rods the amount of signal distortion increased as the nominal rod power increased, but for PWR rods, signal distortion was most significant at low power levels. The amount of signal distortion observed at a specific power level suggest that the PWR design fuel rods maintain a more stable fuel stack geometry during a power oscillation. The fuel pellet central expansion is possibly compensated by the dished ends in the PWR fuel pellets, but it contributes to an unstable geometry in the initially flat-ended BWR pellets during a power oscillation.

4. EVALUATION OF THE POWER OSCILLATION EXPERIMENTAL METHOD

A major objective of the PBF gap conductance tests has been to provide experimental data for evaluating the power oscillation method for obtaining gap conductances. On the basis of the results obtained from Tests GC 2-1, GC 2-2, and GC 2-3, the power oscillation

method does not provide reliable and consistent gap conductance values for BWR design rods over the range of power levels of interest. These results are in contrast to the evaluation of the power oscillation method based on the "piggyback" tests with PWR design rods. The analyses should continue in an attempt to determine why the power oscillation method appears to provide acceptable results for PWR design rods but not for BWR design rods. Tests GC 2-4 and GC 2-5 will provide additional low power data to better identify the range of applicability of the oscillation method. These results may also provide further insight to why the method works for one rod design but not for the other.

VIII. REFERENCES

1. United States Nuclear Regulatory Commission, Reactor Safety Research Program, *A Description of Current and Planned Reactor Safety Research Sponsored by the Nuclear Regulatory Commission's Division of Reactor Safety Research*, NUREG-75/058 (June 1975).

2. J. A. L. Robertson, *Irradiation Effects in Nuclear Fuels*, London: Gordon and Breach Science Publishers, 1969.

3. B. A. Murdock, *Postirradiation Examination Data Report for Gap Conductance Test Series, Test GC 2-1*, TREE-NUREG-1204 (March 1978).

4. D. K. Kerwin, *Postirradiation Examination Data Report for Gap Conductance Test Series, Test GC 2-2*, TREE-NUREG-1206 (May 1978).

5. B. A. Cook, *Postirradiation Examination Data Report for Gap Conductance Test Series, Test GC 2-3*, TREE-NUREG-1231 (July 1978).

6. G. A. Reymann et al, *MATPRO – Version 10: A Handbook of Materials Properties for Use in the Analysis of Light Water Reactor Fuel Behavior*, TREE-NUREG-1180 (February 1978).

7. J. A. McClure, *TOODEE: A Two-Dimensional, Time-Dependent Heat Conduction Program*, IDO-17227 (April 1967).

8. A. M. Ross and R. L. Stoute, *Heat Transfer Coefficient Between UO_2 and Zircaloy-2*, AECL-1552 (June 1962).

9. R. K. Otnes (ed.), *MACRAN-III Time Series Data Analysis System, Reference Manual*, Agbabian Associates, El Segundo, California (1973).

DISTRIBUTION RECORD FOR NUREG/CR-0300

(TREE-1268)

Internal Distribution

1 - Chicago Patent Group - DOE
9800 South Cass
Argonne, IL 60439

2 - R. L. Blackledge
Idaho Operations Office - DOE
Idaho Falls, ID 83401

3 - R. J. Beers, ID

4 - P. E. Litteneker, ID

5 - R. E. Tiller, ID

6 - H. P. Pearson
Information Management, EG&G

7-12 - INEL Technical Library

13-32 - Author

33-87 - Special Internal

External Distribution

88-89 - Saul Levine, Director
Office of Nuclear Regulatory Research, NRC
Washington, D.C. 20555

90-91 - Special External

92-118 - Technical Information Center - DOE
Box 62
Oak Ridge, TN 37830

119-411 - Distribution under R3, Water Reactor Safety Research - Fuel Behavior